



**Politecnico  
di Torino**

**Politecnico di Torino**

Master of Science in Biomedical Engineering

2020/2021

July 19<sup>th</sup>, 2021

***“In vitro* microfluidic 3D platform  
as a pathological model of the  
pancreatic acino-ductal unit”**

**Supervisors:**

Prof. Gianluca Ciardelli

Prof. Matteo Cocuzza

Prof. Chiara Tonda Turo

Dr. Simone Luigi Marasso

**Candidate:**

Beatrice Minervini

# Table of Contents

Abstract.....	5
1. Introduction .....	6
1.1 The clinical problem: Pancreatic Ductal Adenocarcinoma (PDAC).....	6
1.2 Overview of the Pancreas Tissue.....	7
1.2.1 Exocrine pancreas .....	7
1.3 Pathogenesis of PDAC.....	9
1.3.1 PDAC- Stroma crosstalk.....	10
1.3.2 The pancreatic stellate cells .....	13
1.4 Tissue Engineering and PDAC <i>in vitro</i> models.....	15
1.4.1 Animal models .....	16
1.4.2 Two-dimensional (2D) models .....	17
1.4.3 Three-dimensional (3D) culture models to mimic the exocrine pancreatic tissue	18
1.4.4 Microfluidic Systems .....	25
1.5 Organs-on-a-chip in detail.....	26
1.5.1 Materials: PDMS and smart materials.....	26
1.5.2 Fabrication techniques.....	28
1.6 Scientific Background: Cases of Study .....	32
2. Aim of the work .....	37
3. Materials and Methods .....	38
3.1 Device Design.....	38
3.1.1 Bottom layer .....	38
3.1.2 Top layer .....	39
3.1.3 Membrane.....	39
3.1.4 Reservoirs layer .....	40
3.2 Device fabrication .....	41
3.2.1 Replica molding.....	41

3.2.2	Bottom layer mold fabrication: SU-8 photolithography.....	42
3.2.3	Top layer mold fabrication: Laser ablation.....	46
3.2.4	Membrane fabrication .....	47
3.2.5	Microfluidic device assembly.....	50
3.3	Physical characterization of the microfluidic device.....	52
3.3.1	Surface roughness analysis: Profilometer .....	52
3.3.2	Digital microscope analysis of single device layers.....	53
3.3.3	Field Emission Scanning Electron Microscope (FESEM).....	53
3.4	Fluidic test of the microfluidic device.....	54
3.4.1	Capacity test.....	54
3.4.2	Diffusivity test.....	55
3.5	Biological characterization.....	58
3.5.1	Human Foreskin Fibroblasts cells .....	58
3.5.2	PSCs cells.....	59
3.5.3	HPDE cells with KRAS mutation.....	59
3.5.4	Procedure of cell seeding .....	59
3.5.5	Vitality assays.....	61
3.5.6	Biological experiments.....	63
4.	Results and Discussion .....	72
4.1	Mold characterization .....	72
4.2	Device characterization.....	73
4.3	Fluidic characterization.....	77
4.3.1	Capacity test.....	77
4.3.2	Diffusivity test.....	78
4.4	Biological characterization.....	79
4.4.1	HFF-1 culture .....	79
4.4.2	PSCs culture .....	82
4.4.3	HPDE-KRAS culture .....	85
4.4.4	Co-culture .....	89

5. Conclusion and future work.....	95
6. Bibliography.....	97



# Abstract

Pancreatic ductal adenocarcinoma (PDAC) is one of the deadliest tumours that affect the exocrine pancreas and it has a poor survival rate. These unfortunate data are ascribed to the absence of symptoms in the early stages, invasive metastasis, and high resistance to the therapeutic options. For these reasons, *in vitro* models that can reproduce the microenvironment of the pancreatic tissue are required to develop therapies and to predict drug safety and efficacy in humans. Organ-on-chips can be a powerful technology to achieve these goals. In this thesis project, a microfluidic device for modelling the pancreatic acino-ductal unit, is developed. The function of the platform is to investigate the crosstalk between PDAC and the stromal components which plays a fundamental role in cancer progression. To this aim a multilayers device in Polydimethylsiloxane (PDMS) composed by two layers separated by a membrane: a bottom layer loaded with collagen hydrogel mimicking the stromal component and a top layer reproducing the tumour component were fabricated using replica moulding. The connection between the two components was realized by the microporous membrane in polycaprolactone and gelatin (PCL/Gel) that was obtained by the electrospinning technique. SU-8 photolithography and laser ablation techniques have been also implemented to produce the molds of the bottom and top layers, respectively. The surface characterization of the mold was carried out through the use of a profilometer while the morphological characterization of the microfluidic device was performed using optical microscopy and Field Emission Scanning Electron Microscopy (FESEM) proving how the geometries reproduced were of the desired dimensions. In addition, a fluidic characterization was carried out through capacity and diffusivity tests. *In vitro* studies were implemented to evaluate the cell proliferative capability and the cellular response of cells cultured in the device. Moreover, different cell lines, specific of the pancreatic tissue, were used as mono- and co-culture. Specifically, Pancreatic Stellate Cells (PSCs) and Human Pancreatic Duct Epithelial Cells with mutation in oncogene KRAS (HPDE-KRAS) have been employed to reproduce the stroma and PDAC tissue that characterize the tumoral microenvironment *in vivo*. Vitality assays and fluorescence imaging were performed to analyse the cellular activity and the morphological structure of cells seeded in the bottom layer, in the top layer, and in the assembled device. Results suggest that HPDE cells adhered and proliferated on PCL/Gel membrane and PSCs were vital when loaded into collagen hydrogel for the whole culture period.

# 1. Introduction

## 1.1 The clinical problem: Pancreatic Ductal Adenocarcinoma (PDAC)

Pancreatic ductal adenocarcinoma (PDAC) is one of the deadliest tumours that affect pancreas. In general, there are two different classes of pancreatic cancer as a function of tissue: Pancreatic Endocrine Tumours and Pancreatic Exocrine Tumours. These types of tumours have different causes, signs, and symptoms. Endocrine tumours start in the hormone producing cells of the pancreas and they account for less than 5% of all pancreatic tumours and are considered rare while the Pancreatic Exocrine Tumours is the most common types of pancreatic tumours, in particular 90% of pancreatic tumour is born by exocrine component. About 5% of exocrine pancreas cancers are acinar cell carcinomas which begin in the acinar. While 95% of cancers of the exocrine pancreas are adenocarcinomas that starts in the ducts of the pancreas, PDAC that actually is the fourth cause of cancer related mortality in the industrialized countries, in particular in the United States. PDAC is a mortal condition with poor five-year survival rates between 2% and 9%<sup>1</sup>. PDAC is expected become the second reason of death related to tumour in the next decade<sup>2</sup>. These unfortunate data are attributed to no symptoms in the early stages and in the late stages the symptoms are non-specific and similar to other neoplasms, early and invasive metastasis, and the high resistance to possible therapeutic options such as chemotherapy and radiotherapy<sup>3,2</sup>.

The high resistance is partly due to the heterogenous tumour microenvironment (TME), consisting in a mix of biochemical, biomechanical and cellular components, that cooperate in complex ways with extracellular matrix (ECM) and concur to the disease progression<sup>4</sup>. For these reasons, it is necessary continue studies to the development of effective drugs is currently constrained by the lack of a robust preclinical models.

## 1.2 Overview of the Pancreas Tissue

Pancreas is a glandular, parenchymatous and unequal organ that is connected to the digestive system. Pancreas location is in the left part, behind the peritoneum and the stomach, anterior to the first and second lumbar vertebrae (Figure 1.2.1). It is because of its location that its pathologies show vague and non-specific signs and symptoms. The shape of pancreas has individual variation but, anatomically, it can be divided into three main parts: the head, the body and the tail. The head is surrounded by duodenum and it is the largest section of pancreas<sup>5,6</sup>.

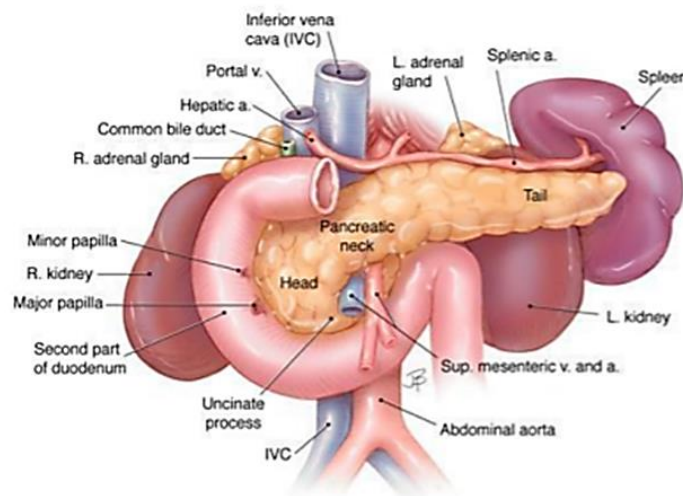


*Figure 1.2.1 Anatomical relationships of pancreas with other organs and structures<sup>6</sup>.*

### 1.2.1 Exocrine pancreas

Pancreas is a secretory mixed gland with both exocrine glandular formations and endocrine glandular formation. Every microscopic lobule is compounded of a great quantity of exocrine cells and a small measure of endocrine cells<sup>5</sup>.

The exocrine component makes up 80-85% of the organ and has the fundamental task of secreting pancreatic juice and pouring it into the duodenum in order to allow complete digestion<sup>5</sup> (Figure 1.2.2-b). The exocrine pancreas is composed by two fundamental types of cells: acinar cells and ductal cells<sup>5</sup>.

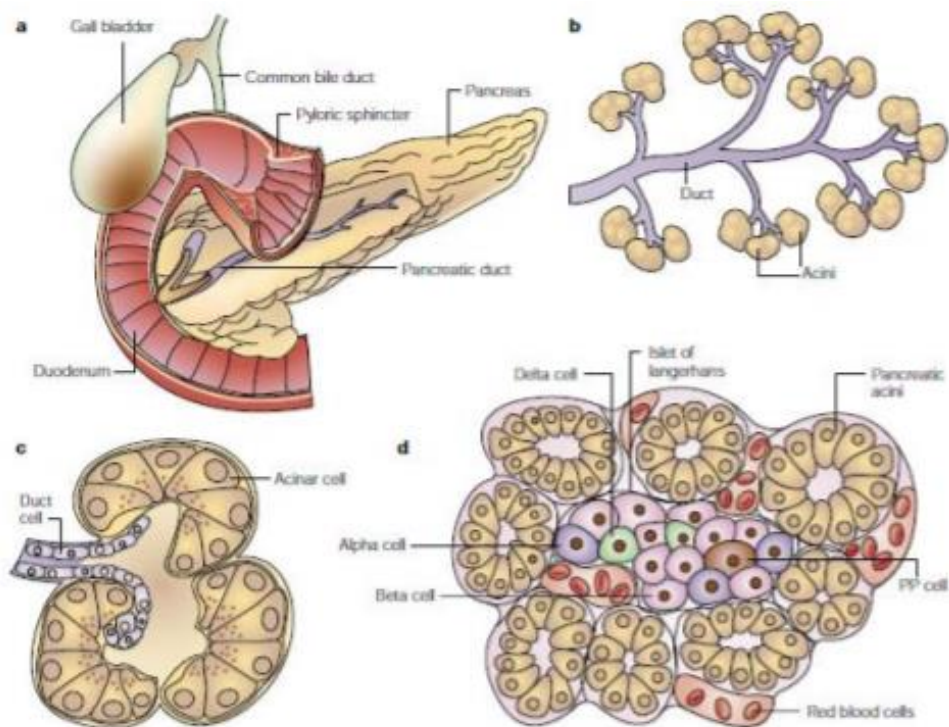


**Figure 1.2.2** a) anatomy of the pancreas; b) the exocrine pancreas; c) a single grape; d) pancreatic island immersed in the exocrine tissue.

**Acinar cells** are parenchymal cells with a pyramidal geometry, these cells are organized to form a convoluted, often interconnecting with a tubular-acinar network within the lobules. The apexes of these cells delimit a small central lumen which represents the terminal part of the secretory ducts, known as acino-ductal unit (Figure 1.2.2-c). Acinar cells have a developed Golgi apparatus and an abundant rough endoplasmic reticulum that are the anatomical areas responsible for exocrine secretion<sup>8</sup>.

**Ductal cells** have a single nucleus and are smaller than acinar cells (Figure 1.2.2-c). Cuboidal cells form a single layer which delimits the interlobular and normal ducts. Duct cells secrete water and bicarbonate that are necessary to carry enzyme proteins into the duodenum. This secretion is regulated by the vagal nerves and by secretin.

The tubules and acini are surrounded by a basement membrane (basal lamina) and delicate fibrous stroma which contains a large number of capillaries<sup>7</sup>.

The secretions by acini drain into a highly branched duct system and joins the common bile duct to flow into the ampulla of Vater, which opens into the duodenum at the greater duodenal papilla. Then there is an accessory duct, or Santorini, which is in the upper portion of the head of the pancreas, as a branch of the main duct, and leads into the minor duodenal papilla<sup>6,8,9</sup>.

The study of three-dimensional organization of the exocrine pancreas is very important in order to understand the changes that take places during pancreatic diseases.

### 1.3 Pathogenesis of PDAC

The origin of PDAC is difficult to define because the cellular structure of pancreas is very complex due to the cellular composition. In the most cases the pancreatic ductal adenocarcinoma develops from ductal cells, and it mainly occurs in the head and in the end of pancreas <sup>10,11</sup>.

PDAC is divided into two diverse compartments, one composed by differentiated and mature cells and the other compartment is constituted by constantly proliferating and self-renewing cells, called cancer stem cells (CSC). CSC have been showed to be resistant to traditional anticancer therapy, and they are implicated in process of cancer spread. Pancreatic cancer stem cells present a combination of specifical markers, such as CD44, CD24, CD133(stem cell markers in hematopoietic and neural stem cells), ESA (epithelial-specific antigen) and ATP-binding cassette sub-family G member 2 (ABCG2) <sup>12</sup>.

PDAC is characterized by a dense fibrotic reaction called Desmoplastic Reaction (DR), which consists in the recruitment and activation of pancreatic stellate cells (PSC) and fibroblasts in the tumour site that release extracellular matrix proteins. This action contributes to the growth of the cancer tissue, to the aggressive nature of tumour and to the drug resistance by PDAC. The PDAC cells live in an extremely hostile environment with low nutrients concentration and hypoxic conditions since the pancreatic cancer microenvironment has a very poor vascularization <sup>13</sup>.

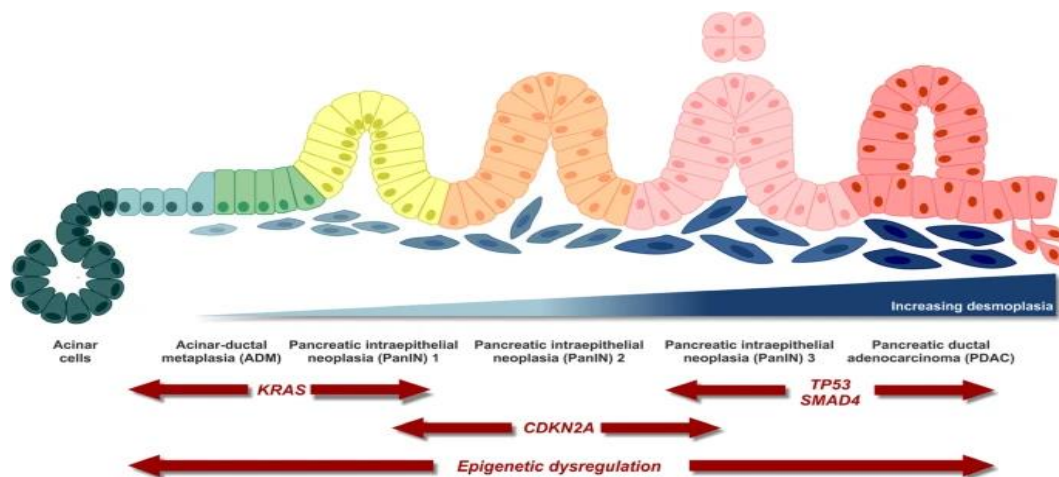


*Figure 1.3.1 Evolution of PDAC* <sup>123</sup>.

The main precursor lesions of this tumour are the pancreatic intraepithelial neoplasia (PanIN), mucinous cystic neoplasms (MCN) and intraductal papillary mucinous neoplasms (IPMN). Pancreatic intraepithelial neoplasia is a microscopic and non-

invasive lesion that develops in the pancreatic ducts with diameters less than 0.5 cm, and it represents the most prevalent precursor of PDAC (Figure 1.3.1). These lesions are divided into three different classes, from 1 to 3, in increasing order of severity. *PanINs-I* are due to mutations in the *KRAS* oncogene and show telomere shortening that it has been linked to the instability of chromosomes, inconspicuous nucleoli, minimal nuclear atypia, and deficient mitotic figures. The *PanINs-II* develop mutations in the *p16* oncogenes, and these lesions show pseudo stratification, modest nuclear atypia, loss of cell polarity, and hyperchromasia of nucleus. In higher grade *PanINs-III* also show mutation in the *CDNK27*, *DPC4*, *p53* e *SMAD4* oncogenes, these lesions have a marked atypia, a micropapillary, a papillary and a flat architecture. Lower grade PanIN lesions have a small amount of stroma around the pancreatic ducts. On the contrary, PanINs-III have a high amount of stroma that leads to a large stroma in invasive tumour<sup>1,14,15,9</sup>.

Another group of PDAC precursors are intraductal papillary mucinous neoplasms, *IPMN*, these lesions develop in the main pancreatic duct or in the secondary branches and they are mucin-secreting epithelial neoplasms. IPMN of the main pancreatic duct are called “*main duct type*” and they have a papillary architecture, while IPMN of the secondary branches are called “*branch duct type*” and they have a papillary or flat structure<sup>16</sup>. Furthermore, the main duct type IPMNs are more malignant than the branch duct type IPMNs<sup>1</sup>. The least common of these precursor lesions are macroscopically visible cystic neoplasms MNC, that present a mucinous epithelial lining and an ovarian-like stroma, for these reasons MNC show hormonal receptors such as progesterone and oestrogen<sup>16,14</sup>. MCN do not connect with the pancreatic ductal system and develop in the body or in the end of pancreas with dimension from 1 to 3 cm<sup>15,17</sup>. In addition to the genetic changes, epigenetic alterations have a central role in the progression of pancreatic cancer. Non-coding RNAs, alterations in DNA methylation and histone modifications contribute to neoplastic progression<sup>18</sup>.

### **1.3.1 PDAC- Stroma crosstalk**

Tumorigenesis is a multistage process where cancer cells develop multiple genetic alteration, throughout different stages that are the primary transformation, the amplification, the local invasion and, finally, the metastatic circulation. The tumour microenvironment is composed by malignant cells, lymphatic/blood vessels, inflammatory/immune cells and a rich extracellular matrix. This tumour environment promotes cancer cells survival and their development<sup>13</sup>. It is composed by abnormal cells that constitute the cancer compartment itself and the stroma that define the connective-tissue framework of the tumoral tissue. The tumour’s progression is due to an evolving crosstalk between the different tumour cell types and the stroma. Cancer cells release

different growth factors such as VEGF(vascular endothelial growth factor), bFGF(basic fibroblast growth factor), EGFR-ligand(epidermal growth factor receptor), PDGF(platelet-derived growth factor), HGF (hepatocyte growth factor), IGF-1 (insulin-like growth factor 1) and TGF $\beta$ (transforming growth factor- $\beta$ ) that change the healthy tissue homeostasis, stimulate the formation of new blood and lymphatic vessels, and are associated with the recruitment of the inflammatory cells and the activation of the PSCs<sup>13,19</sup>. The cell groups main present in the PDAC microenvironment are three. The first type of cells is *fibroblasts* that are more heterogeneous population of cells, which typically compose connective tissue. Fibroblast under stimulation, activate themselves, then proliferate and produce a large amount of ECM proteins. These activated cells, called myofibroblasts, have contractile properties and form the group of 'tumour-associated fibroblasts TAFs 'or 'cancer associated fibroblasts CAFs'.<sup>19</sup> In the PDAC this type of cells is composed by bone marrow-derived cells Pancreas Stellate Cell named PSC. PSC are stromal cells around pancreatic exocrine glandular units which acquire myofibroblast-like properties during an injury<sup>20</sup>. Another group of cells is *inflammatory/immune cells* which are innate immunity cells such as dendritic cells, lymphocytes, macrophages, neutrophils, eosinophils and mast cells. PDAC shows a low amount of tumour infiltrating lymphocytes (TILs) but a high quantity of myeloid-derived suppressor cells (MDSCs) and T regulatory cells (Tregs) that permit to reduce the tumour-specific immune reaction<sup>21</sup>. Tumor-associated macrophages, TAMs, are the major type of immune cells, and they have two different phenotypes, M1 with tumor-suppressing activity and M2 tumour-promoting activity<sup>2</sup>. PDAC cells and growth factors syntheized by CAFs, chemokines and cytokines, in particular interleukines IL-6, IL-8 and IL-10 promote M2 phenotype of TAMs<sup>2</sup>. Neutrophils are another group of Immune cells which secrete cytotoxic factors and reactive oxygen species for this reason their presence in the TME is associated to bed prognosis. Neutrophils expel into extracellular space their intracellular proteins, histones and DNA, and extracellular traps which capture circulating tumour cells in order to simplify metastasis formation<sup>2</sup>. The last main group is composed by *vascular cells*, which make the base for blood vessels<sup>22</sup>. PDAC has a poor vascularization, one reason are PSCs that product a large amount of ECM proteins. These ECM proteins cause compression and distortion of tumour vasculature and contribute to tumour hypoxia and chemoresistance. Furthermore, hypoxia itself stimulates the formation fibrotic/hypoxic tissue; this is the Hypoxia-fibrosis cycle, an autocrine-positive feedback loop<sup>2,13</sup>. In the other hand, in non-adjacent to tumour area there is an increase in vascularization due to the low amount of PDAC cells and the high quantity of macrophages and PSCs that produce VEGF. Other causes of the poor

vascularization are endostatin that is product by type-VIII collagen degradation and HA secrete by PDAC cells and CAFs<sup>2</sup>.

The tumour ECM is the microenvironment that supports the tumour and the structural changes in the ECM have an important role in the survival and the progression of cancer, in the inflammation and in the fibroblast activation which deposit a large amount of ECM proteins<sup>23,2</sup> (Figure 1.3.2).

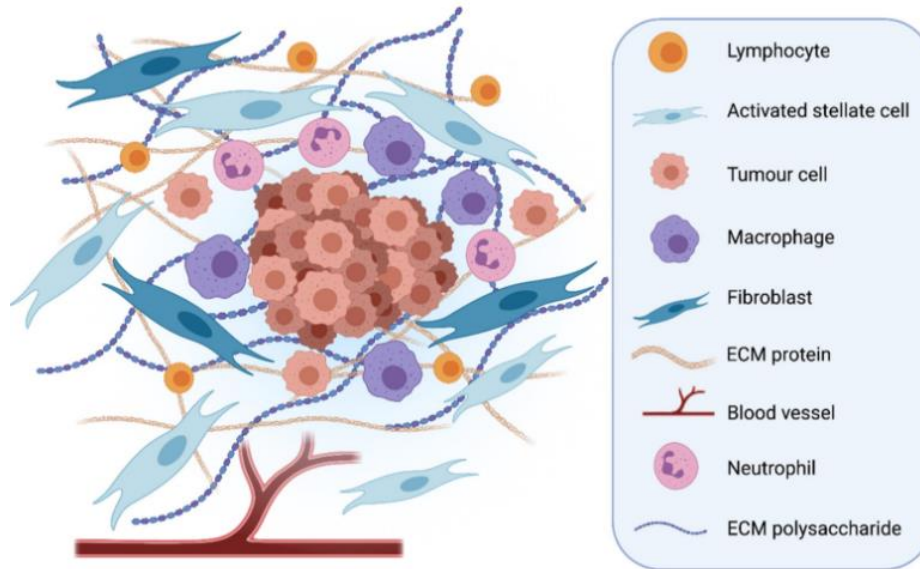


*Figure 1.3.2 Crosstalk Stroma-PDAC<sup>124</sup>.*

PSCs secrete tissue inhibitor of metalloproteinases (TIMP) and metalloproteinases (MMP) that control matrix turnover setting pancreatic fibrosis. Normally basement membrane in pancreas is rich of IV-type collagen but MMP degrades this type of collagen, for this reason in PDAC tumour cells are in direct contact with ECM proteins and this binding provides pro-growth, maintenance and migration signals. Furthermore, MMP stimulate ECM to release growth factors and cytokines that have a relevant effect on cancer proliferation, angiogenesis and metastasis<sup>23,13</sup>.

In general, the extracellular matrix in the PDAC site is mainly composed by fibronectin, fibrin, type I and III collagens, different proteoglycans, hyaluronan acid, and also blood and lymphatic vessels, inflammatory cells, fibroblasts and pancreatic stellate cells (PSCs)<sup>24</sup>.

Collagens are the main important proteins in TEM, in particular type-I collagen is linked to a disruption of the E-cadherin adhesion complex in PDAC cells. Collagen type-I active focal adhesion kinase which increases tyrosine phosphorylation of  $\beta$ -catenin and this is linked to a disruption of the E-cadherin adhesion complex. High protein levels of type-I collagen lead to the development of pancreatic cancer<sup>23</sup>.

Another important protein of the extracellular matrix is fibronectin (FN1), that is produced by fibroblasts and tumour cells. FN1 links with cell surface integrin and this bond trigger FN1 signaling pathways in pancreatic tumour cells in order to promote tumour cell survival, cell invasion and metastasis formation<sup>25</sup>.

Hyaluronic acid produced by cancer cells and CAFs is non-sulphated glycosaminoglycan which interact with CD44 an important stem cell marker that promotes the loss of E-cadherin and accumulation of  $\beta$ -catenin. Low molecular weight HA has been linked with metastatic and aggressive type of tumour because modified cell spreading, promoted mobility and improved drug resistance.<sup>12</sup> Proteoglycans influence protein inhibition and activation, in PDAC one of the most important is Sparc/osteonectin, Cwcv and Kazal-like domains proteoglycan (SPOCK1) which transforms the reception of TGF- $\beta$  ligand into stromal support for cancer cell progression<sup>26</sup>.

All of these cellular and non-cellular component that compose an avascular and fibrotic microenvironment form a barrier that compromitted therapeutic susses, decreasing drug delivery, appropriating of drugs in the peritumoral stroma and reducing drug concentration in cancer cells<sup>13</sup>.

### **1.3.2 The pancreatic stellate cells**

From what emerged in the previous paragraph PSCs have a central role in tumour progression. PSCs are cells of pancreas positioned in the periductal, periacinal and perivascular space of pancreas. In a normal condition PSCs are in their quiescent phenotype and they express defined markers for GFAP, glial fibrillary acidic protein, and for desmin and contain lipid droplets with cytoplasmic vitamin A. The PSCs with this phenotype control ECM turnover and synthetize ECM proteins. Furthermore, PSCs regulate enzymes secretion from acinar cells because they synthetize and produce acetylcholine.

During a pancreas injury or pancreas carcinoma, in response to proinflammatory cytokines such as IL-1 and IL-6 and grow factors such as TGF $\beta$ 1 and TNF $\alpha$ , PSCs commute their phenotype into an active myofibroblast-like (Figure 1.3.3). In this phenotype PSCs increase the expression of cytoskeletal protein  $\alpha$ -smooth muscle actin ( $\alpha$ -SMA), TGF $\beta$ -receptor, and PDGF-receptor, and they loss cytoplasmic- vitamin-A lipid droplets. In this state, PSCs product excessive amount of ECM proteins in particular collagen I and III and fibronectin, and they secrete growth factors and cytokines that change cell growth and migration<sup>20,13</sup>.

PSCs and pancreatic cancer cells have a bidirectional interaction that permits tumour progression. Cancer cells produce mitogenic and fibrogenic mediators which activate and attract the PSCs to the cancer site<sup>13</sup>. Furthermore, cancer cells secrete EMMPRIN, the

ECM metalloproteinase inducer which stimulates PSCs to secrete MMP2. MMP2 has a central role for degradation of basement membrane and thus favours cancer progression<sup>13</sup>. Furthermore, PSCs produce ECM proteins as fibronectin and laminin that inhibit pancreatic cancer cells apoptosis<sup>27</sup>. The direct cell contact between PSCs and cancer cells facilitates both the tumour's growth *in loco* and the formation of distant metastasis. Histological analyses demonstrate that the volume of tumour is composed in a large part of cancer cells and only a small part is fibrotic, this is possible because the presence of PSC stimulates pancreas tumour growth rate<sup>20,27,28</sup>.

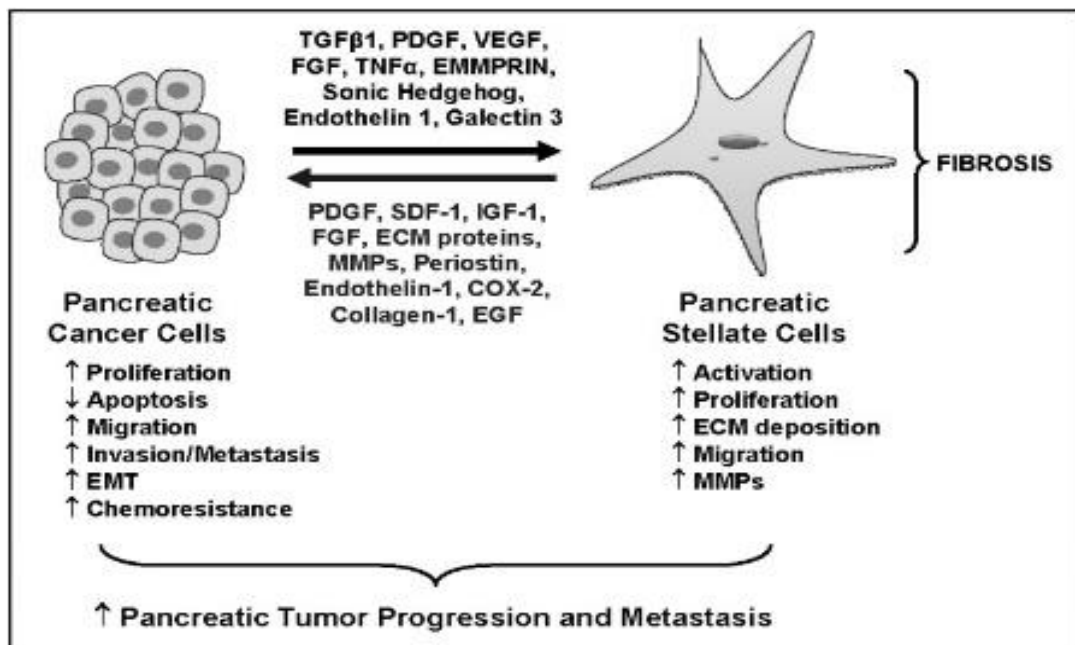


**Figure 1.3.3** Pancreatic stellate cell activation (TGF = transforming growth factor; PDGF = platelet derived growth factor; VEGF = vascular endothelial growth factor; TNF = tumor necrosis factor; IL = interleukin; EMMPRIN = extracellular matrix metalloproteinase inducer; ET-1 = endothelin-1; CTGF = connective tissue growth factor; COX-2 = Cyclooxygenase)<sup>13</sup>.

## 1.4 Tissue Engineering and PDAC *in vitro* models

Tissue engineering (TE) is a multidisciplinary field which involves the development of three-dimensional (3D) tissues and organs substitutes by combining cells, scaffolds, and bioactive molecules (Figure 1.4.1). TE principles allow to produce a large amount of biomedical tools with prospective applicability in the replacement, repair and regeneration of the tissue and permit to achieve a deeper knowledge of pathologies through the establishment of innovative and biomimetic *in vitro* models<sup>29</sup>. The *in vitro* models represent powerful devices to perform cell culture studies and analyses of pathologies like PDAC.

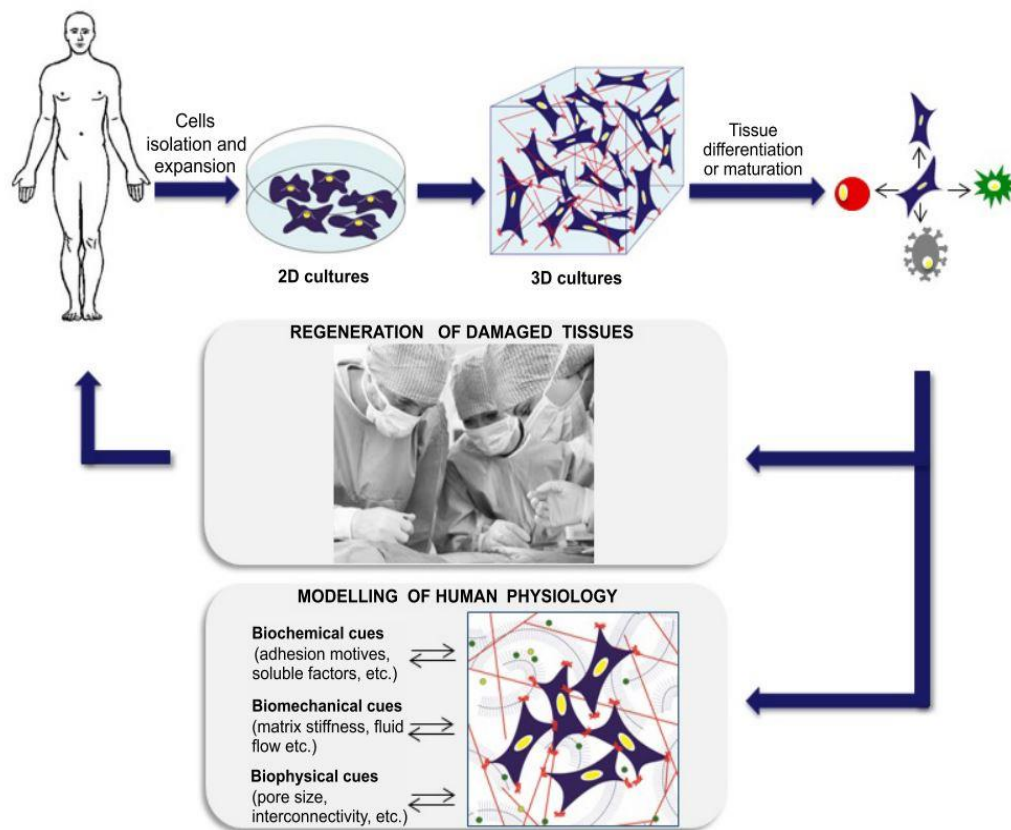


**Figure 1.4.1** Tissue Engineering Principles. Cells are isolated from human or animal sources and expanded on two-dimensional cultures. Cells are then embedded in an extracellular matrix analogue (scaffold), which facilitates proper cellular organization with bioactive molecules<sup>29</sup>.

At the beginning, cell culture experiments have been implemented on Petri dishes, micro-well plates, and tissue culture flasks because these two-dimensional (2D) surfaces have been easy to use and cells have been a high viability on its. Thanks to these 2D surfaces have been possible to increase the knowledge of base of cell biology but in the body, cells live in a 3D fibrous network, ECM which is rich in molecular signals,

mechanical stimuli and concentration gradients. For these reasons 2D surfaces have been demonstrated to be insufficient to describe the correct cells behaviour and their complex 3D microenvironment<sup>30</sup>.

Improvements in tissue engineering approaches, materials fabrication and chemistry have contributed to the development of 3D cell culture matrices that better mimic the mechanical and biochemical signals of natural ECM<sup>30</sup>. Three-dimensional cell culture can be separated into two main groups: clinical application and *in vitro* 3D model. Clinical applications mainly are equivalent of regenerative medicine which has the goal to develop functional implants using fabricated 3D matrices. On the other hand, *in vitro* 3D model systems allow to increase the knowledge of tissue physiology and pathophysiology by reproducing the specific tissue found *in vivo*<sup>30</sup>.

Afterwards, it is recapitulated the different tissue models that have been developed to study the pancreas physiology, with a focus on the PDAC pathophysiology. Firstly, a short overview of animal models and two-dimensional (2D) models is described. Following, three dimensional (3D) systems will be analysed with greater detail, due to their better similarity to the *in vivo* environments.

#### **1.4.1 Animal models**

Living systems both human and animal are very complex physiological environment. Animal models have been used to study the progression of a specific disease, the human risk factors and implement appropriate interventions<sup>31</sup>. The animal models have been employed for the study of PDAC by Sunil R Hingorani et al<sup>32</sup>. The group, for example, has studied the role of oncogenic KRAS mutations in pancreatic tumorigenesis. They have induced endogenous expression of KRAS (G12D) to progenitor cells of the mouse pancreas, and they have demonstrated that this endogenous expression initiates the development of PanINs identical to all three stages found in the evolution of human tumour. Also, they have identified serum proteomic signature in mice with PanINs as possible resources of identifying the preinvasive state in patients<sup>32</sup>.

Another study of PDAC also conducted on animal models is the one carried out by Hideaki Ijichi et al. at from the Vanderbilt University in Nashville<sup>33</sup>. The group studied the TGF-beta signalling which works a prominent role in PDAC progression. TGFBR2 is a transmembrane protein that composes a heterodimeric complex with TGF-beta receptor type-1, and binds TGF-beta. They have studied the TGF-beta receptor type-2 (Tgfr2) knockout mice combined with KRAS (G12D) and they have demonstrated that this model recapitulated human PDAC, highlighting that the blockade of TGF-beta and activated RAS signalling collaborate to stimulate PDAC evolution<sup>33</sup>.

Briefly, there are different types of animal models. Genetically engineered mouse models, GEMMs that fail to summarize the process of mutagenesis; the xenograft mouse models that are direct transplantation of already transformed tumour cells, and the carcinogen induced cancer mouse models that cannot mimic the tissue specificity of the PDAC and reduce their utility in the study of target therapies<sup>34</sup>. Furthermore, these models are resource-intensive, time-consuming and no always reproducible<sup>3</sup>. As pharmac- and toxicokinetic of substances are generally different in humans<sup>3</sup>. The ethical aspect is another important problem, the test on animals are cruel. Principal advantages and disadvantages of animal models were summarized into Table 1.4-1.

*Table 1.4-1 Summary of advantages and disadvantages of animal models<sup>3</sup>.*

Model	Advantages	Disadvantages
Animal	Study evolution of disease  Use to study new therapies	High difference between animals and humans  Animal tests do not reliably predict results in human being  No always reproducible  Resource-intensive  Ethical aspect

#### **1.4.2 Two-dimensional (2D) models**

Two-dimensional (2D) cultures represent robust platforms for the *in vitro* investigation due to the relative ease cell life on this cultures and simply and accessible imaging<sup>35,30</sup>. They have considerably provided to the comprehending of cell behaviours, mechanisms of drugs action, and so on. Studies progressively favour 3D models, because *in vivo* tissue microenvironment, cell-cell interaction and cell-ECM interaction are better mimic by these models, however, 2D models still preserve their role<sup>35</sup>. In general, 2D models are widely used models to study the biology of PDAC, because they are easy to manipulate and they can grow indefinitely at low cost, but these models have different problems. Tissue culture plastic and glass are particularly rigid and inflexible substrates and this lead to an alteration of the cells phenotype as a result of the adaptation of cells<sup>30</sup>. Furthermore, 2D models cannot simulate the complex gradient nature of soluble signals observed *in vivo*, and cannot replicate neoplastic cellular polarity, cell-cell contact and cell-extracellular environment interactions<sup>36,37</sup>. Moreover, cells in 2D culture have access to the components of the medium, but *in vivo*, owing to the architecture of the cancer area the availability of nutrients is more different <sup>37</sup>. For these reasons, the promising results obtained in drug testing in 2D monolayer cultures often cannot be reproduced *in*

*vivo*, using animal models, or in 3D cultures, for instance Longati and co-workers in their work studied the difference chemoresistance between 2D and 3D models. 3D model showed an high amount of ECM, this involved an increase of resistance to chemotherapeutic reagents as compared to a 2D monolayer<sup>38</sup>.

Overall, several studies of PDAC are performed on 2D *in vitro* systems but these are not able to correctly reproduce important 3D *in vivo* TME characteristics<sup>3</sup>. For these reasons, the passage to 3D cultures have been very important to reproduce the 3D aspects of the tissue and to study the drugs safety and efficacy in humans.

### **1.4.3 Three-dimensional (3D) culture models to mimic the exocrine pancreatic tissue**

In cancer research, 3D *in vitro* cultures replicate native pancreas microenvironment, in particular they permit to replicate the cancer TME by using tumour cells combining with scaffold or matrices. 3D *in vitro* models have been shown superior to 2D *in vitro* cultures because 3D models allow cell-cell and cell-ECM interactions and therefore describe the tumour heterogeneity and permit to replicate the correct reaction to different treatments. In addition, 3D *in vitro* models can facilitate to transform the simply research into a customised medicine<sup>39</sup>.

Among the 3D approaches used to reproduce the PDAC tissue, the most common are scaffolds, 3D bioprinted constructs, decellularized matrices, spheroids and organoids.

#### *1.4.3.1 Scaffolds*

Scaffold are three-dimensional cell culture matrices that allow to replicate the native ECM structure where stromal and tumour cells live, proliferate and migrate<sup>2</sup>. Scaffolds can be synthesized by combining different parameters, such as porosity and stiffness, in order to mimic the structure, morphology and composition typical of the natural tissue and to maintain cell viability in a 3D microenvironment<sup>39</sup>. The new tools and knowledges in the tissue engineering have made possible the development of scaffold-based models, where cells are stimulated to colonize the macro-, micro- or nano- porous architectures<sup>39</sup>. Specifically, the pore size and the porosity of scaffolds are important parameters that affect the cell activity and have to be considered during the scaffold design process<sup>40</sup>. Different types of cells, and biological factors can be employed in combination with the scaffold material in order to develop a suitable environment for cell growth. It has been demonstrated that the scaffolds provide cells with a 3D structure that is a preliminary ECM and permits cell 3D self-positioning, proteins secretion and effective drug response<sup>2</sup>.

Various materials can be used to produce scaffolds suitable for the PDAC tissue reproduction; biocompatible materials software, for instance, agar, gelatin or polyvinyl alcohol/gelatin mixture<sup>2,39</sup>.

Moreover, scaffolds allow to control physicochemical and mechanical features of TME such as cell–cell forces, cell–substrate interaction, substrate stiffness, the transport phenomena as fluid dynamics or drugs penetration, cellular kinetics such as metabolism, intracellular signalling and proliferation, that can be studied at selected stages of tumour’s evolution<sup>3</sup>.

For instance, Puls et al developed an *in vitro* 3D model by using PDAC cells embedded in Matrigel and type I collagen in order to study the importance of ECM composition and physical properties in guiding the epithelial to mesenchymal transition EMT. This study demonstrated that fibrillar type I collagen actually involves the EMT<sup>41</sup>.

In order to produce a biomimetic TME architecture model, Totti et al. improved a 3D highly porous polyurethane PU scaffold coated with fibronectin (FN). They showed that this system was able to support the long-term cellular growth and tumour proliferation, and they found that the pancreatic cells seeded on the scaffold were able to produce collagen type I and other ECM proteins<sup>3</sup>.

In general, scaffold-based 3D culture models can mimic the architectures and complexity present *in vivo* using naturally originated ECM components or synthetic polymers and combining different cell lines. Moreover, these models allow to reproduce *in vitro* the physiological mechanical forces and the chemical stimuli experienced by cell *in vivo*. On the other hand, these models are generally more expensive than 2D cultures, not easy to use and require complex methods to retrieval cell and specific imaging methods. Despite these disadvantages scaffolds represent one of more popular options of 3D models to study PDAC<sup>39</sup>.

#### 1.4.3.2 3D Bioprinting

3D bioprinting is a new technique which allows to produce more biomimetic constructs in terms of materials used and geometrical features. This approach combines different cell types and bio-ink in order to print structures with a controlled geometry. Extrusion-based printing (EBP), inkjet printing, stereolithography, laser-assisted bioprinting (LAB), generally are called bioprinting and permit a high control on temporal and spatial distribution of cells into the scaffold thanks to a controlled layer-by-layer assembly of biomaterials. 3D bioprinting allows to mimic *in vivo* architecture and complexity, furthermore, it is possible to develop vascularized constructs<sup>39</sup>. As regards, the study of Langer et al. involves the use of the 3D bioprinting technology to co-culture primary human PSCs and umbilical vein endothelial cells (HUVECs) in order to realize a vascularized PDAC model. The group showed that this multi-cell-type bioprinted scaffold

allows to reproduce the characteristics of the *in vivo* cancer, therefore this model represents an interesting system for the analysis of different tumorigenic stages in the proper microenvironment<sup>42</sup>.

3D bioprinting techniques require special equipment that generally are expensive. Furthermore, the optimization of the parameters to obtain a fully biomimetic and vascularized constructs is difficult and time expensive<sup>39</sup>.

To overcome the limitation of oxygen and nutrient, microfluidics has born as innovative technology for combining patient-derived tissue models with the flow control of a tumor-on-a-chip devices. This technology will be dealt in a dedicated paragraph<sup>39</sup>.

#### 1.4.3.3 Decellularized matrices

The type of engineered matrix on which pancreatic cells grow is very important because it provides the environments where tumour cells adhere, proliferate, and migrate. Sometimes, synthetic scaffolds have structures which are largely different respect with the physiological tissues and the complex tumor-stroma system remains ignored. To overcome this issue, more biologically relevant scaffolds can be used, as the decellularized matrices<sup>43</sup>. These are decellularized tissues, obtained by the removal of cells from an organ or tissue using a correct mix of cleansing agents by leaving a complex mixture of functional proteins and structures that composed the native ECM. Generally, the final aim of decellularized matrices is *in vivo* implantation, where decellularized organ or tissue can be reseeded with stem cell populations for tissue substitution, and they can also be used to study and catalogue ECM and angiogenic modifications in pancreatic tumors<sup>44</sup>.

Currently, the research about the decellularized pancreas tissues is focused only on the endocrine pancreas, for instance the group of Wan et al. has combined decellularized rat pancreatic scaffolds with mouse GFP (+)-iPSCs (-) derived pancreatic  $\beta$ -like cells. It has been observed that decellularized pancreatic scaffolds have favourable biochemical properties, they support the survival of  $\beta$ -like cells and accelerated the expression of the insulin as compared to plate-based cell culture<sup>45</sup>.

A model combining 3D cell culture and decellularized matrix scaffolds produces a very supple system, enabling to the interaction between different cell types in a biologically relevant 3D environment while still detaining the efficiency seen *in vitro*<sup>43,44</sup>. Therefore, decellularized matrices can be used as scaffold to culture cells *in vitro* in a complex, native matrix but it is necessary evaluate if cells cultured in these decellularized matrices interact with the ECM in similar way as *in vivo* contexts because decellularization could cause a loss of unbound soluble factors to the tissue such as growth factors<sup>44</sup>.

Another problem is that the decellularized matrices are more variable due to the difference among donors. Moreover, the decellularized tissue cannot mimic the

physiological evolution process of tissue during the tumorigenesis because of its mature state<sup>43</sup>.

#### 1.4.3.4 Spheroids

Spheroids are the easiest 3D models which allow to study structure and composition of diseased tissue. Spheroids can be produced by embedding cells in different templates such as gelatine, collagen or alginate hydrogels and so on, or by growing single-cell suspensions in ultralow attachment plates such as coverslip or multiwell plastic lid in order to improve cell-cell interactions and to decrease the adhesion to plastic plates<sup>39</sup>. Another possibility is embedded cells inside matrices of Matrigel, type I collagen, fibronectin, methylcellulose or inside synthetic scaffolds composed of biocompatible polymers<sup>36</sup>. Cells are forced to self-assembling by the absence of direct contact with the surfaces, by forming a cell cluster with a low oxygen perfusion in the centre which mimics the chemo-resistant core of a tumor<sup>2</sup>.

These techniques do not mimic perfectly PDAC, cancer microenvironments or cancer stem cell-like features found in patient tissues. For this reason, hanging drop method can be modified incorporating methylcellulose allows to generate a co-culture of PDAC and stroma cells such as pancreatic stellate cells (PSCs), in order to reproduce native desmoplastic reaction and tissue architecture<sup>2</sup>.

Ware et al. developed an *in vitro* spheroid model combining PSCs and PDAC cells using a modified hanging drop method avoiding any addition of extracellular components. This 3D PDAC-stroma model has been used for the drug testing, showing an increase in collagen content and a decrease of cytotoxicity of gemcitabine. Despite the promising results suggesting that this model is very close to the native tissue, spheroids were grown only for 7/10 days and they had a low PSC seeding ratio<sup>46</sup>. This is only an example of application because this type of culture has a large variety of use; for instance, they have been used to reproduce and analyse the 3D interactions found *in vivo* and to consequently study the self-renewal capability of cells or to evaluate the characteristics of cancer stem cells. However how such cells mimic to tumour cells *in vivo* remains still unclear<sup>36</sup>.

Different studies have shown that spheroid cultures have the capability to produce ECM, to increase the resistance to drug therapies, and to develop polarized cell junctions<sup>36</sup>. This type of cultures is easy to use, scalable to different plate formats and is possible a long term-culture; nonetheless, spheroids mimic only simple architectures and the composition is not scalable, making them difficult to obtain consistent biologically meaningful results. Furthermore, this 3D model is characterised by a low grade of vascularization<sup>39,47</sup>.

In order to improve this type of model a new type of 3D models, organoids, has been established.

#### 1.4.3.5 Organoids

Currently, there is no a standard definition of “organoid”, but this term can be associated to a group of different cell types that is generated from embryonic stem cells, pluripotent stem cells or primary cells that can come from health or diseased tissues and are capable of self-organization and self-renewal, maintaining an organ-like structure that mimics the original tissue. Organoids are developed by the dissociation of primary tissue into tissue fragments that are embedded and propagate in a synthetic matrix or in an ECM came from animal tissues. Typically, Collagen type I or Matrigel combining with specific differentiation modulators and growth factors are used to generate the specific model<sup>2, 48</sup>. Normally, organoids have the capability to preserve the genetic stability and to be maintained stable through different passages<sup>48</sup>.

Pancreatic 3D organoids can be produced starting from small tissue fragments of biopsy, surgical or endoscopic needle aspiration samples. Organoids are a novel model for the studies of gene characteristic in epithelial cells without alteration of immune, mesenchymal and hemopoietic cells. These 3D models can be utilized to analyse the cancer progression, associated genetic alteration with it and to find gene associated with all stages of cancer from early stage to late stages<sup>48</sup>.

Chio et al developed an organoid in order to study the influence of redox master regulator, NRF2, in PDAC progression. The study revealed that NRF2 is very important to maintain a high proliferation in PDAC. In particular, they observed that organoids without NRF2 have shown a low proliferation rate and they tested that combining the EGFR effector AKT with the glutathione antioxidant pathway is possible mimic NRF2 ablation *in vivo*<sup>49</sup>.

Another example of organoids application is provided by Huang L. et al., who used organoids to test different drugs. In this study, they tested gemcitabine, the most common treatment for PDAC, on five different patient tumour derived organoids with a low response. Then they tested the effects of organoids by targeting epigenetic regulators such as *KRAS* and *TP53*, showing dose-dependent decrease in proliferation<sup>50</sup>. Thanks to capabilities of organoids, such as indefinite passaging capability and genetic stability, they can be used to study a particular gene manipulating them genetically, this is possible carrying out modification with plasmid transfection or retroviral transduction. Furthermore, organoids are an important tool for therapeutic research, they can be used for drug testing and to implement personalized medicine. In the last years, the formation of biobanks of 3D organoids has become relevant to study genetic profiles and drug response of singular patients<sup>48</sup>. Therefore, the 3D organoids models

have many applications and represent attractive approaches, but they are very expensive and time-consuming. In addition, 3D organoids don't show important cell components present *in vivo*, such as immune cells, fibroblasts, and endothelial cells. Additionally, to develop them is possible require access to human samples and require a validation to recognize outgrowth of undesirable cells<sup>48, 39</sup>.

#### 1.4.3.6 Bioreactors

3D suspension bioreactors are dynamic culture systems that permit to mimic the physiological conditions of tumours; in particular, these platforms can better reproduce the shear forces and the interaction of different type of cells typical of a tumour microenvironment<sup>39</sup>. Bioreactors may surpass the loss of specialized cellular functions and their growth as monolayers. 3D suspensor bioreactors permit to control oxygen, CO<sub>2</sub>, pH and evaporation and for this capability it is possible use them not only to study the physiology of tumours, but also to evaluate the infusion of chemotherapies at concentrations similar to those found *in vivo* and the response<sup>39</sup>. There are different bioreactor systems, between bioreactor cartridges, spinner flask bioreactors or rotating wall vessel (RWV)<sup>39</sup>.

Brancato et al., for instance, developed human PDAC microtissues by co-culturing cancer-associated fibroblasts (CAFs) or normal fibroblasts with PC cells (PT45) with gelatine micro scaffolds cultured in a spinner flask bioreactor. After 6 days it was possible to observe the development of stromal microtissues and after 12 days the culture was stopped, then by histological and morphological analyses they observed the deposition of a stromal matrix composed prevalently of collagen<sup>39</sup>.

However, these platforms are very expensive, and are not easy to use as they require long time to optimize the cell procedures and the biomaterial features. Furthermore, excessive hydrodynamic shear stresses are destructive for cells<sup>39</sup>.

In Table 1.4-2 were collected the advantages and disadvantages of the main 3D approaches used to reproduce the PDAC tissue.

**Table 1.4-2** Summary of advantages and disadvantages of different 3D models <sup>39</sup>.

Models	Advantages	Disadvantages
Scaffolds	<p>Allow co-culture</p> <p>High reproducibility</p> <p>Scalable to different formats</p> <p>Use in tissue engineering and transplantation</p> <p>Versatile</p> <p>Use of naturally derived ECM components and/or synthetic polymers</p>	<p>Expensive</p> <p>Not easy-to-use protocol</p> <p>Simple architecture</p> <p>Require specific imaging methods</p> <p>Variability of natural matrixes</p>
3D Bioprinting	<p>High reproducibility</p> <p>Allow co-culture</p> <p>Versatile</p> <p>Vascularized</p> <p>Mimic <i>in vivo</i> complexity</p>	<p>Costly</p> <p>Require special equipment</p> <p>Need optimization</p> <p>Issues with tissue maturation</p>
Decellularized matrices	<p>Allow co-culture</p> <p>Mimic <i>in vivo</i> complexity</p> <p>Mimic <i>in vivo</i> architecture</p>	<p>Require access to human samples</p> <p>Optimization of decellularized protocol</p> <p>Variable samples</p> <p>No mimic the development tissue</p>
Spheroids	<p>Easy to use</p> <p>Scalable to different formats</p> <p>Long term-culture</p>	<p>Simple architectures</p> <p>Composition is not scalable</p> <p>Poor vascularization</p>
Organoids	<p>Patient-specific</p> <p>Scalable to different formats</p> <p>Allows co-culture</p> <p>Mimic <i>in vivo</i> architecture</p> <p>Use in tissue engineering and transplantation</p>	<p>Expensive</p> <p>Not easy-to-use protocol</p> <p>No control uniformity (size, composition)</p> <p>Lack vasculature</p> <p>Require validation to identify outgrowth of unwanted cells</p> <p>Require access to human samples</p>
Bioreactors	<p>High density cell expansion</p> <p>Controllable culture parameters</p>	<p>Costly</p> <p>Require optimization of cell parameters and biomaterial</p> <p>Hydrodynamic shear stress</p>

#### 1.4.4 Microfluidic Systems

Microfluidic “organs-on-a-chip” devices are used to culture cells in a controlled microenvironment, using glass, polymers, or plastic<sup>51</sup>. These devices were initially employed as substitutes for the vascular perfusion in the body, since the perfusion in micrometer-sized channels provides oxygen and nutrients to cells and allows the waste removal in an automated manner<sup>2,51</sup>. Organs-on-a-chip combine two or more types of cells that can interact across a porous membrane or a gel within the micro-channels, in order to reproduce one or more features of the *in vivo* organ’s functionality and physiology response *in vivo* under a real-time monitoring<sup>52</sup>. Organs-on-a-chip allow to reproduce different diseases including tumours and their microenvironment. These approaches are important to recapitulate the tissue-tissue interface and the *in vivo*-like architecture; in particular, they are decisive to model the different organ levels architectures and the function<sup>51</sup>. Organ on chip is more versatile 3D culture because allow co-cultures including primary cells or cell lines, furthermore the culture parameters are easy to control. One of the main advantages of these platform is their transparency to light, for this reason, it is possible to use a large variety of microscopy-based imaging techniques, which allow to observe cell–cell interactions, spatial relations among different cell types and cells morphology<sup>39</sup>.

In general, microfluidic devices for PDAC can be used to gain new knowledge into fundamental processes of cancer and the study of new drugs and therapeutic plan<sup>51</sup>.

In order to mimic the key tissue processes such as infiltration, separation, cell-cell interaction and vascularization, microfluidics devices should be fabricated with similar resolutions, a few hundred micrometres. For this reason, they are composed by different microchannels or microchambers whose geometry depends on the desired environment and flow conditions.

Furthermore, mechanical, chemical and/or electrical stimuli play a central role in a physiological tissue and therefore they should be considered in an *in vitro* model. Organs-on-a-chip allow to integrate these stimuli on the same platform. For example, the incorporation of bio-surfaces and hydrogel permit to recapitulate barriers or interfaces between tissue and ECM and are more common<sup>52</sup>.

Although organ-on-chip microfluidic devices are a robust technology for mimicking the key structures and functions of pancreatic tissue, they have limitations. Firstly, there are limitations associated to the production of these platforms, as the processes are very long and require special expensive technologies and machines. Moreover, the selection of appropriate device material, cell sources, correct matrices that mimicking 3D support and the choice of appropriate flow and forces are important problems. Another potential

limitation is the permanent bonding between PDMS layers, which is used to build chips, interfering to access and process tissues produced in the microchamber for certain types of assay and analysis. Furthermore, there are other limitations like microbial contaminations that are often associated with long-term culture system, contraction/degradation of gels and degradation of membrane<sup>39</sup>.

Principal advantages and limitations of microfluidic systems were recapitulated in the Table 1.4-3.

**Table 1.4-3** Summary of advantages and disadvantages of microfluidic devices<sup>39</sup>.

Models	Advantages	Disadvantages
Microfluidic systems	Microscopy-based imaging techniques High reproducibility Allows co-culture Mimic <i>in vivo</i> complexity Mimic <i>in vivo</i> architecture Controllable culture parameters Vascularized	Expensive Require specific apparatus Difficult to scale up Possible microbial contaminations

## 1.5 Organs-on-a-chip in detail

It is clear 3D systems are superior in that they better mimic the architecture, dimension, chemistry, and signaling environment of human organ or portion of organ. As already mentioned, organs-on-a-chip are a good way to recapitulate organs substructures in a controlled microenvironment<sup>52</sup>. There are different organ-on-a-chip for PDAC using polydimethylsiloxane (PDMS) and soft lithography to fabricate chip, more of them load type-I collagen and HA combined with PDAC cells, PSCs or fibroblasts in the device to recapitulate PDAC microenvironment<sup>2</sup>. Another group of organs-on-a-chip for PDAC mimics tumour–blood vessel interactions and vascular invasion, in order to study the infiltration of immunosuppressive cells that is an important features in the maintenance of an immunosuppressive environment in this tumour<sup>39</sup>.

In the following sections these platforms are discussed in detail since this thesis work involves the use of a microfluidic device.

### 1.5.1 Materials: PDMS and smart materials

Different physicochemical properties of the material can be required for the device production, depending on the design and the application of the microfluidic device.

Among potential materials polydimethylsiloxane (PDMS), polymethylmethacrylate (PMMA) and polycarbonate (PC), have been widely used in microfluidics<sup>52</sup>.

In general, the most important properties to develop an effective microfluidic device are the following.

*Biocompatibility.* The degree of biocompatibility can vary depending on the application, and requires low toxicity, an high capability of materials to perform the desired functions with correct cellular responses <sup>52</sup>.

*Optical transparency.* The microfluidic device is made of an optical transparent material and/or an integrate optical window to easily observe the culture inside the chip by optical microscopy<sup>52</sup>.

*Gas permeability.* Human cells require a supply of oxygen and therefore the choice of permeable materials permits a correct and controlled cell culture without the need of separate oxygenators<sup>52</sup>.

*Adsorption of molecules to the surface.* Physiological cell behaviour in the device can potentially alter by the adsorption of molecules to the surface<sup>52</sup>.

*Resistance to chemicals.* Chemical degradation of materials causes a release of compounds that could alter the mimicked organ functions and could also cause the introduction of air plugs. For these reason device material must have a good chemical resistance<sup>52</sup>.

*Thermal resistance.* In order to maintain the geometry properties of the system is important that material should not undergo contraction or dilatation caused by variations in temperature<sup>52</sup>.

*Stiffness.* To reproduce organ the use of material with similar mechanical properties is important. High flexibility of the chip is an advantage to microfabricating integrated microfluidic channels, valves, or pumps but at the same time is a disadvantage, because deformation during the application of experimental conditions could alter flow and shear stresses could be inserted<sup>52</sup>.

Typically, PDMS is mostly used for the fabrication of microfluidic device as it is a silicon organic polymer with Young's modulus among 0.5 MPa and 3.5 MPa ( in base of the amount of crosslinker agent) and interesting physical properties for these biomedical applications<sup>53,52</sup>. PDMS is a soft transparent material with an excellent biocompatibility and a high oxygen permeability<sup>52</sup>. In particular, PDMS can transmit incident light with a little absorption and reflection that make it a very good candidate to fabricate chips which are visible by optical microscopy<sup>52</sup>. Furthermore, PDMS is a no-toxic material and allows the culture of cells in direct contact with it<sup>52</sup>. Moreover, PDMS is a permeable material which guarantees enough oxygen to the cells in the microfluidic devices<sup>52</sup>. In addition, sterilization of materials is necessary to eliminate eventually microorganismal

contamination and PDMS can be sterilized with different techniques such as autoclave, ultraviolet light and ethanol. For all of these reasons PDMS is the elite material for the organs-on-a-chip<sup>52</sup>.

To develop the physiological and pathological tissues in microfluidic devices, it is possible to incorporate smart materials into the device, which change one or more fundamental properties in response to the application of specific stimulus<sup>52</sup>. These materials could alter their rigidity, shape, or porosity in response to an alteration in physiological characteristics such as temperature, enzyme concentrations or pH or after the application of an external stimulation like magnetic field, light or electrical current<sup>52</sup>. To better mimic the 3D microenvironment a hydrogel could be integrate and porous membrane could be employed to model the interfaces of specific tissues. Hydrogels are networks of hydrophilic polymer chains, characterized by a high quantity of water, an excellent biocompatibility, a correct stiffness and a good permeability to oxygen that can be insert in order to mimic a similar native microenvironment where cells grow, spread, and proliferate<sup>52</sup>. Hydrogels can be natural or synthetic; for instance Collagen type-I is a protein present into native ECM and it is used to mimic physiological microenvironments due to its biocompatibility and similarity to the native ECM<sup>54</sup>.

Furthermore, as already mentioned, to control the cell-cell interactions among different types of cells is possible to use electrospun membranes. Different techniques can be used to combine microfluidic devices and membranes<sup>52</sup>. These can be fabricated with specific materials and properties and later assembled within the chip elements<sup>52</sup>.

In general, the material into a microfluidic device should be biocompatible, easy to sterilize and with desirable physicochemical properties<sup>52</sup>.

## **1.5.2 Fabrication techniques**

### *1.5.2.1 Replica molding*

Replica molding or soft lithography is a widely used technique to produced macroscale and microscale things. Through this technique a prepolymer is poured onto a master produced by lithography, moulding or other techniques, and then the prepolymer is cured.

Normally, in order to reduce master surface free energy, the surface of the master is modified chemically by coating it with a polymer or a fluorinated molecule thanks to this functionalization the separation of the master from the replica after molding is helped. One problem of replica moulding is the separation between master and polymer layer because the pattern of master could be damage, to reduce this problem it is important the use of elastomeric polymer, such as PDMS<sup>55</sup>.

As reported above, the most used material for this type of techniques is PDMS, a precursor of PDMS is poured onto a master, then it is cured and finally it is peeled off<sup>52,56</sup>. The figure 1.5.1 shows the schematic process of molding replication.

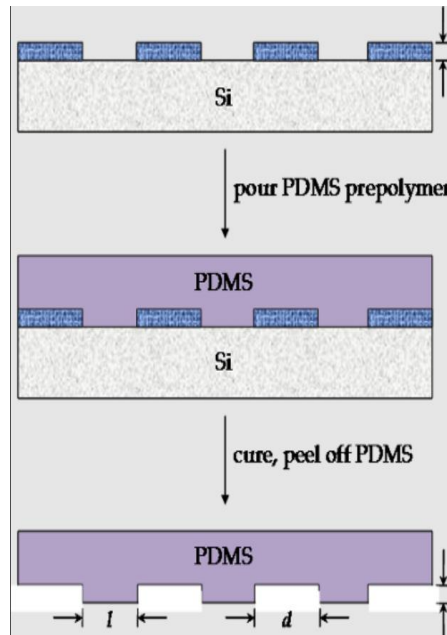


**Figure 1.5.1** Schematic illustration of PDMS replica molding<sup>125</sup>.

### 1.5.2.2 Lithography techniques

Lithography is a general term used to indicate different top-down techniques used for nanomaterial fabrication in industry<sup>57</sup>. Light, an ion beam, or an electron beam are used to transfer a specific pattern on a substrate known as resist. Resist is a photosensitive material, which can be negative or positive resist<sup>57</sup>. In the negative resist bonds became stronger during the irradiation with photons, electrons or ions, while in the positive resist bonds break as consequence of the irradiation<sup>58</sup>. After irradiation the sample is developed in a solution to eliminate the no-irradiated part (for the negative resist) or irradiated part (for the positive resist).

To transfer the pattern to the substrate it possible to use two different methods.

- *Software method or scanning method* where a computer-controlled software is used to transfer the pattern on the sample<sup>57</sup>.
- *Physical mask method or mask lithography* where a mask is applied in contact or nearness with the surface of the resist. In this method the mask is produced with a laser writing that transfer the CAD model directly on the glass or quartz substrate<sup>57</sup>.

Among vary lithography techniques, one of the most commonly used is SU-8 photolithography, which is discussed in the next paragraph<sup>56,58</sup>.

This technique has some problems, the process required instruments and material extremely expensive and this process requires a clean room. Nevertheless, lithography is a highly successful technique and it is typically used in biomedical fields, principally for the high resolution and the high reproducibility of samples<sup>58</sup>.

The figure 1.5.2 shows the schematic process of lithography.

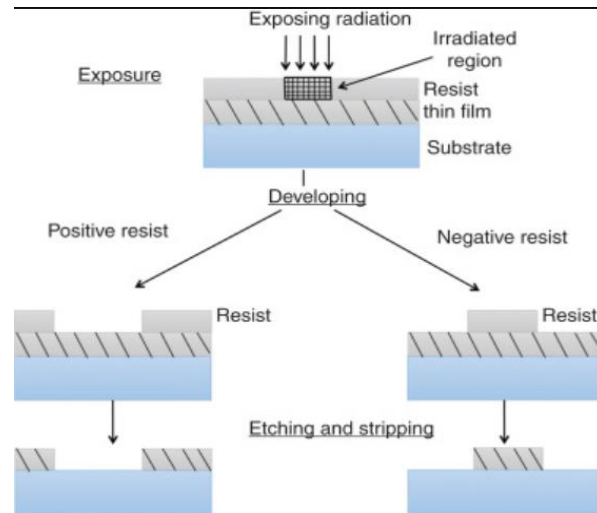


**Figure 1.5.2** Schematic illustration of lithography process<sup>126</sup>.

### 1.5.2.3 SU-8 photolithography

Photolithography is a lithography technique that employs a UV-light to pattern a substrate and SU-8 photolithography refers to the use of SU-8 photoresist as substrate to the photolithography process, since it is an acid-catalysed negative photoresist<sup>59</sup>.

SU-8 photolithography is divided into five fundamental phases: deposition of photoresist, soft bake, UV light exposure, post bake, and developing<sup>59</sup>.

First of all, photoresist is deposited on a clean substrate, normally a wafer made of Silicon (Si), glass or quartz. To deposit the resist various techniques can be used, but spin coating is more common than other, using this technique more important parameters are spin time, speed, and acceleration. After this process, the evaporation of casting solvent is necessary, and SU-8 is treated for different time a different temperature. Then an UV irradiation generates a low concentration of a strong acid and opens the epoxide rings in the resist. UV light represents the catalyst of the chemically amplified cross-linking reaction. In this phase the energy dose, the power intensity and the exposure time are important parameters to set the pattern on photoresist. It is necessary a postexposure treatment with a bake at different temperature to polymerize SU-8. Finally, unpolymerized SU-8 eliminates with the immersion of the substrate in a developer agent such as propylene glycol methyl ether acetate (PGMEA). This technique allows to obtain samples with a high resolution and a high reproducibility<sup>59</sup>.

#### 1.5.2.4 Laser ablation

Laser ablation of polymers is an alternative technique used to fabricate master of microfluidic devices or directly devices. This technique substitutes the traditional photolithography-based techniques, which is very expensive, and it requires specific tools and environments<sup>60</sup>.

Laser ablation is simply and cheap method to fabricate device with different materials, it consists in a breaking down one part of material using a laser beam directed by a computer in order to replicate the pattern on the surface<sup>56</sup>. The interaction between material surface and laser beam can produce melting, electronic excitation or de-excitation, evaporation and material expulsion, dissociation or decomposition. Broken chemical bonds produce the material to dissociate or decompose from the area of the pattern to transcript<sup>61</sup>. There are different factors to consider in order to have good results. The most critical factor is the timescale of the interaction between the material and the laser beam<sup>56,61</sup>. Other important parameters to consider are laser wavelength, power of laser beam and material properties, such as thermal conductivity, specific heat, reflectivity, and evaporation. The source of laser can be different:

- ❖ *Gas laser*, where gas is normally a mixture of dioxide gas CO<sub>2</sub> stimulated by electrical discharges<sup>62</sup>.
- ❖ *Solid state laser*, is a low power diode laser<sup>62</sup>.

Laser ablation is a technique with vary problems whatever the source, it produces poor surfaces quality with burning, contraction, buckle, large heat-affected zone and resolidification near the perimeter of the patterns. Most of these impurities are normally produced during laser ablation by heat accumulation and they are caused by low sensitivity of traditional engineering polymers, such as polymethylmethacrylate (PMMA) or polycarbonate (PC), which are normally use as material of master. Furthermore, being limited with the spot size of laser beam and the heat affection, the pattern feature size is usually larger than it established by CAD<sup>60</sup>.

Notwithstanding, this technique is used because is versatile, fast and low-cost method.

## 1.6 Scientific Background: Cases of Study

As mentioned before, tumours-on-a-chip systems are microfluidic devices that allow to recreate relevant aspects of the tumour's physiology. The use of microfluidics is another dimension of physiological helpful to supply continuously nutrients and test pharmaceutical drugs. The use of tumour-on-chip platforms is increasing in many different areas of cancer research, including the study of the physiology of solid tumours, the testing of novel anticancer pharmaceutical compounds, and the development of personalized treatments.<sup>63</sup> In this section three studies have been reported where different platforms are analysed by highlighting distinct aspects of PDAC tumour. Two studies focus on PDAC microenvironment while the last one aims attention at PDAC extravasation, two very important features of PDAC progression.

In the work of Beer et al.<sup>64</sup>, a microfluidic device is combined with the dielectrophoresis (DEP) to permit the culture of vary PDACs human cell lines into the HepaChip and specifically in a cyclic oleif polymer (COP) chamber. In order to mimic the tumour microenvironment, they loaded the extracellular matrix collagen into the device. To obtain robust results, they studied three different cell lines: PANC1, MiaPaCa2 end BxPC3, seeded on HepaChip, by comparing 2D and 3D models. Furthermore, they studied the PDAC progression by performing *in vivo* experiments on mice. Moreover, they studied cell vitality *in vitro* using Live/Dead assay and they observed the cell morphology by DAPI/Phalloidin staining. Furthermore, they studied the effect of different concentration of Cisplatin after 72h of culture in all the experiments.

In 2D culture, the PDAC cells proliferate with similar kinetics; particularly, flattened morphology is shown by BxPC3 cells, and they grow as small "islands". On the contrary, MiaPaCa2 cells are at the same time adherents with a mesenchymal morphology or less adherents. PANC1 are more adherent and with an intermediate morphology, epithelial and mesenchymal. In 3D culture conditions, PANC1 and MiaPaCa2 cells grew and form big and compact spheroids during 10 days' culture period, while, BxPC3 had a minimum growth rate. PANC1 cells has branches of cells coming out from the originary spheroid mass and they showed a distinction between tightly formed round central cells and loosely peripheral cells. The PDAC cells in the spheroids showed an actin cytoskeleton compactly arranged, there were cell-cell interaction and aggregation and the peripheral cells were characterized by distribution of actin filament. In HepaChip culture, both BxPC3 and PANC1 cells stayed viable for different days and the cellular density significantly increased into chip (Figure 1.6.1-C). Both BxPC3 and PANC1 cells suffered mitosis, this was a sign of their state and functionality. While, MiaPaCa2 cells showed

very less adhesion to the collagen into device, because the integrin adhesion receptors of these cells have a lower affinity for collagen. PANC1 cells inside the chip forms spheroids. Actin appeared denser along the cell membrane stained of both BxPC3 and PANC1 (Figure 1.6.1-B). Furthermore, PANC1 had pro-migratory and cancerous features because they showed also short actin filaments that extend from the membrane both into the cell and outside (Figure 1.6.1-B).

Compared with conventional 2D cultures, chip cultures required higher Cisplatin concentration, this could be due either to differences in cellular functions or to a low adsorption of the drug onto the microfluidic device.

Overall, their results show the capability of HepaChip to obtain vital culture of PDAC cells attached to collagen and cells shown vitality, morphological and growth characteristics more like 3D cultures. Furthermore, in HepaChip cells maintained their actin organisation and a pro-migratory and neoplastic behaviour<sup>64</sup>.

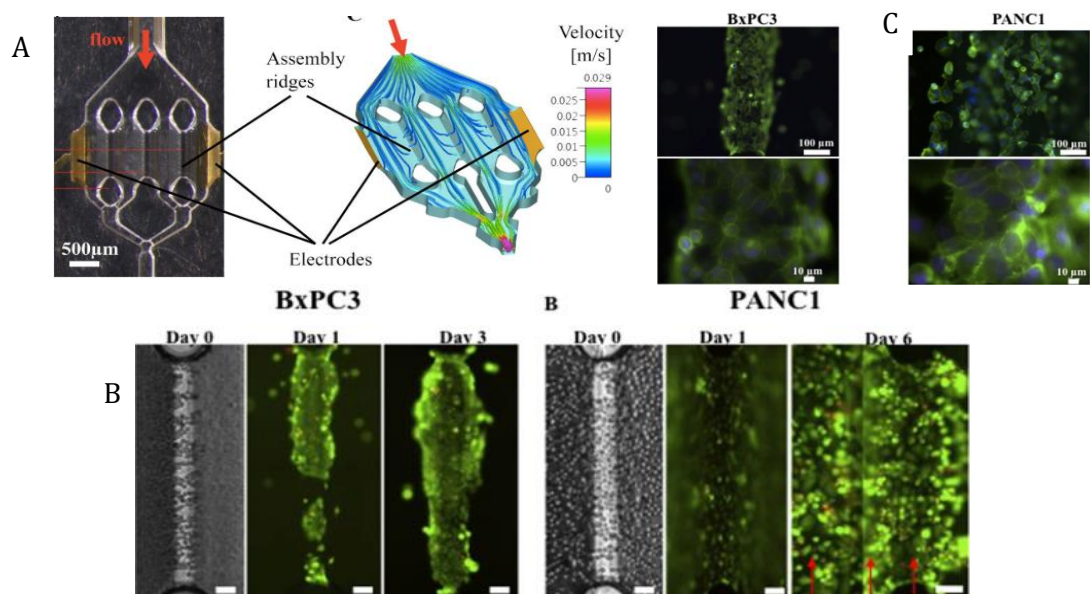


**Figure 1.6.1** (A) Chamber with collagen and simulation of flow velocity and trajectories of cells inside a culture chamber. (B) Live/Dead cell staining of BxPC3 and PANC1 (C) Morphological characterization of BxPC3 and PANC1: Fluorescence images after actin and nucleus staining with Phalloidin and DAPI<sup>64</sup>.

Another example of study which mimics the PDAC microenvironment is the one made by Ji-Hyun Lee et al. <sup>65</sup>, where a co-culture model is fabricated by combining tumour spheroids and PSCs embedded in a three-dimensional (3D) collagen matrix.

Particularly, the device is made in PDMS and it is composed by four units containing three channels and four media channels each unit, all in a single plate. To produce the device in PDMS soft lithography has been used on SU-8 master. Through oxygen plasma the open side of PDMS replicas were closed with a PDMS film or a glass coverslip. The microchannels were then coated with a solution of poly-dopamine in order to facilitate type I collagen adhesion. In this study have been employed three human pancreatic cancer cell lines: PANC-1, AsPC-1 and MIA PaCa-2, human hepatic cancer cell line Huh-7 and human colorectal cancer cell line HT-29 co-cultured with human pancreatic stellate cell line PSCs. They cultured mono- and co-culture with PSCs in co-culture the number of spheroids increased and into co-culture of PSCs and PAN-1 cells (Figure 1.6.2-A), PSCs showed an elongated shape, a decrease in F-actin area, and these were the indexes of their activation (Figure 1.6.2-B).

Another element that supported their activation, were the increase of  $\alpha$ -SMA expressed by PSCs (Figure 1.6.2-B). In co-culture there were increased the proliferation marker (Ki-67), the transforming growth factor beta (TGF- $\beta$ ) and the connective tissue growth factor (CTGF) expression (Figure 1.6.2-C,D).

They analysed different drugs and the only interesting results were showed by the mixed of gemcitabine and paclitaxel, probably due to sensitivity of PSCs to paclitaxel. This study shown how microfluidic co-culture of pancreatic tumor spheroids with PSC were an important tool to understand EMT effects and drug resistance (Figure 1.6.2-E) <sup>65</sup>.

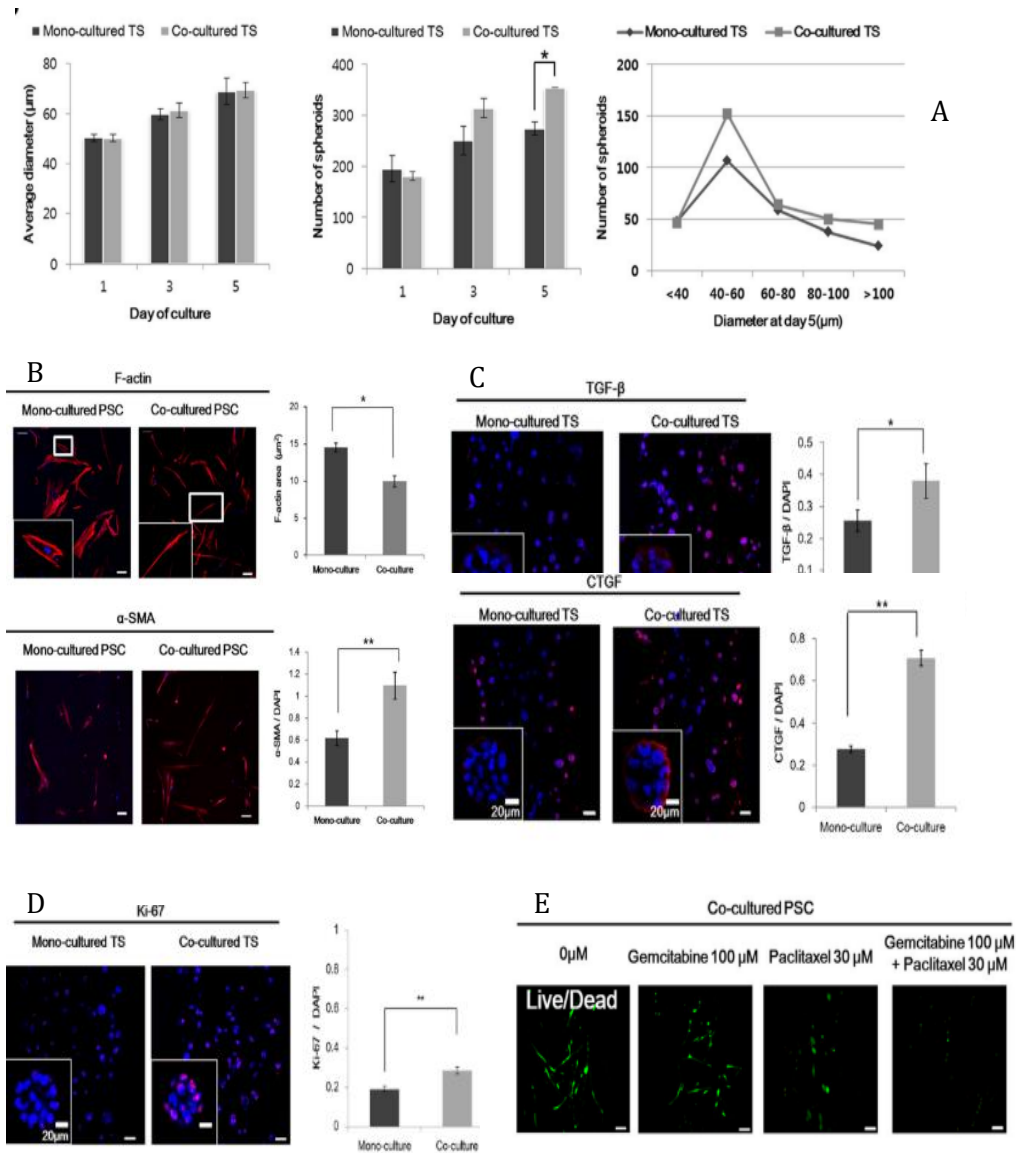


**Figure 1.6.2** (A) Comparison of growth of PANC-1 spheroids for 5 days with or without PSCs. (B) Changes in morphology and  $\alpha$ -SMA expression level of PSCs in co-culture. (C) Expression of cytokines in PANC-1 tumor spheroids in co-culture and stained for TGF- $\beta$ , and CTGF. (D) Expression of Ki-67 in co-culture. (E) Sensitivity of PANC-1 tumor spheroids and PSCs to anti-cancer drugs Gemcitabine, Paclitaxel and Gemcitabine + Paclitaxel. <sup>65</sup>

In the last important case of study realized by Duc-Huy T. Nguyen and his group<sup>66</sup>, an organotypic PDAC-on-a-chip culture model has been developed in order to mimic tumour-blood vessels interaction and vascular invasion by cancer cells. Two PDMS gaskets with two channels, produced by soft lithography, were bonded after plasma etching and embedded with a 3D collagen matrix containing a PDAC cells in one channel and endothelial cells in the other. In this work have been employed primary murine pancreatic cancer cell lines isolated from primary tumours of GEMM, two type of human pancreatic cancer cell lines, PANC-1 and BxPC-3, and human umbilical vein endothelial cells (HUVECs). They observed that PDAC cells passed through collagen and invaded vessel lumen, in particular tumour cells ablated the endothelial cells. At the same time, they observed endothelial ablation also *in vivo* PDAC models. Testing ALK7, ALK5 and ALK4 to cellular invasion and endothelial ablation of PD7591 was showed that ALK7 played an important role. This was tested also in mice and in both cases, it was confirmed that ALK7-deficient tumours displayed a significantly higher vessel density and less apoptotic endothelial cells within the tumour mass (Figure 1.6.3). The group of work proposed a new model of PDAC that other to study endothelial cell ablation by tumour cells via the activin-ALK7 signalling pathway it could be used to investigate other mechanisms affecting PDAC extravasation<sup>66</sup>.

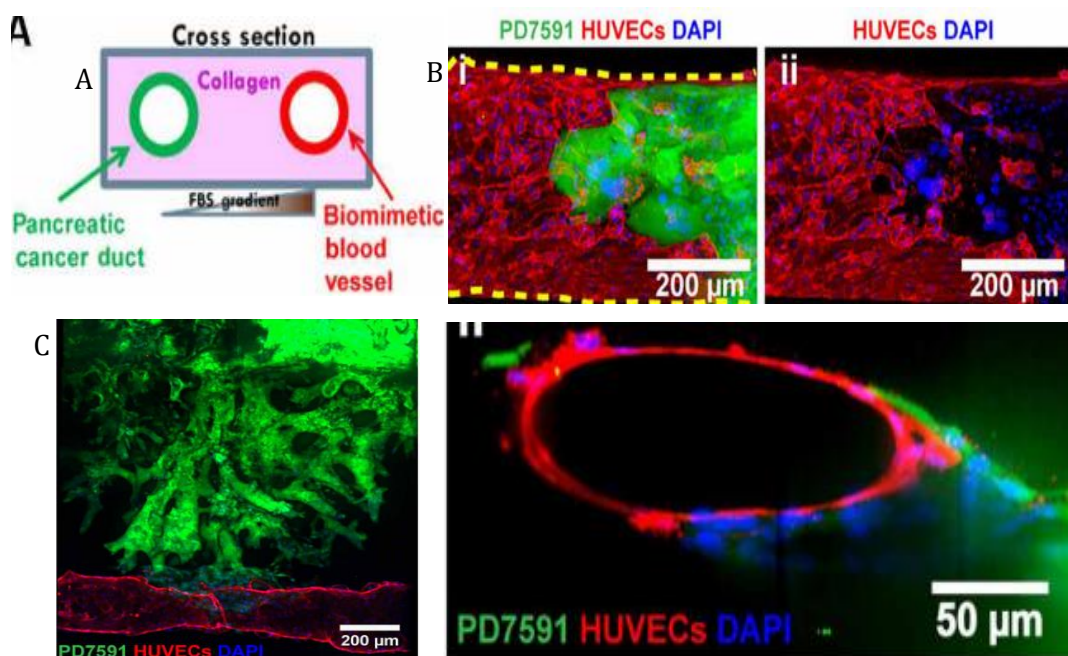


**Figure 1.6.3:** (A) Schematic of PDAC-on-a-chip: biomimetic blood vessel and pancreatic cancer duct. (B) A confocal image of a section of the blood vessel (in red) invaded by YFP PD7591 (in green). (C) YFP PD7591 (in green) invaded toward the biomimetic blood vessel (in red) <sup>66</sup>.

## 2. Aim of the work

The aim of this project is to realize an *in vitro* model of pancreatic acino-ductal unit using a microfluidic device in order to study PDAC. As described above, PDAC is a deadly disease due to late stages diagnosis, invasive metastasis, and the high resistance to therapeutic treatments. One of the causes of this resistance is the interaction between the tumour and the stromal component. For this reason, a multilayer microfluidic device has been developed to study the stroma-PDAC physiological crosstalk. The PDMS microfluidics device combining with a thermosensitive collagen-based hydrogel was fabricated with soft lithography and electrospinning.

The microfluidic device developed in this project is composed by two layers: a bottom layer loaded with pancreatic fibroblast embedded into a collagen hydrogel mimicking the stromal component and a top layer which resembles the tumour component. The crosstalk between the two components is allowed by a microporous membrane obtained by electrospinning.

Morphological characterization of the microfluidics device was performed by FESEM and optical microscopy. Concerning the fluidic characterization, both capacity and diffusivity tests were implemented. Finally, a biological characterization was performed in order to study the cellular response.

# 3. Materials and Methods

## 3.1 Device Design

In order to mimic stroma-PDAC physiological crosstalk in a dynamic environment, such as the one present *in situ*, the 3D model has to show important characteristics:

- ❖ Physiological crosstalk between stromal cells and PDAC cells.
- ❖ A matrix that mimics the tumoral microenvironment.

For these reasons a multilayer microfluidic device was developed. The microfluidic device has been designed using Rhinoceros, an application software for 3D modeling of sculptured surfaces. This platform is composed by two layers a *bottom layer* and a *top layer* connected by a *membrane*.

### 3.1.1 Bottom layer

Bottom layer is composed of three channels separated by two rows of micropillars (Figure 3.1.1). The middle channel is loaded with a collagen hydrogel in order to mimic the stromal component. The lateral channels allow the media passage while the central channel is the culture one that mimics the stromal component. To optimize the design there are only two inlets (for the media and the culture respectively) and one general outlet. The micropillars are cylinders with diameters and distances between them such as to allow the passage of nutrients from the lateral channels to the central one, for this reason they were fabricated four variants of bottom layers with different diameters of pillars and distance between them. Diameters of inlets and outlet are of 2 mm to permit the insertion of tubes. Lateral channels measure 6,4 mm long, 500  $\mu\text{m}$  wide, and 200  $\mu\text{m}$  high each one, while central channel measure 6,4 mm long, 900  $\mu\text{m}$  wide, and 200  $\mu\text{m}$  high. The Figure 3.1.1 shows bottom layer layout designed in Rhinoceros. The features of micropillars of the four layouts are summarized in Table.3.1-1.

**Table 3.1-1** Pillar features (diameter, distance and height).

$\mu\text{m}$	$\emptyset$	d	h
Model A	100	50	200
Model B	100	75	200
Model C	50	15	200
Model D	50	25	200

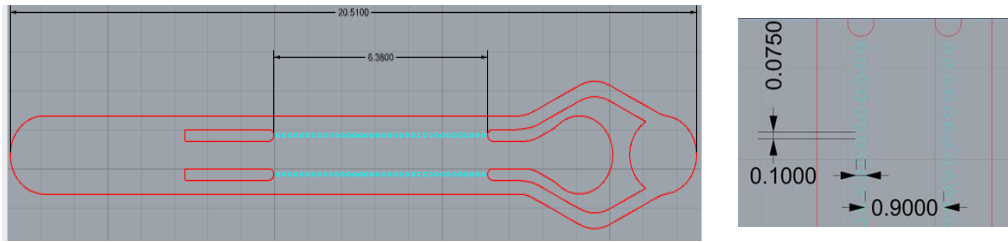


**Figure 3.1.1** Bottom layer layout: **A)** it is composed by a central channel (6,4 mm long, 900  $\mu\text{m}$  wide, 200  $\mu\text{m}$  high), filled with hydrogel and PSCs, between two lateral channels (6,4 mm long, 500  $\mu\text{m}$  wide, 200  $\mu\text{m}$  high). **B)** one typology of pillars (75  $\mu\text{m}$  diameter, 100  $\mu\text{m}$  pitch, 200  $\mu\text{m}$  high) confine the hydrogel in the central channel.

### 3.1.2 Top layer

Top layer is composed by only one channel in correspondence of the central channel of the bottom layer (Figure 3.1.2). Channel of top layer allows to culture PDAC cells. Furthermore, there are three inlets, two for the bottom layer and one for the top one, and there are two outlet each for layer. Diameters of inlets and outlet are of 2 mm to permit the insertion of tubes, and channel is 5.4 mm long, 1 mm wide and 250 $\mu\text{m}$  high.

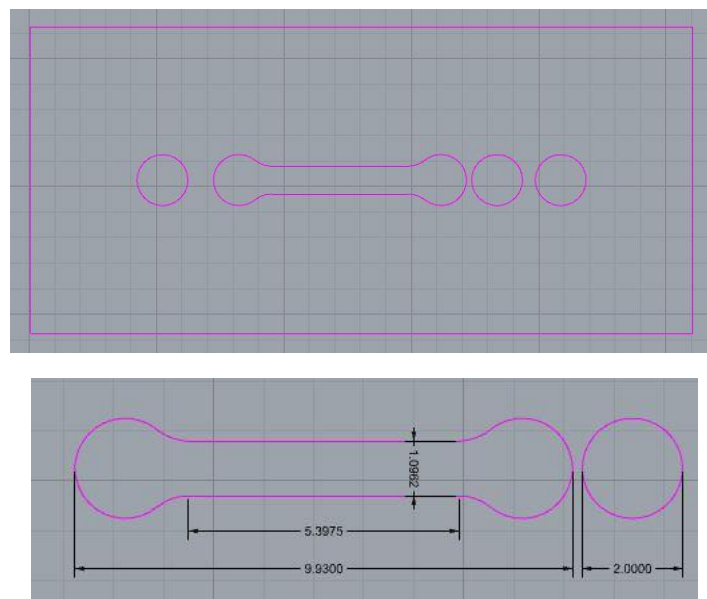


**Figure 3.1.2** Top layer layout: it is composed by a central channel (5,4 mm long, 1 mm wide, 250  $\mu\text{m}$  high), three inlet (2 mm diameter) and two outlets (2 mm diameters).

### 3.1.3 Membrane

The thin microporous membrane is used to separate top and bottom layers. Membrane allows a communication between PSCs cells culture in the bottom channel and PDAC cells culture in the top channel. Membrane is made in polycaprolactone/gelatine (PCL/GEL) and it was produced by solution electrospinning.

The Figure 3.1.3 shows the layout of complete device.

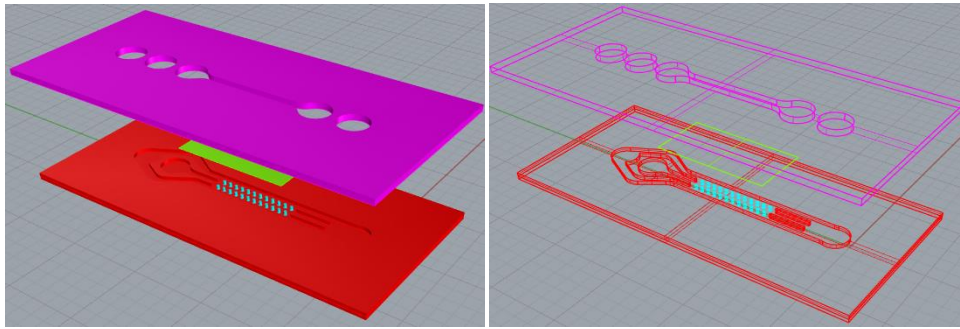


*Figure 3.1.3 Complete device layout.*

### **3.1.4 Reservoirs layer**

Reservoirs layer is an additional layer produced to facilitate culture in static conditions. It is composed by a PDMS layer with two cylindrical cavities of respectively 700  $\mu\text{m}$  and 540  $\mu\text{m}$  diameters, and 250  $\mu\text{m}$  high. The largest cavity is positioned above the inlets while the smallest is located above the outlets (Figure 3.1.4).

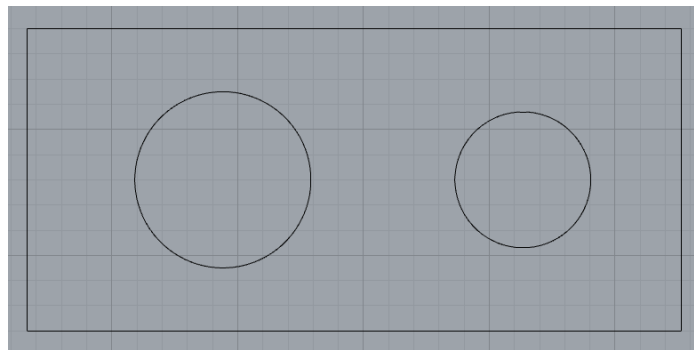


*Figure 3.1.4 Reservoir layout.*

## 3.2 Device fabrication

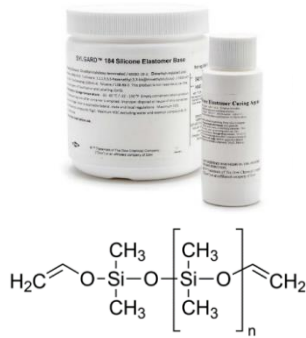
### 3.2.1 Replica molding

#### 3.2.1.1 PDMS

In this work, PDMS was used to produce the layers of the microfluidic device, starting from SYLGARD®184. SYLGARD®184 is a commercial PDMS based kit that is composed by a polymeric base and a curing agent, which is the cross-linker<sup>67</sup>. PDMS has excellent physical and chemical properties such as optical transparency, chemical inertness, and good permeability to gases but it is hydrophobic<sup>52,68</sup>. Table 3.2-1 summarize the main properties of SYLGARD®184.

*Table 3.2-1 A) PDMS SYLGARD 184 and chemical structure of the PDMS. B) Properties of PDM STLGARD 184<sup>67</sup>.*

PROPERTIERS	
Color	Colorless
Viscosity (Base)	5100 cP
Viscosity (Mixed)	3500 cP
Cure Time at 25°C	48 hours
Dielectric Strenght	19 kV/mm
Tensile Strenght	6,7 MPa



The image shows two bottles of SYLGARD 184 Silicone Elastomer Base and Curing Agent. Below the bottles is the chemical structure of PDMS, which is a linear chain of silicon atoms connected by oxygen atoms, with methyl groups attached to the silicon atoms. The structure is shown as  $\text{H}_2\text{C}=\text{O}-\text{Si}(\text{CH}_3)_2-\text{O}-\left[\text{Si}(\text{CH}_3)_2-\text{O}\right]_n-\text{CH}_2$ .

#### 3.2.1.2 Replica molding

PDMS solution was prepared under chemical hood and mixing polymeric base and curing agent respectively in the ratio 10:1 volume / volume (v/v). PDMS prepolymer and curing agent solution were inserted inside a plastic cup, and then the solution was stirred manually. After, using a vacuum pump, the air bubbles in the solution were removed, and the degassed solution was poured into the molds of top layer and bottom layer. The solution was cured in the oven at 70°C for 1 hour and 30 minutes. Replicas were removed from the mold inserting ethanol between the replicas and the molds.

After the top layer replica was peeled off from the master mold, the fluidic access into the device was produced with a manual biopsy puncher of 1.5 mm diameter.

### 3.2.2 Bottom layer mold fabrication: SU-8 photolithography

In this work, to produce the mold of bottom layer SU-8 photolithography technique has been used. This technique is divided into two phases, the first phase consists in the mask fabrication and the second is the real production of mold in SU-8. The entire process was done in a ISO clean room under yellow light illumination (Figure 3.2.5).

#### 3.2.2.1 SU-8 resist

SU-8 is an epoxy photoresist. It is formed by EPON resin (Bisphenol A Novolak epoxy oligomer) and photo acid generator (triarylsulfonium hexafluoroantimonate salt) which are dissolved in the GBL (gamma-butyrolactone) organic solvent<sup>69</sup>. The viscosity of the resist, and therefore the thickness that can be obtained depends on the amount of organic solvent used<sup>69</sup>. SU-8 absorbs light in the UV region, when light irradiate epoxy photoresist, the photo acid generator dissociates in order to generate hexafluoroantimonic acid that protonates the epoxides on the oligomer<sup>69</sup>. After irradiation, the structures with a high degree of reticulation can be obtained since each monomer molecule has eight reactive epoxy sites<sup>69</sup>. Cross-linked resin has high mechanical and thermal stability, and has a glass transition temperature about 200°C, a degradation temperature near 380°C and a 4-5 GPa Young E module<sup>69</sup>. In this work, SU-8 photoresist by MicroCHEM (Figure 3.2.1) was used to fabricate the mold of bottom layer. Specifically, SU-2150, one type of SU-2000, was employed and it is characterized by 80000 cSt of viscosity and 1,238 g/mL of density<sup>70</sup>.

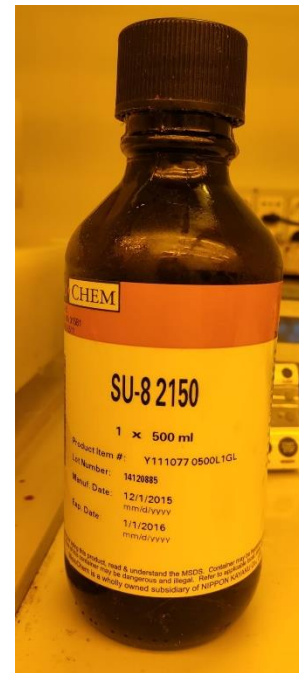


Figure 3.2.1 SU-2150

#### 3.2.2.2 Mask fabrication

The mask was produced on chromium/glass substrate using MICROTECH LASERWRITER LW405 A<sup>71</sup>, a laser writer machine (Figure 3.2.2).



Figure 3.2.2 MICROTECH LASERWRITER LW405 A<sup>71</sup>.

LaserWriter system is a machine that permits patterning planar structures on chromium/glass substrate to produce the mask or directly on the final substrate.

The system is composed by:

- ❖ *Write unit*: is the fundamental unit and it is composed by the GaN laser, the substrate microtranslation system and the electro-optical components. It allows to control the laser beam and the its exposure energy. The write unit leads the laser beam through specific optics tuned to the laser wavelength in order to write the structures on the mask.
- ❖ *Cabinet*: encases the write unit to shield it by the air flow of the clean room, that may induce tremors.
- ❖ *Control unit*: drives the write unit using a group of electronic subsystems<sup>71</sup>.

To produce a mask, the CAD was designed by using Rhinoceros and then it was converted in .CIF by *CleWin* (Figure 3.2.3), a layout editor. At the end of this operation, the CAD was imported, the write mode was selected, the mask was loaded and the write process has started. The writing process takes 24 hours and then mask is ready to use.

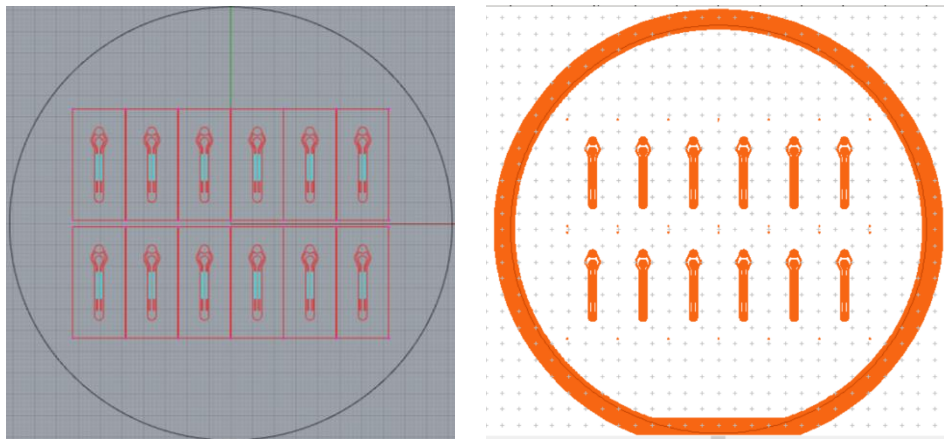


**Figure 3.2.3** A) CAD of mask designed in Rhinoceros. B) CAD of mask converted in .CIF by CleWin.

### 3.2.2.3 SU-8 photolithography

The initial substrate was a standard 4-inch single-side-polished Si wafer and to obtain a pattern with 200  $\mu\text{m}$  of thickness the following process was applied:

- ❖ *Coat*: distribute 10 mL of resist in the center of the wafer (Figure 3.2.4).
- ❖ *Spin coating*: using a spin coater, spin at 500 rpm for 10 seconds with acceleration of 100 rpm/second and then at 2000 rpm for 60 seconds with acceleration of 300 rpm/second. The first step allows for spreading the photoresist over the wafer and the second step at higher speed allows for controlling the layer thickness<sup>59</sup>(Figure 3.2.4<sup>72</sup>).

- ❖ *Soft bake*: on a hotplate for 8 min at 65 °C, ramping till 95 °C, 1 h at 95 °C, cooling at room temperature out of the hotplate. The aim of this phase is to evaporate the solvent to make the SU-8 photoresist more solid (Figure 3.2.4).
- ❖ *Exposure*: add a long pass filter to remove UV radiation under 365 nm and expose the wafer to Near UV (350-400 nm) radiation for 50 s at 7 mW/cm<sup>2</sup>. During this step the parts exposed to the UV light start the cross linkage (Figure 3.2.4).
- ❖ *Post-exposure bake*: on a hotplate for 5 min at 65 °C, ramping till 95 °C, 20 min at 95 °C, cooling at room temperature out of the hotplate. This phase provides energy to obtain cross linkage<sup>59</sup> (Figure 3.2.4).
- ❖ *Development*: immerse the wafer in MicroChem's SU-8 developer (Propylene glycol monomethyl ether acetate, PGMEA) and stir the solution to facilitate the development.
- ❖ *Rinse and dry*: Wash the developed wafer with fresh solution of SU-8 developer for 10 s, then wash with 2-Propanol Alcohol (IPA) for another 10 s. Finally blow drying with nitrogen.
- ❖ *Hard bake*: on a hotplate for 5 min at 150 °C.

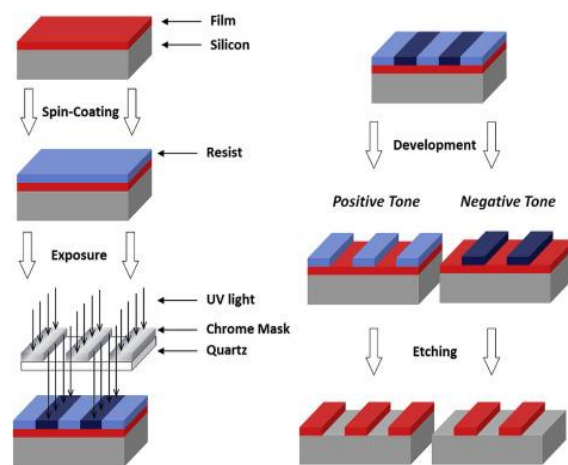


Figure 3.2.4 SU-8 photolithography process<sup>72</sup>.



Figure 3.2.5 Workbench: Spin coater – Hot plate- SU-8 2150 - UV photolithography system

This process was optimized, and the various tests are listed in Table. 3.2-2

*Table 3.2-2 List of SU-8 photolithography tests conditions.*

TEST	SPIN COATING	SOFT BAKE- T1	SOFT BAKE- T2	REST- Tamb	UV	POST BAKE- T1	POST BAKE- T2	DEVELOPED
T1	2500rpm 30sec	65°C 6min	95°C 35 min	/	20sec	65°C 5min	95°C 13min	30 min
T2	3000rpm 30sec	65°C 6min	95°C 35 min	/	15sec	65°C 5min	95°C 13min	30 min
T3	3000rpm 30sec	65°C 6min	95°C 40min	50 min	10sec	65°C 5min	95°C 15min	20 min
T4	500rpm 30sec 3000rpm 60sec	65°C 6min	95°C 40min	30 min	10sec	65°C 5min	95°C 15min	30 min
T5	500rpm 30sec 3000rpm 60sec	65°C 6min	95°C 40min	30 min	15sec	65°C 5min	95°C 15min	35 min
T6	500rpm 30sec 3000rpm 60sec	65°C 6min	95°C 40min	30 min	15sec	65°C 5min	95°C 15min	40 min
T7	500rpm 10sec 2000rpm 60sec	65°C 8min	95°C 40min	/	50sec	65°C 5min	95°C 20min	15 min

In consideration of Si has a strong compatibility with PDMS, an anti-adhesive layer was required to simplify peel off PDMS. This layer was obtained with salinization process and the procedure followed was the following:

- ❖ *Solution:* toluene and trichloromethylsilane was poured into a glass petri dish with a 1:10 ratio between trichloromethylsilane and toluene.
- ❖ *Exposure:* the wafer was dipped in the solution for 3 hours.

- ❖ *Cleaning and bake*: the wafer was washed with IPA and it was baked for 15 min at 160 °C.

To produce the mold, the wafer was positioned into a petri dish and it was used a Kapton tape to confine the PDMS. Kapton is a polyimide film that remains stable between -269 °C and +400 °C<sup>73</sup>.

### 3.2.3 Top layer mold fabrication: Laser ablation

In this work, laser ablation technique was used to produce the top layer mold, the reservoir mold and the chip housing. CAD was patterned on polymethylmethacrylate (PMMA) using CO<sub>2</sub> laser of LASER Slider Marker System by Microla<sup>74</sup> (Figure 3.2.6).

LASER Slider is marker template and it is constituted of:

- ❖ *laser system* with a CO<sub>2</sub> source that work at 25-50 W of power and a wavelength of 10.6 μm.
- ❖ *galvanometric head* used to drive laser beam towards samples
- ❖ *slider* used to positionate the samples
- ❖ *integrated computer* used to load the CAD and regulate the parameters of process<sup>74</sup>.

The PMMA sheet of 5mm of heigh was placed in the laser machine. Then the laser beam was focused on the top of PMMA. Finally, the parameters were set, and the process was started. After this process the mold of the top in PMMA was obtained, it is the negative of the final geometry and it is a 2D pattern. To fabricate a thickness to confine the PDMS, the laser machine was used, and a rectangular edge was cut from PMMA sheet of 2 mm of thick, which was the desired height of the final layer of PDMS. Finally, the edge was glued to the 2D mold using a double-sided tape.



Figure 3.2.6 LASER Slider Marker System by Microla<sup>74</sup>

Several samples of line spacing and speed of passage were tested to obtain optimized mold. The test parameters were summarized in the Table 3.2-3.

*Table 3.2-3 Laser ablation conditions.*

Test	Line	Line spacing [mm]	Angle	Steps	Time_on	Frequency [Hz]	V <sub>p</sub> [mm/s]
P1	Crisscross	0,05	45°	1	5%	2000	100
P2	Crisscross	0,05	45°	1	5%	2000	75
P3	Crisscross	0,03	45°	1	5%	2000	75

### 3.2.4 Membrane fabrication

Membrane is constituted by polycaprolactone (PCL) and gelatin (GEL), obtained by solution electrospinning technique.

#### 3.2.4.1 PCL: polycaprolactone

PCL is a thermoplastic, biodegradable, biocompatible, hydrophobic, and aliphatic polymer that appertains to the group of polyesters. It is composed by five non-polar methylene groups and one polar ester group, which makes it biodegradable in physiological environments<sup>75</sup>. PCL has good mechanical properties, such as toughness and flexibility, at low temperature, because it is a semi-crystalline thermoplastic polymer with a melting temperature of between 59 °C and 64 °C and a glass transition temperature of -60 °C<sup>75,76</sup>. It is obtained using the stannous octate that catalyzes ring-opening polymerization of the cyclic monomer  $\epsilon$ -caprolactone (C<sub>6</sub>H<sub>10</sub>O<sub>2</sub>)<sup>76,75</sup>, (Figure 3.2.7<sup>77</sup>).

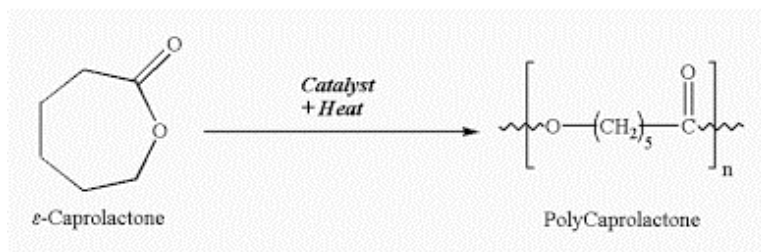


**Figure 3.2.7** Scheme of the ring opening polymerization through which the PCL is obtained<sup>77</sup>.



solution. After 30 minutes of stirring, polymer chains of the gelatin and of the PCL were intertwined and the transparent solution was ready.

#### 3.2.4.4 Solution electrospinning process

The solution, obtained by means of the previously described protocol, was electrospun thanks to the solution electrospinning set-up of the NovaSpider instrument<sup>81</sup> (Figure 3.2.9). The NovaSpider is constituted by different components:

- ❖ *Glass syringe* is loaded with a volume of 5 mL of polymer solution.
- ❖ *Volumetric pump* imposes continuous pressure on the plunger of the syringe, thus it allows to extruding the solution at an established constant speed.
- ❖ *Voltage generator*: generates a potential difference.
- ❖ *Flat collector*: a plastic plate coated with aluminium foil to allow the random deposition of the nanofibers.



Figure 3.2.9 NovaSpider Instrument<sup>81</sup>.

Once the syringe was placed on the pump, the needle was connected, and the process parameters were set. The process parameters are summarized in the Table 3.2-4.

Table 3.2-4 Solution electrospinning conditions.

MATERIAL	VOLTAGE	FLOW RATE	NEEDLE-COLLECTOR DISTANCE
PCL/GEL	4 kV	500 $\mu$ L/min	12 cm

### 3.2.5 Microfluidic device assembly

To manufacture the complete device, it was necessary to combine the different layers, and therefore a chip housing was fabricated and PDMS surfaces were treated in order to decrease the hydrophobicity and to facilitate the bond between the different layers.

The chip housing was fabricated with the same measures of microfluidic device (26 mm long, 12 mm wide and 2 mm high) using laser ablation technique and as a protocol was followed the same used to produce top layer mold.

#### 3.2.5.1 Plasma Oxygen

To turn PDMS hydrophilic can be used different chemical or physical processes and, in this work, it was used oxygen plasma. The oxygen plasma treatments can increase the wettability of surface and it allows the production of strong-hydrophilic surface of PDMS<sup>68</sup>. PDMS is composed by repeated units of  $\text{—O—Si(CH}_3)_2\text{—}$ , which on exposure to oxygen plasma develops silanol groups ( $\text{—OH}$ ) and loses methyl groups ( $\text{—CH}_3$ ), (Figure 3.2.10<sup>82</sup>). Silanol groups make the exposed surface greatly hydrophilic because the silanol groups are polar. These silanol groups then condense with those on another surface of PDMS and this reaction produces Si-O-Si bonds and a leak of a water molecule. This reaction produces a covalent strong bond between the two layers<sup>83</sup>.

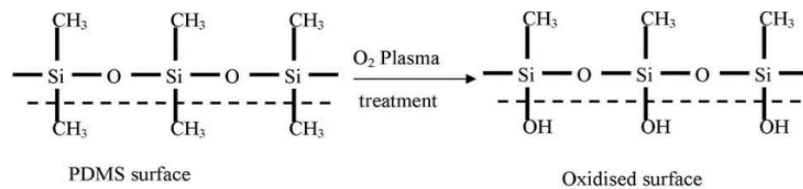


Figure 3.2.10 Chemical process of PDMS activation<sup>82</sup>.

In this work oxygen plasma by Electronic Diener Plasma-Surface-Technology<sup>84</sup> was used to bond the layers (Figure 3.2.11).

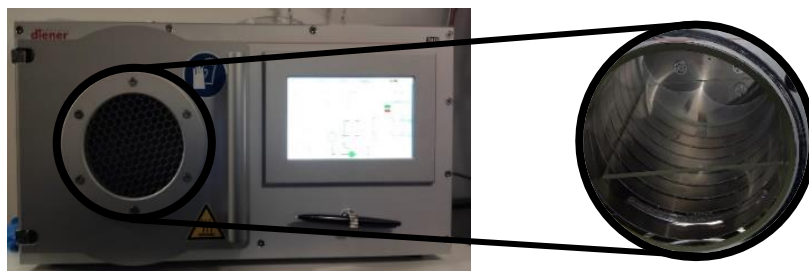


Figure 3.2.11 Electronic Diener plasma reactor system used for surface modification of substrates<sup>84</sup>.

The PDMS layers were cleaned in the ultrasound bath with 2-propanol for 1 min and then dried for 1 min with nitrogen flux. The membranes were cut with a 3 mm wide and 10 mm long, they were placed in the plasma system together with the samples and they exposed to plasma oxygen treatment. The process is divided into five phases, in the first phase, called pumping down period, the pressure in the chamber drops to 0.3 mbar. In the second phase the working gas (oxygen) is blown in the chamber with samples with a pressure of 0.70 mbar for one minute, after the high frequency generator is activated and plasma takes place for 30 seconds with a power of 22%. The last step is the vent in which the chamber is filled with air. After the surfaces treatment, device was assembled under the optical microscope. The lower layer was inserted into the chip housing, the membrane was placed and then blocked by aligning the top layer with the lower layer. Later, the same procedure was carried out to bond the complete chip with the reservoir. Finally, the device was heat treated for 10 minutes at 70 °C to ensure a stronger PDMS-PDMS bond.

The process parameters of oxygen plasma were summarized in the Table 3.2-5.

*Table 3.2-5 Optimized Plasma oxygen parameters.*

<b>PARAMETERS</b>	
Pumping down period	
PRESSURE	0,3 mbar
Gas supply period	
DURATION	1 min
GASES	O <sub>2</sub> 100%
PRESSURE	0,70 mbar
Plasma process period	
DURATION	30 sec
POWER	22%
Venting period	
DURATION	1 min

### 3.3 Physical characterization of the microfluidic device

The molds and the device layers after production were analyzed using the profilometer, digital microscope and FESEM to investigate physical features such as dimensions and surfaces.

#### 3.3.1 Surface roughness analysis: Profilometer

Profilometer is a microscopic technique that provides the quantitative measure of the steps between layers and surface roughness. The probe follows each point of the surface, and the height of the probe is register for each point, then at end of the measurement a 2D map is returned and tanks to this is possible measurement the total height of the observed area of the samples. In contact profilometer, a stylus is moved vertically in contact with the sample for a specific distance and with a specific contact force. Normally mechanical probe is used to measure a large area, around 100 mm, with a z-resolution of 0.01  $\mu\text{m}$  and a x-y resolution of 5  $\mu\text{m}$  and with a contact force of 5 mN<sup>85</sup>.

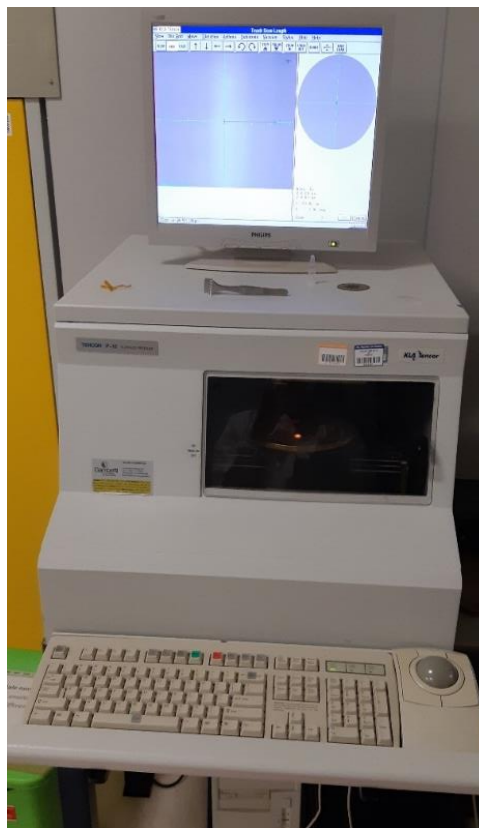


*Figure 3.3.1 TENCOR P.10 SURFACE PROFILER<sup>86</sup>.*

In this experimental procedure, the contact profilometer was used to measure the surface's profile of the mold in SU-8 of the bottom layer (Figure 3.3.1<sup>86</sup>). After the hard bake step, the samples of SU-8 were loaded inside the sample holder chamber of

profilometer, the probe was positioned on the area to observe and then the high was measured.

### **3.3.2 Digital microscope analysis of single device layers**

In this work digital microscope by Leica<sup>87</sup> was used to observe the different layers of the device and to investigate the dimension using the dedicated software LAS VA.1.

Focusing on replicas of bottom layer, digital microscope was used to observed the development of the pattern on PDMS replica and to measure the diameters of inlets and outlets, to measure the diameter of micropillars and the distance between them, to measure the dimension of different channels and to observe if all micropillars were developed. Instead, on replica of top layer were measured the diameters of inlets and outlets and the dimension of different channels. To measure the heights, the replicas section was evaluated, then in the bottom layer replicas the distance among the base of channel and the top of the pillars was measured, while in the top layer replicas was measured the distance among the base and the top of channel.

### **3.3.3 Field Emission Scanning Electron Microscope (FESEM)**

Field Emission Scanning Electron Microscope or FESEM is a microscope which involves the use of electrons. Electrons source is a cold tungsten needle which generates a high electrical field gradient<sup>88</sup>. These primary electrons are focussed and deflected by a set of electronic lenses within the high vacuum column in order to produce a beam that hits the samples, thus emitting a secondary electrons beam<sup>88</sup>. A detector catches these secondary electrons and makes an electronic signal that is increased and elaborated in a digital image<sup>88</sup>. Therefore, the surface structure of samples is described by the velocity and angle of the secondary electrons <sup>88</sup>.



*Figure 3.3.2 ZEISS MERLIN FE-SEM<sup>89</sup>.*

The FESEM (Zeiss Supra 40) shown in Figure 3.3.2 has been used to analyse the structure of bottom layer replica <sup>89</sup>.

The sample preparation consisted in the slicing of the samples into a smaller specimen along three dimensions and placement on a FESEM stub. Finally, the sample was coated with a 10 nm chrome layer using the sputtering instruments, Quorum Q150s. The morphology was observed at an accelerating voltage of 3 kV.

## 3.4 Fluidic test of the microfluidic device

In this work the sealing and diffusive tests were carried out to evaluate respectively the tightness of the assembled device and to evaluate which bottom layer layout to use for biological characterizations. For these analyses both feeding and fluorescent dyes were used, then investigated using the confocal microscope.

### 3.4.1 Capacity test

Capacity test has been made on assembled chip and on bottom layer bonded with microscope slide (Figure 3.4.1).

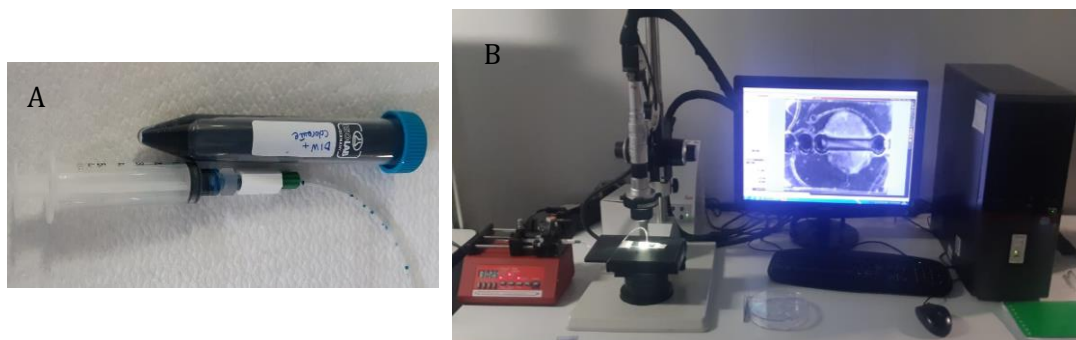


**Figure 3.4.1** A) Blue food dyed solution. B) Capacity test set up: Syringe pump and Leica digital microscope.

#### 3.4.1.1 Assembled device

Capacity test on complete device has been made to observe if the bond between two layers held and if there were no losses. The solution of blue food dye and deionized water was prepared respectively in the ratio 1:3 (v/v), and after the bonding of layers, the solution was loaded into inlets of bottom layer and inlet of top layer using a syringe pump with 2,4  $\mu\text{L}/\text{h}$  as flow rate and tube with an external diameter of 1,5mm. Then it was observed if there were losses.

#### 3.4.1.2 Only bottom layer

Capacity test on bottom layer bonded with microscope slide has been made to observe if the two rows of micropillars kept liquids inside the central channel. The solution of blue food dye and deionized water was loaded into inlets of central channel of bottom layer

with a manual micropipette load with 1,5  $\mu\text{L}$  of solution. Then it was observed if there were losses into lateral channels. This test was repeated using a collagen gel, to understand if the two rows of micropillars could confine it.

### 3.4.2 Diffusivity test

The microfluidic chip was tested to verify proper gradient formation into the central channel of bottom layer filled with a collagen hydrogel and to choose the typology of bottom layer.

#### 3.4.2.1 Collagen

Collagen is a natural and structural protein and its basic unit is a helical quaternary structure called triple helix, which is composed of three left-handed  $\alpha$ -chains held together by hydrogen bonds. Generally,  $\alpha$ -chains are composed by a series of triplet Gly-X-Y sequences in which X and Y can be any amino acids, often X is proline and Y is hydroxyproline<sup>90</sup> (Figure 3.4.2<sup>91</sup>).

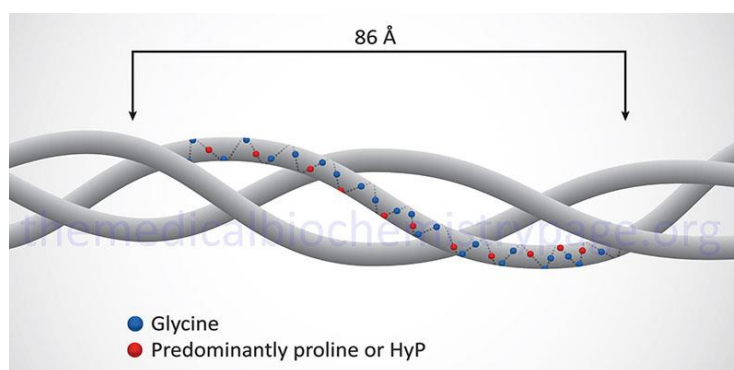


Figure 3.4.2 Structure of collagen<sup>91</sup>.

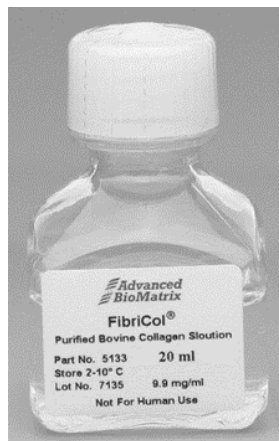
In type I collagen two of the chains are identical and the third has a similar but distinct sequence<sup>92</sup>. Collagen is composed by polar groups and hydrophobic section that came from hydrophobic amino acids<sup>93</sup>. For its component collagen has high hydrophilicity, and variable ionic character, and it can be involved in many interaction systems with other micro- and macromolecular components<sup>93</sup>.

Type I collagen gels and solutions are commonly used to obtain medical biomaterials. Gel is a system with both solids and fluidics properties, moreover hydrogels are three-dimensionally hydrophilic polymeric systems derived from the cross-linking of gels<sup>93</sup>. Hydrogels are insolubility in water for the presence of ionic interaction and hydrogen bonding in the structures of the hydrogels, this ensures mechanical strength and physical integrity to the hydrogels. Collagen gels and solutions correspond to a polydispersed colloidal network<sup>93</sup>. Collagen gel can be crosslinked with two methods, physical and chemical. In the chemical cross-linking a residual cross-linking agent, that can be toxic,

remains and therefore a further physical treatment could be used. Among physical methods there are heat-drying and exposure to UV and  $\gamma$  radiation<sup>93</sup>.

In this work, Type I Collagen Solution (Bovine) by FibrCol<sup>®</sup> was used. FibrCol collagen is composed by 97% Type I collagen and the remainder 3% corresponds to Type III collagen. The concentration of collagen in FibrCol<sup>®</sup> is about of 10 mg/mL. collagen in FibrCol<sup>®</sup> comes from bovine hides <sup>94</sup>. The main properties were summarized in the Table 3.4-1.

**Table 3.4-1** Propertiers of FibrCol Type I Collagen Solution (Bovine) <sup>94</sup>.



*FibrCol collagen properties*

Form	Solution
Storage Temperature	2-10°C
Collagen Concentration - Biuret	9.0-11.5 mg/mL
Collagen Purity - Silver	≥99.9%
Staining	
pH	1.9-2.1
Source	Bovine Hide

**3.4.2.2** *Collagen hydrogel solution*

Collagen hydrogel solution was prepared mixing 1 part of PBS 10X and 8 parts of collagen solution (at 4°C) and then the solution was stirred for a few minutes. To obtain a 7.2-7.8 pH, sterile 0.1 M NaOH was added to solution and pH was monitored using a pH paper. Then 1 part of sterile water was added, and the solution was stirred. This process it was carried out into a crystallizer with ice in order to maintain the collagen solution at 4°C. To reticular the solution it was maintained at 37°C for 90 minutes.

**3.4.2.3** *Confocal laser scanning*

Laser scanning confocal microscopy is an imaging technology that emits a laser excitation able to interact with the fluorophore generating an emission radiation which is detected. The confocal microscope allows to achieve high resolutions since it has a stenopeic hole between the lenses and the sensor, which blocks the unfocused light and allows the passage of the focused one<sup>95</sup>.

In this work, confocal laser scanning microscopy (Figure 3.4.3) was used for the diffusivity test and for cell models using the Nikon Eclipse Ti2 microscope<sup>96</sup> that is available at Polito<sup>BIO</sup>Med Lab.



*Figure 3.4.3 Nikon Ti2 inverted microscope<sup>96</sup>.*

#### *3.4.2.4 Diffusivity test procedure*

The experiments were conducted on bottom layer replicas bonded on specific glass slides, and the central channels were filled with the collagen gel.

Collagen gel solution was prepared, 1,5  $\mu\text{L}$  of collagen were inserted inside the central channels, and the samples positioned in incubator at 37°C and with 90% of humidity for 40 minutes in order to reticular the collagen solution. Meantime, the fluorescent solution was prepared, FICT and deionized water were inserted inside a tube and they were stirred for two minutes. When collagen gel was reticuled, 10  $\mu\text{L}$  of fluorescent solution was inserted in the lateral channels and then the samples were observed with Nikon Ti2 inverted microscope for 30 minutes and every 30 seconds was captured an image.

## 3.5 Biological characterization

*In vitro* studies were performed to analyse the cell proliferative capability in the microfluidic device. In this work, four different experiments were performed. Firstly, HFF-1 fibroblasts were cultured on collagen hydrogel in the bottom layer; in the second experiment the same protocol was performed using the PSCs; then HPDE were cultured on PCL/GEL membrane in the top layer and the last experiment involved the co-culture of PSCs and HPDE within the complete device. The cell proliferation was evaluated after 24 h, 48 h and 72 h purpose, vitality assays and fluorescence imaging were performed. All the biological procedures were conducted in a laminar flow hood that is designed to provide a barrier against bacteria. It protects the environment and the user from inhaling toxic gases and prevents contamination of experiment from dust and microorganisms. All items placed in the hood were disinfected with ethanol 70%, sterilized with autoclave or UV light, in order to preserve the sterility of the environment.

### 3.5.1 Human Foreskin Fibroblasts cells

The HFF-1 (Human Foreskin Fibroblasts) cell line was used for cellular testing on Collagen Hydrogel, inserted into microfluidic devices, to mimic the stroma of PDAC. HFF-1 were purchased from the American type culture collection (ATCC). The cells were grown in DMEM, Dulbecco's Modified Eagle Medium (Gibco, ThermoFisher scientific). DMEM contains low or high concentrations of glucose and phenol red. Glucose is the principal energy source for cells, while phenol red is pH indicator that controls modifications of pH as results of the change in metabolic activity of cells<sup>97</sup>. DMEM was supplemented with:

- ❖ 15% fetal bovine serum (FBS, Gibco ThermoFisher scientific), it is composed by embryonic growth promoting factors, hormones, inorganic minerals and vitamins and it allows for cell maintenance and vitality<sup>98</sup>.
- ❖ 2% L-glutamine, 200 nM (Gibco, ThermoFisher scientific), it is an aminoacid<sup>99</sup>.
- ❖ 1% penicillin streptomycin (P/S, Gibco, ThermoFischer scientific), it is an antibiotics used to impede bacterial contamination due to their action against both gram-positive and gram-negative bacteria<sup>100</sup>.

The HFF-1 cells are fibroblasts, connective tissue cells that produce some components of the extracellular matrix such as collagen, glycosaminoglycans and glycoproteins. When active, fibroblasts show an elongated shape<sup>101</sup>. These cells can be employed as an alternative for primary human pancreas endothelial cells for pancreatic cancer research, for studying the role of stroma in the development of cancer.

### 3.5.2 PSCs cells

The PSCs cell line was used for cellular testing on Collagen Hydrogel, inserted into microfluidic devices, because this cell line is the main cellular component of stroma of PDAC. The PSCs were kindly provided by Prof. Cauda. The cells were grown in Stellate Cell Growth Medium kit (iXCells BIOTECHNOLOGIES)<sup>102</sup> composed by Stellate Cell Basal Medium supplemented with:

- ❖ 10 % Fetal Bovine Serum.
- ❖ 0,2 % Stellate Cell Growth Supplement, a medium supplement designed for the optimal growth of normal human stellate cells.
- ❖ 1 % Antibiotic – Antimycotic (100X), it is a mixture of antibiotic that contains penicillin, streptomycin and amphotericin B. Normally it is used against the most common types of cell culture contamination, as bacteria and fungi<sup>103</sup>.

As mentioned above, PSCs are the main cells of the stromal tissue of the pancreas, which in the presence of lesions are activated becoming myofibroblast like cells. They are widely used to study the role of the PDAC progression stroma.

### 3.5.3 HPDE cells with KRAS mutation

The HPDE (Human Pancreatic Duct Epithelial) cell line with mutation KRAS was used for cellular testing on PCL/GEL membrane, inserted into the microfluidic device, to mimic the PDAC tissue. HPDE were purchased from the American type culture collection (ATCC). The cells were grown in RPMI, Roswell Park Memorial Institute (Gibco, ThermoFisher scientific)<sup>104</sup>. RPMI is composed by reducing agent glutathione and it presents high concentrations of vitamins, including biotin, vitamin B12, and PABA. RPMI also contains phenol red as pH indicator. RPMI was supplemented with:

- ❖ 15% fetal bovine serum (FBS)<sup>98</sup>.
- ❖ 1% L-glutamine, 200 nM<sup>99</sup>.
- ❖ 1% penicillin streptomycin (P/S)<sup>100</sup>.

The HPDE with KRAS are cell line derived from normal human pancreatic duct epithelial with a mutation on gene KRAS, which is a DNA mutation typical of many cancer cells like the PDAC ones<sup>105</sup>.

### 3.5.4 Procedure of cell seeding

In this work the cell splitting was made using 0.05% trypsin. Trypsin is a proteolytic enzyme that links specific amino acid sequences and cuts them.

The protocol used for this operation was described above:

- ❖ Removal of the culture medium from the flask.
- ❖ Flush cells with Dulbecco's phosphate-buffered saline (DPBS, Gibco) to eliminate all trace of serum that could alter the action of trypsin.
- ❖ Remove DPBS and addition of 2 ml of trypsin in the flask, trypsin must be at 37 °C.
- ❖ Incubate of the flask at 37 °C for 3 minutes.
- ❖ Observe of cell morphology at the microscope, if cells are rounded the detachment from the surface happened.
- ❖ Add the growth medium in the flask to stop the action of trypsin.
- ❖ Aspire the cell suspension and placement in a tube.

After this procedure, a 10 µL drop of cell suspension is poured into the Burker chamber and covered by cover glass, cells were observed at optical microscopy and they were counted using it. Burker chamber has 2 cells, each divided into 9 squares of 1 mm<sup>2</sup>, each with 16 squares of 0.2 x 0.2 mm, there are also 9 squares smaller, (0.05 mm and 1/400 mm<sup>2</sup>), and 24 rectangles with an area of 1/100 mm<sup>2</sup> interposed to the nine squares of 1 mm<sup>106</sup>. Cells are counted in the four square grid engraved on the bottom of the cells.

The total cells in the suspension is calculated as follows:

$$N^{\circ}cells = \left( \frac{Conted\ cells}{4} \right) * 10000 * Suspension\ volume$$

The number of cells to culture is used to calculate the appropriate volume of cellular suspension with a proportion:

$$N^{\circ}cell: Suspension\ volume = N^{\circ} cell\ to\ culture: X$$

After, the correct volume of cells was placed in a tube or Eppendorf and it was centrifugated at 1000 rpm for 8 minutes, at the end the solid phase represented by cells, called pellet is deposited at the tube bottom. As regards the pellet of PSCs and HFF-1, they were re-suspended in a correct amount of collagen gel and fresh media while the pellet of HPDE was re-suspended only with the right volume of fresh media, and then by repeatedly gently pipetting the pellet were broken. In the vary experiments, this volume has been placed in the device and in the 48 well plates for the controls. After seeding the cells were placed into the incubator at 37 °C in a 5% CO<sub>2</sub> humidity saturated atmosphere. Cell culture medium was changed every day in the device and every two days in the control.

### 3.5.5 Vitality assays

In this work to evaluate the vitality of cells resazurin cell viability assay (Invitrogen, ThermoFischer SCIENTIFC), Live/Dead (Invitrogen, ThermoFischer SCIENTIFC) assay<sup>107</sup>, DAPI/Phalloidin assay (Invitrogen, ThermoFischer SCIENTIFC) and CellTiterGlu 3D (Promega)<sup>108</sup> were implemented.

#### 3.5.5.1 Resazurin cell Viability Assay

In this work, Resazurin Cell Viability Assay by ThermoFisher has been used to study cellular vitality of fibroblasts loaded in the collagen and seeded on plastic control. Resazurin Cell Viability Assay is based on resazurin (Figure 3.5.1<sup>109</sup>). Resazurin is an active and no-toxic substance that has the capability of permeable to cell. In normal condition it is blue and no-toxic, when the resazurin enter in the cells, the cellular environment reacts with it and reduces it to resorufin. Resorufin is a fluorescent red compound. The higher the intensity of fluorescence can be read through absorbance-based plate readers, and this intensity is an index of cell viability<sup>110</sup>.

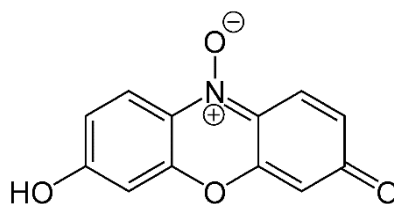


Figure 3.5.1 Chemical structure of Resazurin<sup>109</sup>.

#### 3.5.5.2 CellTiterGlo 3D Cell Viability Assay

In this work, CellTiter-Glo® 3D Cell Viability Assay by Promega has been used in preliminary tests to study cellular vitality of fibroblasts loaded in the collagen hydrogel to assess the optimal cellular density for the subsequent tests. CellTiter-Glo® 3D Cell Viability Assay allows to determinate cell viability in 3D cell cultures, such as hydrogels. In this assay relies the molecules of thermostable luciferase react with ATP, that came from to the cell lysis, and oxygen generating a luminescent signal, that can be read through an absorbance/luminescence- based plate reader (Figure 3.5.2)<sup>108</sup>.

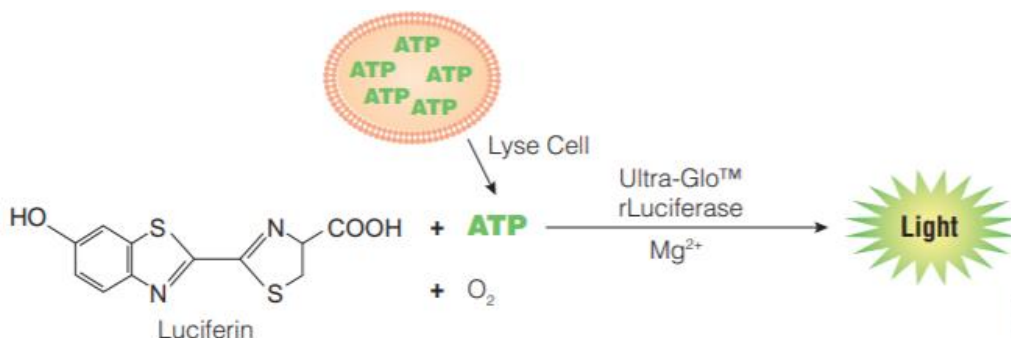
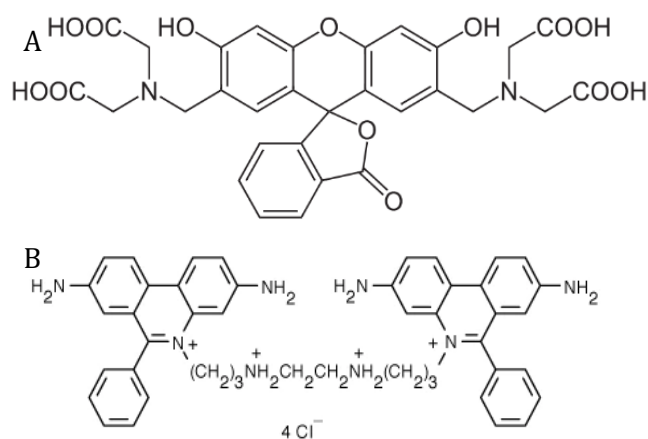


Figure 3.5.2 Reaction between Luciferin and ATP<sup>108</sup>.

### 3.5.5.3 Live/Dead Cell Viability Assay

LIVE/DEAD™ Viability/Cytotoxicity Kit, for mammalian cells by ThermoFischer was used to evaluate the living and dead cells present in the devices and in the respective controls. In this assay two probes (Figure 3.5.3<sup>111, 107</sup>), calcein AM and ethidium homodimer (EthD-1) allow to determine live and dead cells. Calcein AM enters vital cells and marks them because vital cells present an intracellular esterase activity, which allows the enzymatic conversion of non-fluorescent calcein into fluorescent. Calcein within live cells, raises an intense uniform green fluorescence with a wavelength between 495 nm and 515 nm. While EthD-1 enters cells with damaged membranes, and it links with nucleic acids. This bond raises a bright red fluorescence in dead cells with wavelength between 495 nm 635 nm. EthD-1 fails to enter vital cells because the membrane is not damaged. In this work both the devices and the controls after they were marked, they were observed with a microscope. The images were captured on two different channels and then they were made the merges of the images<sup>107</sup>.



**Figure 3.5.3 A)** Chemical structure of Calcein AM. **B)** Chemical structure of EtdH-1 AM in the right<sup>98, 107</sup>.

### 3.5.5.4 DAPI and Phalloidin staining

DAPI/Phalloidin staining was used to mark the nuclei and cytoskeletons cells present in the devices and in the respective controls. DAPI or 4',6-diamidin-2-phenylol is a fluorescent organic dye that binds A-T sequences in DNA with a strong bond. This link between DAPI and DNA produces a blue fluorescence with a wavelength around of 460 nm<sup>112</sup>. While Phalloidin is a bicyclic peptide, a toxin isolated from the Amanita phalloides mushroom. Phalloidin binds F-actin in the cytoskeleton of cells, this link allows F-actins to be identified and quantified in cells<sup>113</sup>. In this work both the devices and the controls were marked with DAPI and phalloidin and then were observed with a confocal microscope. The images were captured on two different channels and then merged.

### 3.5.6 Biological experiments

In this work six different experiments were carried out, where HFF-1 or PSCs and HPDE-KRAS cells were seeded as mono and co-culture.

#### 3.5.6.1 1<sup>st</sup> Experiment

The first experiment was carried out to understand the cellular vitality of fibroblasts within the FIBRICOL collagen gel<sup>94</sup>. In this experiment, 30000 cells for 100  $\mu$ L of hydrogel of collagen and 30000/1.9cm<sup>2</sup> for each control were considered. Four samples and two control were tested for each time step and the time points were set to 24h 72h and 7 days. A total of 360000 cells were considered for a total of 1,2 mL of collagen hydrogel and 180000 cells for controls. After performing the seeding protocol and the counting of cells, the two volumes of cellular suspension have been calculated as follows:

$$N^{\circ}cells = \left(\frac{61}{4}\right) * 10000 * 35mL = 5337500 \text{ cells}$$

$$5337500:35 = 180000:V1_{coll}$$

$$V1_{coll} = 2,36mL$$

$$5337500:35 = 360000:V2$$

$$V2 = 1,18mL$$

These two volumes were taken and inserted into two distinct tubes and then they were centrifuged to generate the two pellets. The first pellet was broken with 1,2 mL of hydrogel and 400  $\mu$ L of medium, then a smear of 100  $\mu$ l collagen and cells was inserted in each well. The gel was made to reticular for 30 minutes in incubator at 37°, then 300  $\mu$ L of medium were added in every wells. While the pellet two was broken with 1,8 mL of medium, then 300  $\mu$ L medium and cells were inserted in each well.

In this experiment cellular vitality was evaluated with the resazurin test and the protocol adopted to this assay was as follows.

#### **Protocol 1:**

- ❖ Add 20  $\mu$ L of resazurin for every 100  $\mu$ L of the medium present in the wells, then add 60  $\mu$ L of resazurin each well.
- ❖ Incubate for 3 hours at 37°C in a cell culture incubator, protected from direct light.
- ❖ Transfer the contents of the wells to a black multiwell.
- ❖ Read fluorescence using a fluorescence excitation wavelength of 525 nm.

This protocol was carried out for three time steps, after 24 hours, after 72 hours and after 7 days. The procedure of 1<sup>st</sup> experiment was summarized in the Table 3.5-1.

**Table 3.5-1** 1<sup>st</sup> Experiment procedure.

	Samples	Control 1
Density	30000cell/100 µL gel	30000cell/300 µL medium
N° of samples for time step	6	2
Time step	24h-72h-7d	24h-72h-7d
Assay	Resazurin Cell Viability Assay <sup>110</sup>	Resazurin Cell Viability Assay <sup>110</sup>

The results of this experiment are not reported as the data are considered not significant due to the variance in the samples number and in the seeding procedure.

### 3.5.6.2 2<sup>nd</sup> Experiment

The second experiment was made to achieve the optimal cell density to use in subsequent experiments. In this experiment, two different densities were studied, 100000 cells /100 µL collagen and 200000 cells/ 100 µL of collagen. Only one control was carried out with 30000 cells in 300 µL of medium. Three samples for every density were tested for each time step and the time points were set at 24h 72h and 7 days. After performing the seeding protocol and the counting the of cells, the two volumes of cellular suspension have been calculated as follows:

$$N^{\circ} cells = \left(\frac{49}{4}\right) * 10000 * 25mL = 3062500 \text{ cells}$$

$$3062500:25 = 900000:V1_{coll}$$

$$V1_{coll} = 7,35mL$$

$$3062500:25 = 1800000:V2_{coll}$$

$$V2_{coll} = 14,7mL$$

$$3062500:25 = 30000:V3$$

$$V3 = 0,245mL$$

The first two volumes were taken and inserted into a tube and then they were centrifuged to generate the two pellets. The two pellets were broken with 900 µL of hydrogel and 300 µL of medium, then 100 µL of collagen and cells was inserted in each well. The gel was made to reticular for 30 minutes in incubator at 37°, then 300 µL of medium were added in every wells. While the third volume was directly taken and inserted into a well, then 300 µL medium and cells were added.

In this experiment cellular vitality was evaluated with CellTiter-Glo® 3D Cell Viability Assay and the protocol adopted to this assay was as follows.

#### **Protocol 2:**

- ❖ Add a volume of CellTiter-Glo® 3D Reagent equal to the volume of cell culture medium present in each well, add 300µL of CellTiter-Glo® 3D Reagent to 300µL of medium containing cells.

- ❖ Mix the contents for 5 minutes to induce cell lysis.
- ❖ Allow the plate to incubate at room temperature on the bascule for an additional 10 minutes to stabilize the luminescent signal.
- ❖ Record luminescence with absorbance/luminescence- based plate readers.

This protocol was carried out for three time steps, after 24 hours, after 72 hours and after 7 days. The procedure of 2<sup>nd</sup> experiment was summarized in the Table 3.5-2.

*Table 3.5-2 2<sup>nd</sup> Experiment procedure.*

	Samples 1	Samples 2	Control 1
Density	100000cell/200 $\mu$ L gel	200000cell/200 $\mu$ L gel	30000cell/300 $\mu$ L medium
N° of samples for time step	3	3	1
Time step	24h-72h-7d	24h-72h-7d	24h-72h-7d
Assay	CellTiter-Glo® 3D Cell Viability Assay by Promega <sup>108</sup>	CellTiter-Glo® 3D Cell Viability Assay by Promega <sup>108</sup>	/

### 3.5.6.3 3<sup>rd</sup> Experiment

This experiment was carried out to evaluate the vitality of fibroblasts in the bottom layer of the device. The bottom layer was bonded to the laboratory slide and two different layouts were assessed, the first presented a needle as reservoir and the second instead the reservoirs in PDMS. Two layout devices were tested with 10000 cells in 3  $\mu$ L collagen and two with only 10000 cells in 3  $\mu$ L medium as controls. Other two types of controls were carried out, one with 30000cells in 300  $\mu$ L of medium and 320000 cells in 150  $\mu$ L of collagen hydrogel. In this experiment only one time step was performed at 72 h. To obtain the volumes of cell suspension that correspond to the correct number of cells the following mathematical calculates has been made:

$$N^{\circ}cells = \left(\frac{40}{4}\right) * 10000 * 20mL = 2000000 cells$$

$$2000000: 20 = 40000: V1_{coll-chip}$$

$$V1_{coll-chip} = 0,4 mL$$

$$2000000: 20 = 40000: V2_{chip}$$

$$V2_{chip} = 0,4 mL$$

$$2000000: 20 = 640000: V3_{coll}$$

$$V3_{ctrl\_coll} = 6,4 mL$$

$$2000000: 20 = 30000: V4_{ctrl\_midium}$$

$$V4_{ctrl\_midium} = 0,3 mL$$

These volumes were taken and inserted into different tubes and then they were centrifugated to generate the pellets. The pellet first was broken with 12  $\mu\text{L}$  of hydrogel and, then 3  $\mu\text{L}$  of collagen and cells were inserted in each device, two for each layout. While the pellet two was broken with 20  $\mu\text{L}$  of medium, then 5  $\mu\text{L}$  of medium and cells were inserted in four devices, two for each layout. The pellet three was broken with 300  $\mu\text{L}$  of hydrogel and 100  $\mu\text{L}$  of medium, then 150  $\mu\text{L}$  of collagen and cells was inserted in each well, two for time step. While the pellet four was broken with 300  $\mu\text{L}$  of medium and inserted into each well, two for time step. The gel was made to reticular for 30 minutes in incubator at 37°, then 300  $\mu\text{L}$  of medium were added in every well and 20  $\mu\text{L}$  were added into every reservoir.

In this experiment cellular vitality was evaluated with LIVE/DEAD™ Viability/Cytotoxicity Kit, for mammalian cells and the protocol adopted to this assay was as follows.

**Protocol 3:**

- Thaw vials.
- Prepare solution following mathematical calculates:
  - $5 \mu\text{L calcein AM} : 10\text{mL DPBS} = X : \text{DPBS volume deiderate}$
  - $20 \mu\text{L EtdH} - 1 : 10\text{mL DPBS} = X : \text{DPBS volume deiderate}$
- Remove medium from cells.
- Add 20  $\mu\text{L}$  of solution in each channel of the device and add 300  $\mu\text{L}$  of solution in each well.
- Incubate 40 minutes at 20–25°C on the bascule.
- Image the cells.

The procedure of 3<sup>rd</sup> experiment was summarized in the Table 3.5-3.

*Table 3.5-3 3<sup>rd</sup> Experiment procedure.*

	Samples 1-Layout 1	Samples 2-Layout 2	Control 1-Layout 1	Control 2-Layout 2	Control 3	Control 4
Density	10000cell /3 $\mu\text{L}$ gel	10000cell /3 $\mu\text{L}$ gel	10000cell /3 $\mu\text{L}$ medium	10000cell /3 $\mu\text{L}$ medium	320000cell/ 130 $\mu\text{L}$ gel	
N° samples	2	2	2	2	2	1
Time step	72h	72h	72h	72h	72h	72h
Assay	LIVE/DEAD <sup>107</sup>	LIVE/DEAD <sup>107</sup>	LIVE/DEAD <sup>107</sup>	LIVE/DEAD <sup>107</sup>	LIVE/DEAD <sup>107</sup>	LIVE/DEAD <sup>107</sup>

#### 3.5.6.4 4<sup>th</sup> Experiment

This experiment was carried out to evaluate the vitality of PSCs in the bottom layer of the device and in the hydrogel of collagen. In this experiment 10000 cells in 3  $\mu$ L collagen were seeded in each bottom layer with reservoir, four for each time steps. Three types of controls were carried out, in the first type, four bottom layers were seeded with 10000 cells in 3  $\mu$ L of medium in each one, four for each time step. In the second type of control 320000 cells in 150  $\mu$ L of collagen hydrogel was seeded in each wells, two for each time step, and in the last control 30000 cells in 300  $\mu$ L of medium was seeded in each wells, two for time step. In this experiment two time step were performed at 48h 72h. To obtain the volumes of cell suspension that correspond to the correct number of cells the following mathematical calculates has been made:

$$N^{\circ}cells = \left(\frac{82}{4}\right) * 10000 * 15mL = 3075000 \text{ cells}$$

$$3075000: 15 = 80000: V1_{coll-chip}$$

$$V1_{coll-chip} = 0,39 \text{ mL}$$

$$3075000: 15 = 80000: V2_{chip}$$

$$V2_{chip} = 0,39 \text{ mL}$$

$$3075000: 15 = 1280000: V3_{coll}$$

$$V3_{ctrl\_coll} = 6,25 \text{ mL}$$

$$3075000: 15 = 120000: V4_{ctrl\_midium}$$

$$V4_{ctrl\_midium} = 0,56 \text{ mL}$$

These volumes were taken and inserted into different tubes and then they were centrifuged to generate the pellets. The first pellet was broken with 24  $\mu$ L of hydrogel and, then 3  $\mu$ L of collagen and cells was inserted in each device. While the pellet two was broken with 40  $\mu$ L of medium, then 5  $\mu$ L of medium and cells were inserted into each device. The pellet three was broken with 600  $\mu$ L of hydrogel and 200  $\mu$ L of medium, then 150  $\mu$ L of collagen and cells was inserted in each well. While the pellet four was broken with 1,2 mL of medium and 300  $\mu$ L of cells and medium was inserted in each well. The gel was made to reticular for 30 minutes in incubator at 37°, then 300  $\mu$ L of medium were added every well and 20  $\mu$ L were added into every reservoir of device.

In this experiment cellular vitality was evaluated with LIVE/DEAD™ Viability/Cytotoxicity Kit, for mammalian cells and with DAPI/Phalloidin assay. For LIVE/DEAD the protocol adopted was the previous one (**Protocol 3**), while for DAPI/Phalloidin the protocol adopted was as follows.

**Protocol 4:**

- Remove medium from each channel of device.
- Rinse with PBS.
- Fix with PFA at 4% (Paraformaldehyde), add 20  $\mu\text{L}$  of PFA each channel.
- Incubation of the device at room temperature for 40 minutes.
- Remove PFA.
- Rinse with PBS for two times.
- Addition of Triton X-100 (0.5%) in PBS for 10 minutes to permeabilize cellular membranes.
- Rinse with PBS for two times.
- Incubate cells with 1% BSA (Stain buffer) in PBS (PBS+ 1% of BSA) for 30 min to block unspecific binding of the antibodies.
- Rinse with PBS.
- Add phalloidin to BSA and PBS with a volume ratio of 1:60.
- Incubate cells with phalloidin-BSA solution for 40 minutes.
- Rinse with PBS.
- Add DAPI to PBS with a volume ratio of 1:1000.
- Incubate cells with DAPI-PBS solution for 5 minutes.
- Rinse with PBS.
- Remove PBS.
- Observe the cells.

The procedure of 4<sup>th</sup> experiment was summarized in the Table 3.5-4.

*Table 3.5-4 4<sup>th</sup> Experiment procedure.*

	Samples 1- Layout 1	Control 1- Layout 1	Control 3	Control 4
Density	10000cell/3 $\mu\text{L}$ gel	10000cell/3 $\mu\text{L}$ medium	320000cell/130 $\mu\text{L}$ gel	30000cell/300 $\mu\text{L}$ medium
N <sup>o</sup> samples	4	4	2	2
Time step	48h-72h	48h-72h	48h-72h	48h-72h
Assay	LIVE/DEAD <sup>107</sup> DAPI/Phalloidine	LIVE/DEAD <sup>107</sup> DAPI/Phalloidine	LIVE/DEAD <sup>107</sup>	LIVE/DEAD <sup>107</sup>

### 3.5.6.5 5<sup>th</sup> Experiment

This experiment was carried out to evaluate the vitality of HPDE-KRAS cells seeded in the top layer and on the membrane of PCL/GEL. The top layer and reservoir were bonded on laboratory slides.

In this experiment four top layers and reservoir for each time step were seeded with 35000 cells in 5  $\mu$ L of medium. Two types of controls were carried out, in the first type of control three wells for each time step was seeded with 40000 cells in 300  $\mu$ L of medium, in the last type of control for each time step, three slides of 1.9 cm<sup>2</sup> of area covered with the PCL/GEL membrane were seeded with a drop of 15  $\mu$ L containing 50000 cells. Cell activity was analysed at 24h, 48h and 72h. To obtain the volumes of cell suspension that correspond to the correct number of cells the following mathematical calculates has been made:

$$N^{\circ}cells = \left(\frac{61}{4}\right) * 10000 * 12mL = 7380000 \text{ cells}$$

$$7380000:12 = 444000:V1_{chip}$$

$$V1_{hip} = 0,72mL$$

$$7380000:12 = 450000:V2_{memb}$$

$$V2_{memb} = 0,73mL$$

$$7380000:12 = 360000:V3_{ctrl}$$

$$V3_{ctrl} = 0,56mL$$

These volumes were taken and inserted into different tubes and then they were centrifugated to generate the pellets and they were seeded correctly. After 40 minutes in incubator at 37°, 300  $\mu$ L of medium were added in every well and 20  $\mu$ L were added into every reservoir.

LIVE/DEAD™ Viability/Cytotoxicity Kit, for mammalian cells and with DAPI/Phalloidin assay were used to study the different samples. For LIVE/DEAD assay the **Protocol 3** was adopted while for DAPI/Phalloidin assay was used **Protocol 4**.

The procedure of 5<sup>th</sup> experiment was summarized in the Table 3.5-5.

**Table 3.5-5** 5<sup>th</sup> Experiment procedure.

	Samples 1-Layout 1	Control 1- membrane	Control 3
Density	35000 cell/5 $\mu$ L medium	50000 cell/15 $\mu$ L medium	40000 cell/300 $\mu$ L medium
N° samples	4	3	3
Time step	24h-48h-72h	24h-48h-72h	24h-48h-72h
Assay	LIVE/DEAD <sup>107</sup> DAPI/Phalloidine	LIVE/DEAD <sup>107</sup> DAPI/Phalloidine	LIVE/DEAD <sup>107</sup>

### 3.5.6.6 6<sup>th</sup> Experiment

Experiment six consisted of the co-culture of the PSCs and HPDE-KRAS. Two complete devices were tested for each time step and three types of controls were carried out, while a complete chip has been tested for each time step with only PSCs, one well for each time

step was seeded with PSCs and collagen and three wells for each time step were seeded with HPDE. In this experiment three time step was performed at 24h, 48h and 72h. To obtain the volumes of PSCs cell suspension that correspond to the correct number of cells the following mathematical calculates has been made:

$$N^{\circ}PSCs = \left(\frac{33}{4}\right) * 10000 * 12mL = 990000 \text{ cells}$$

$$990000: 12 = 990000: V1_{PSCs}$$

$$V1_{PSCs} = 12 \text{ mL}$$

The tube was centrifuged to generate the pellet, that was broken with 297  $\mu$ L of hydrogel and 50  $\mu$ L of medium, then 3  $\mu$ L of collagen and cells was inserted in the bottom layer of each device, and 45  $\mu$ L of collagen and cells was inserted in the six wells. Then 105  $\mu$ L of collagen was added to the six wells. The gel was made to reticular for 30 minutes in incubator at 37°, then were added the HPDE-KRAS cell. To obtain the volumes of HPDE cell suspension the following mathematical calculates has been made:

$$N^{\circ}HPDE - KRAS = \left(\frac{255}{4}\right) * 10000 * 18mL = 11495000 \text{ cells}$$

$$11495000: 18 = 210000: V2_{HPDE}$$

$$V2_{HPDE} = 0,329 \text{ mL}$$

$$11495000: 18 = 360000: V3_{HPDE}$$

$$V3_{HPDE} = 0,595 \text{ mL}$$

These volumes were taken and inserted into different tubes and then they were centrifuged to generate the pellets. The first pellet was broken with 30  $\mu$ L of medium and, then 5  $\mu$ L of medium and cells was inserted in each top layer of device. While the pellet two was broken with 2,7 mL of medium, then 300  $\mu$ L of medium and cells were inserted into each well. After 40 minutes in incubator at 37°, 20  $\mu$ L of medium were added into every reservoir.

In this experiment the PSCs and PDAC cell lines were cultured and maintained in DMEM supplemented with 10% FBS, 1% Pen-Strep, and 1% amphotericin B.

LIVE/DEAD™ Viability/Cytotoxicity Kit, for mammalian cells and with DAPI/Phalloidin assay were used to study the different samples, and the **Protocol 3** **Protocol 4** previously described were applied.

The procedure of 6<sup>th</sup> experiment was summarized in the Table 3.5-6.

**Table 3.5-6** 6<sup>th</sup> Experiment procedure

	Samples 1	Control 1	Control 2	Control 3
Density	10000 cell <sub>PSCs</sub> /3 $\mu$ L Gel + 35000 cell <sub>HPDE-KRES</sub> /5 $\mu$ L medium	10000 cell <sub>PSCs</sub> /3 $\mu$ L Gel	40000cell <sub>HPDE</sub> /300 $\mu$ L medium	150000 cell <sub>PSCs</sub> /150 $\mu$ L Gel
N° samples	2	1	3	1
Time step	24h-48h-72h	24h-48h-72h	24h-48h-72h	24h-48h-72h
Assay	LIVE/DEAD <sup>107</sup> DAPI/Phalloidine	LIVE/DEAD <sup>107</sup>	LIVE/DEAD <sup>107</sup>	LIVE/DEAD <sup>107</sup>

## 4. Results and Discussion

### 4.1 Mold characterization

In the bottom layer, micropillars represent both an added value and a challenging element to be fabricated and for this reason in accordance with the work carried out by Marasso et al. photolithography with SU-8 was chosen to produce the mold in SU-8. The mold of the bottom layer obtained by SU-8 photolithography with the protocols previously described have been analysed with the profilometer and the digital microscope. Profilometer allows measuring the height of pattern in SU-8 while digital microscope allows for observing the pattern surface, only with T7 process is obtained a defect-free master and with 220  $\mu\text{m}$  of thickness, according to the measures already described. To achieve these characteristics, exposure and development times have been optimized. Exposure times have been increased in order to augment the responsiveness of the substrate, whereas, and development time has been reduced to ensure both the development of the cavities used for the pillars and the desired height.

Instead, the mold of top layer was characterized only using the digital microscope, values of the diameters of inlet and outlet, and the channel dimensions were acquired with Leica software and then analysed in Excel. Process three (P3) was employed to produce a mold with the desired dimensions and a low number of defects. In fact, in this process a lower speed has been applied and this allows machining the PMMA efficiently. In addition, the line spacing has been changed to produce patterns with less defects (Figure 4.1.1). The final dimension of the channel in the mold are 12 mm long, 0,4 mm wide and 0,5 mm high. Inlets and outlet result of 2,2 mm of diameters. Furthermore, the wall of channel is not perpendicular, but it is oblique, this is a result of an aberration related to the laser galvo head lens.



*Figure 4.1.1 Top layer mold.*

This technique has a low precision but is a fast process, for this reason it has been chosen for the mold of top layer, which has a simpler geometry than the top layer.

## 4.2 Device characterization

Replicas in PDMS and their heights were evaluated with digital microscope. Figure 4.2.1 shows bottom layer and top layer replicas in PDMS.

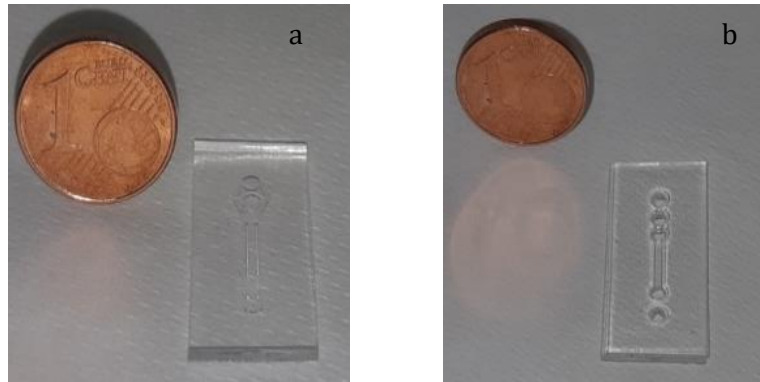


*Figure 4.2.1 a) Bottom layer replica in PDMS. b) Top layer replica in PDMS*

Focusing on bottom layer replica, digital microscope allows for studying the surface of the replica, the development of micropillars and the height of the pattern (Figure 4.2.2). Regarding models A and B, the micropillars are completely developed while the micropillars of models C and D have defects and are not fully developed. The values of the diameters, the distances between the micropillars and the heights were acquired through the Leica software and then they were reported on Excel. Then average values of the diameters, distances and heights relative to the four models of the bottom layer have been calculated.

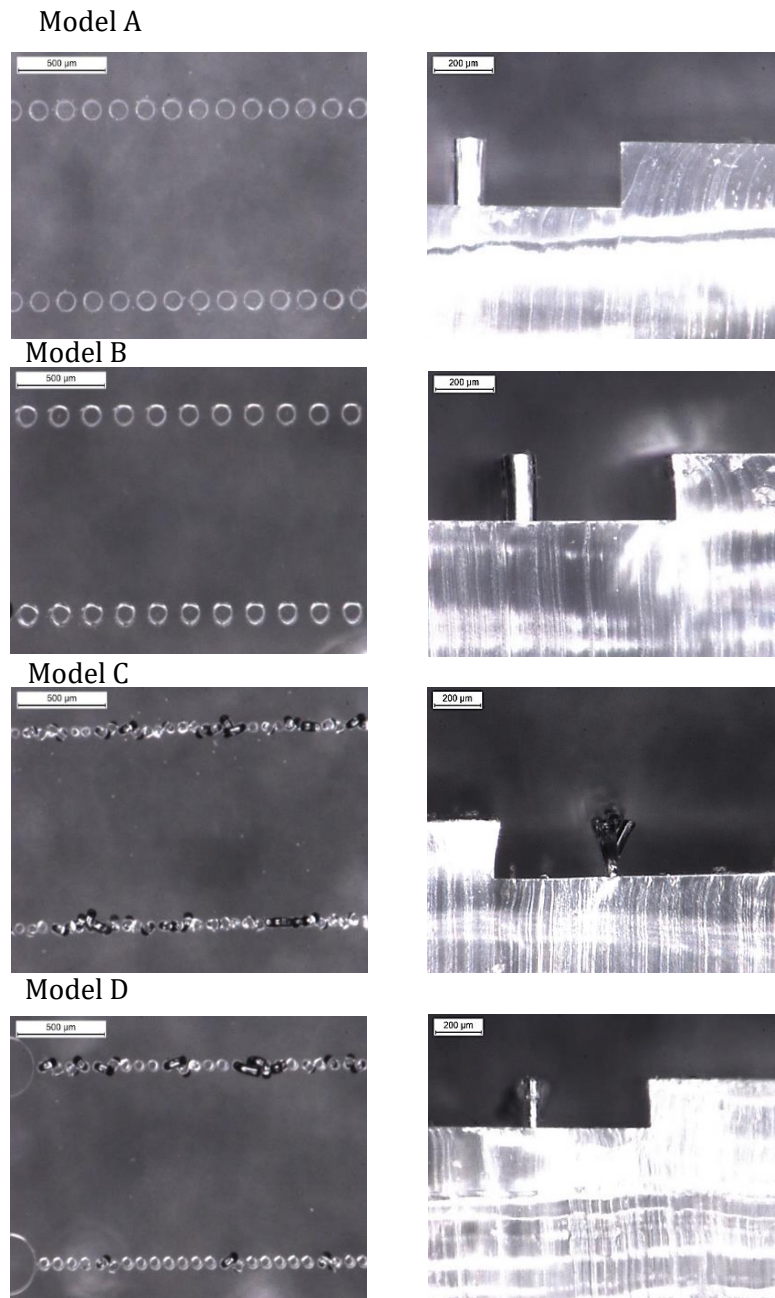


**Figure 4.2.2** Microscopic images of PDMS replicas of the four layouts. On the left are visible the upper views and, on the right, the sectional views of the micropillars.

As shown in Table. 4.2-1, only for models A and B was possible to take the measurements of height and for these models the values of the diameters and the distances between the micropillars resulted similar to the desired dimensions.

**Table 4.2-1** Average values of micropillar diameters, spaces between them, and heights, calculated on six samples for each model.

	DIAMETERS		GAP		HEIGHT	
	Replica[ $\mu\text{m}$ ]	CAD [ $\mu\text{m}$ ]	Replica[ $\mu\text{m}$ ]	CAD [ $\mu\text{m}$ ]	Replica[ $\mu\text{m}$ ]	CAD [ $\mu\text{m}$ ]
<b>A</b>	106 $\pm$ 1	100	47 $\pm$ 1	50	207 $\pm$ 3	200
<b>B</b>	105 $\pm$ 2	100	79 $\pm$ 2	75	212 $\pm$ 3	200
<b>C</b>	43 $\pm$ 3	50	15 $\pm$ 3	25	/	200
<b>D</b>	41 $\pm$ 3	50	19 $\pm$ 5	15	/	200

The FESEM also confirmed that models A and B are the only ones that do not present impurities, are fully developed and with the pre-established measures (Figure 4.2.3).

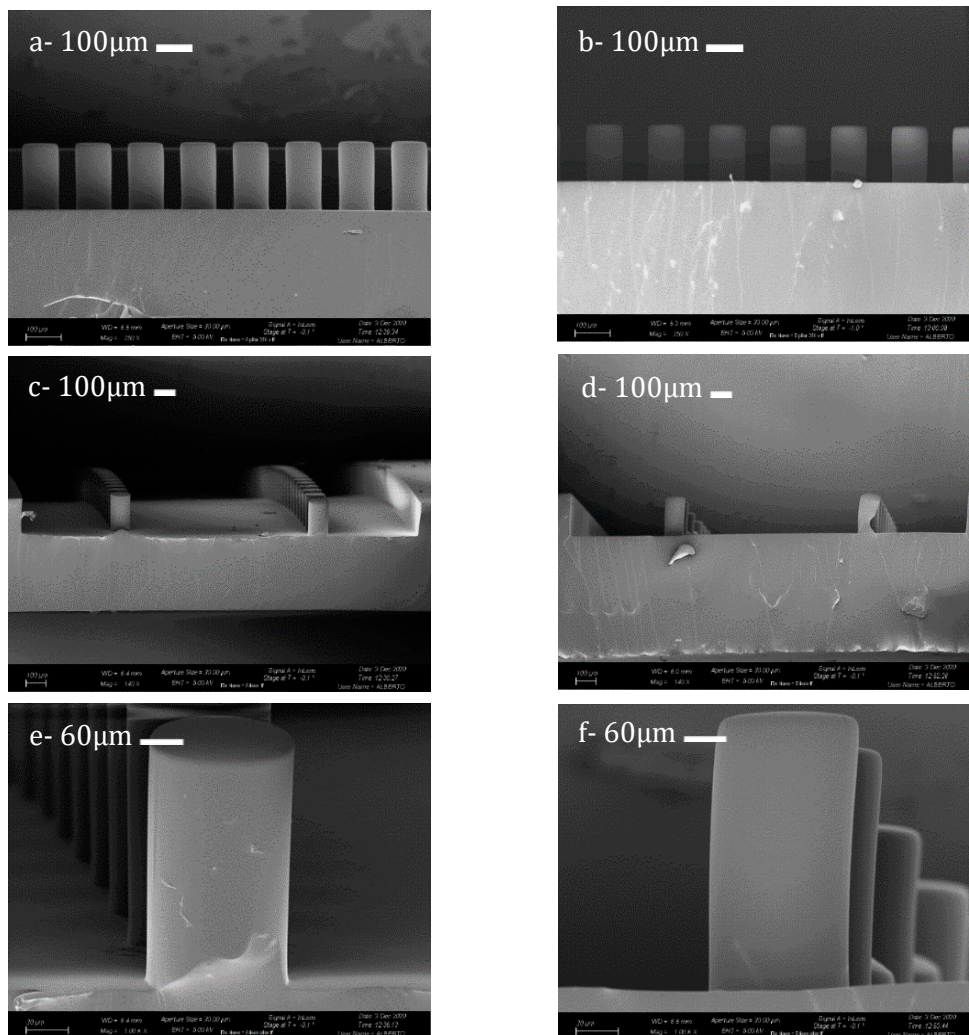


**Figure 4.2.3** FE-SEM images of Bottom layers A (left) and B (right). The first line (a-b) corresponds to the sagittal section of the chip, the second corresponds to the frontal section, and the third line is an enlargement on the micropillars.

Also surface and section of top layer replica were studied using digital microscope (Figure 4.2.4). The channel in the replica are 13 mm long, 0,6 mm wide and 0,5 mm high. Inlets and outlet result of 2,5 mm of diameter despite of 2 mm desired but this is not a problem because to produce the holes it was used a biopsy puncher of 1.5mm.

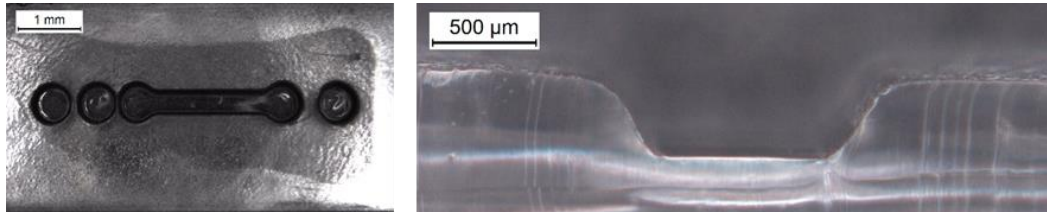


**Figure 4.2.4** Microscopic images of PDMS replica of the Top layer. On the left are visible the upper views and, on the right, the sectional views of the replica.

Furthermore, digital microscope allows for evaluating the section of complete chip. It has been possible observe that membrane in PCL/Gel is perfectly supported by the two rows of micropillars and it results completely flat, how it possible observe in the figure below where a section image at the optical microscopy and a photo of the assembled device were reported (Figure 4.2.5).

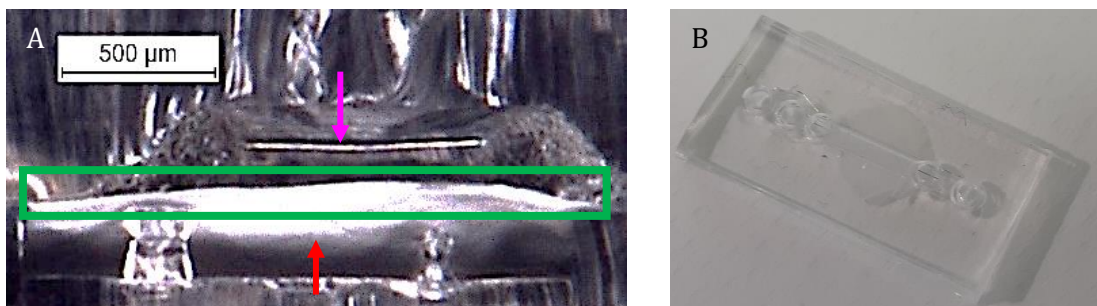


**Figure 4.2.5** A) Image of section of complete microdevice: green rectangular highlight PCL/Gel membrane; pink arrow indicate top layer and red arrow indicate bottom layer. B) complete device

## 4.3 Fluidic characterization

### 4.3.1 Capacity test

Preliminary tests on assembled device to study mechanical stability were performed using dyed solutions. In these tests, the dyed fluid was inserted in the central channel of both bottom and top layers. No losses are observed, and the result is reported in the Figure 4.3.1.

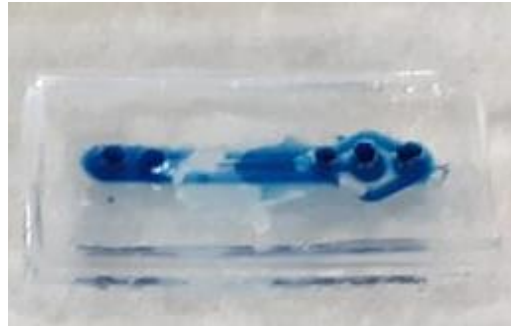


*Figure 4.3.1 Images of capacity test on complete device.*

Although this is not a quantitative test, it clearly confirms the tightness of bonding produced by plasma oxygen with parameters set for the process.

The Figure 4.3.2 reports the results of capacity test on bottom layer bonded on the microscope slide. The micropillars with high aspect ratio represent an added value, and in order to choose between the two typologies, A and B, two different tests have made. In the first tests, the dyed fluid and a collagen hydrogel were inserted in the central channel of bottom layer bonded to microscope slide. From these tests it emerged that both types well confine water-based liquids and collagen hydrogel into central channel.

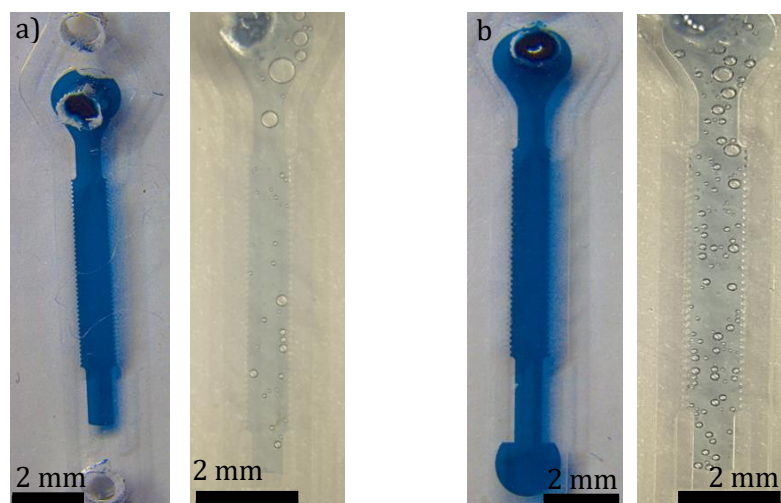
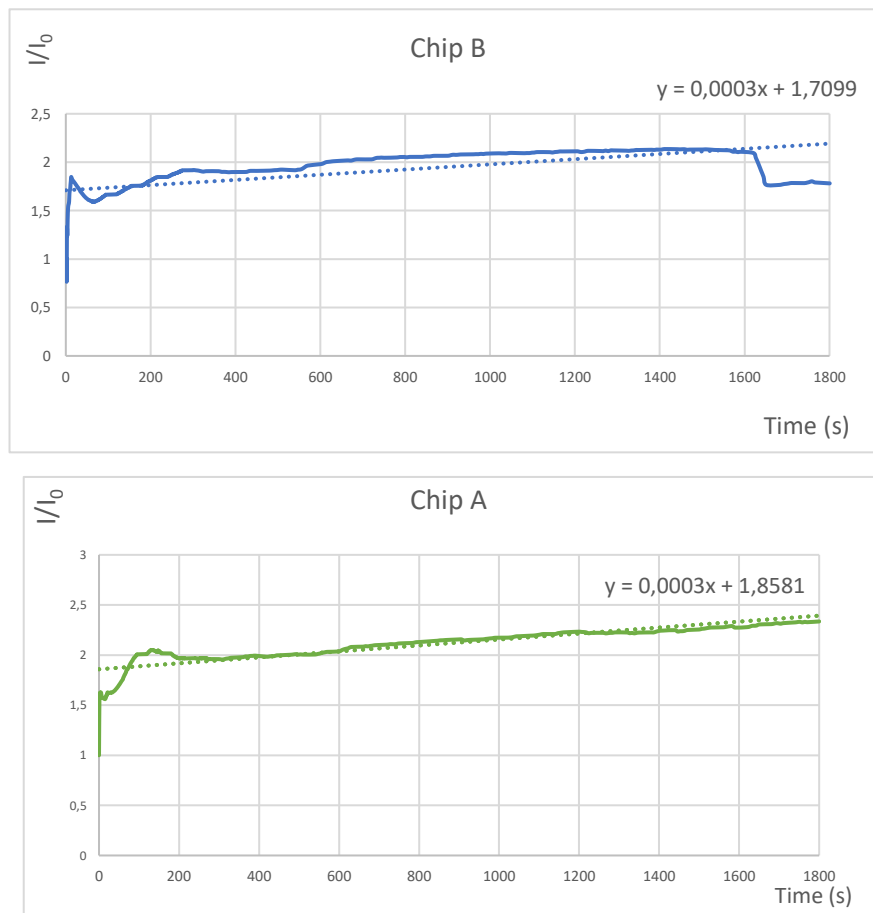


*Figure 4.3.2 a) Images of capacity test on model A bottom layer with dyed fluid and with hydrogel. b) Images of capacity test on model B bottom layer with dyed fluid and with hydrogel*

### 4.3.2 Diffusivity test

Graph 4.3-1 reports plots relative to the measurements of the fluorescence intensity at different time intervals for both typologies of layout. The average fluorescence intensity of the different ROIs was indicated as  $I_0$  at time  $t = 0$  s, while for  $t > 0$  s it was generically indicated as  $I$ . The first peaks of intensity are due to the insertion of the fluorescent dye with the micropipette. In both types, the growth of fluorescence is linear, so the fluorescent dye diffuses linearly within the collagen hydrogel for both 75  $\mu\text{m}$  and 50  $\mu\text{m}$  inter-micropillar distances. In addition, the angular coefficient of the interpolation line which indicates the diffusivity coefficient in the collagen hydrogel is the same for both layouts.

However, the model with pillars of 100  $\mu\text{m}$  of diameter, with a gap of 75  $\mu\text{m}$  and a height of 200  $\mu\text{m}$  has proved to be the most promising model and it is a compromise between dye retention inside the central channel and liquid diffusion through pillars gaps, because the central channel is completely fluorescent in less than 30 minutes, and the replicas of this version has more similar dimension to the predetermined one.



**Graph 4.3-1** Fluorescence intensity at different time intervals. Graphs representing the average fluorescence intensity measured in the Chip A, in the Chip B.

## 4.4 Biological characterization

The response of HFF-1, PSCs and HPDE cells was evaluated in terms of proliferation, viability and cell morphology.

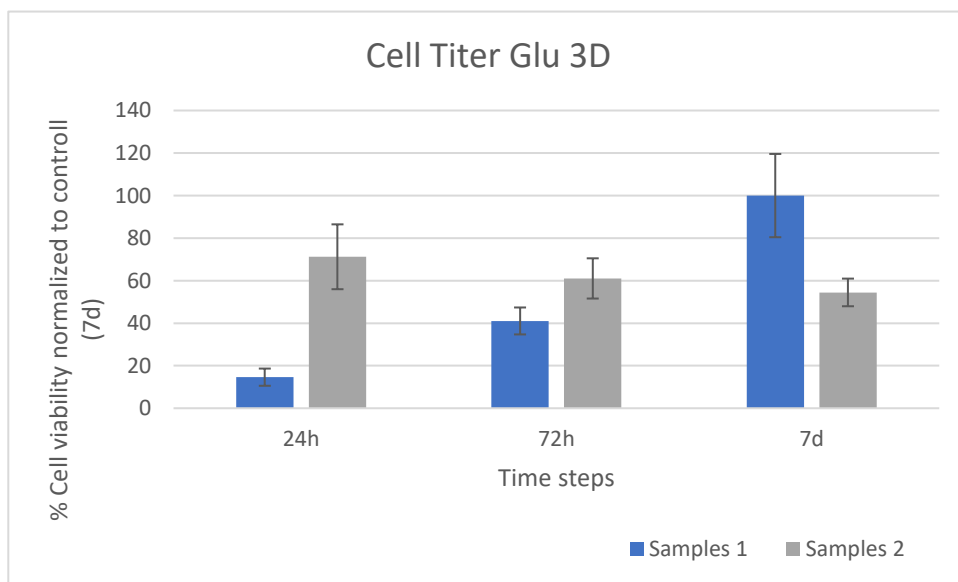
### 4.4.1 HFF-1 culture

Fibroblasts were used because they have a phenotype similar to that of PSCs. Graph 4.4-1 reports the graphs relative to the resazurin assay. However, the results relative to the 1st Experiment are not reported due to collagen volume of the strips were not the same in all the samples. Consequently, the absorbance values were no significant. Nonetheless, collagen hydrogel shows good biological properties for fibroblasts growth as demonstrated in the works of Katrin Bott et al.<sup>114</sup> and Tabatabaei et al.<sup>115</sup>.

This test was repeated by changing some parameters, such as cell densities and collagen matrix shape. CellTiterGlo3D was performed to assess from which cell density to start tests for microfluidic device characterization.

The cell viability showed on the y-axis has been obtained by measuring the light that has been emitted by each sample, and the values were normalized to control at 7 day (Samples 1). Graph 4.4-1 shows the graphs relative to the CellTiterGlo3D.

A lower cell density allows for greater cell proliferation.



**Graph 4.4-1** CellTiterGlo3D Assay performed on two densities of HFF-1 seeded in collagen hydrogel. The measurements were carried out at 24h 72h and 7 days and the results have been normalized to control at 7 day (Samples 1).

The latest culture with fibroblasts was implemented to analyse the effect that the bottom layer of the device has on the cells.

The experiment were performed on 2 typologies of layout to compare the cellular response: the bottom layer with needle as reservoir and the bottom layer with reservoir in PDMS bonded on microscope slide. Both types were tested with collagen hydrogel and without, in addition, the behaviour of fibroblasts within the collagen gel and on the 2D support was evaluated. The culture of HFF-1 cells was monitored and their growth was observed with digital imaging system. The Figure 4.4.1 shows the culture of fibroblasts inside the chip with the PDMS reservoir at 24 hours, 48 hours and 72 hours after seeding.

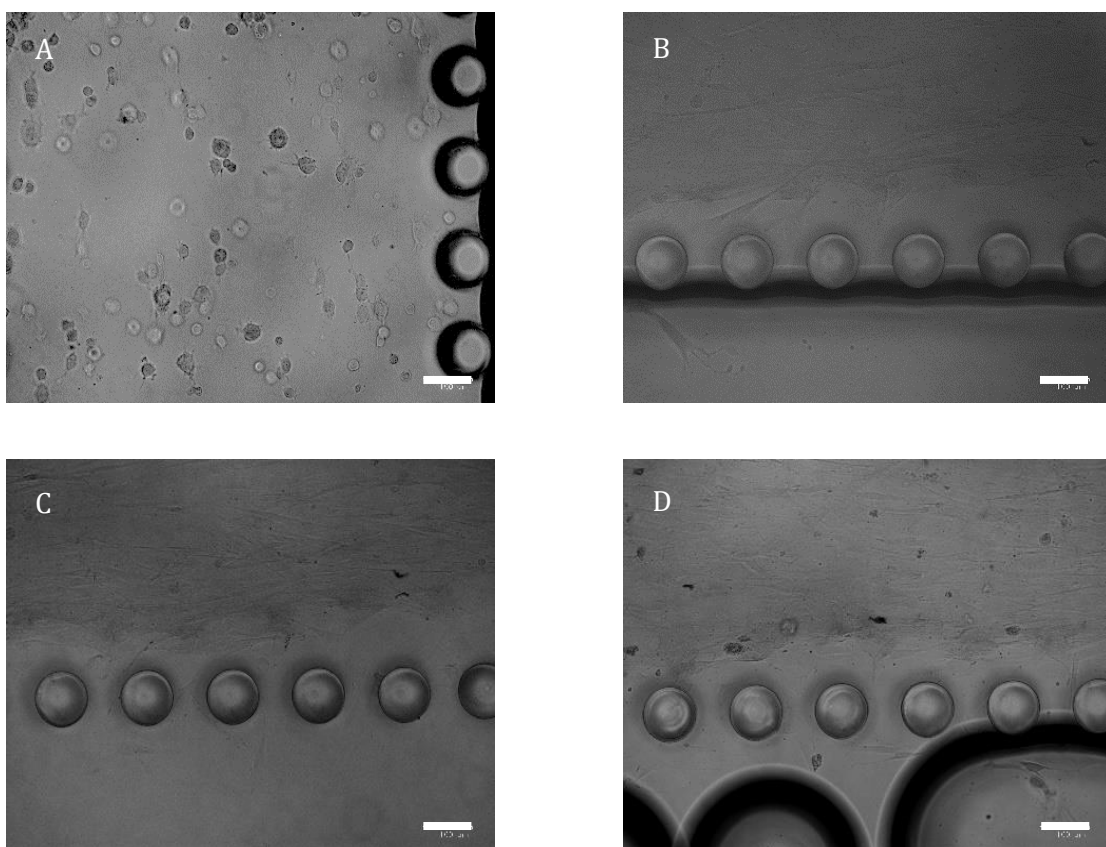


**Figure 4.4.1** HFF-1 growth inside collagen hydrogel in the bottom layer. A) Just seeded B) 24h after seeding c)48h after seeding D) 72h after seeding. The scale bars correspond to 100 µm.

The LIVE/DEAD assay was performed at 72 hours after seeding to study the cellular vitality in the different samples.

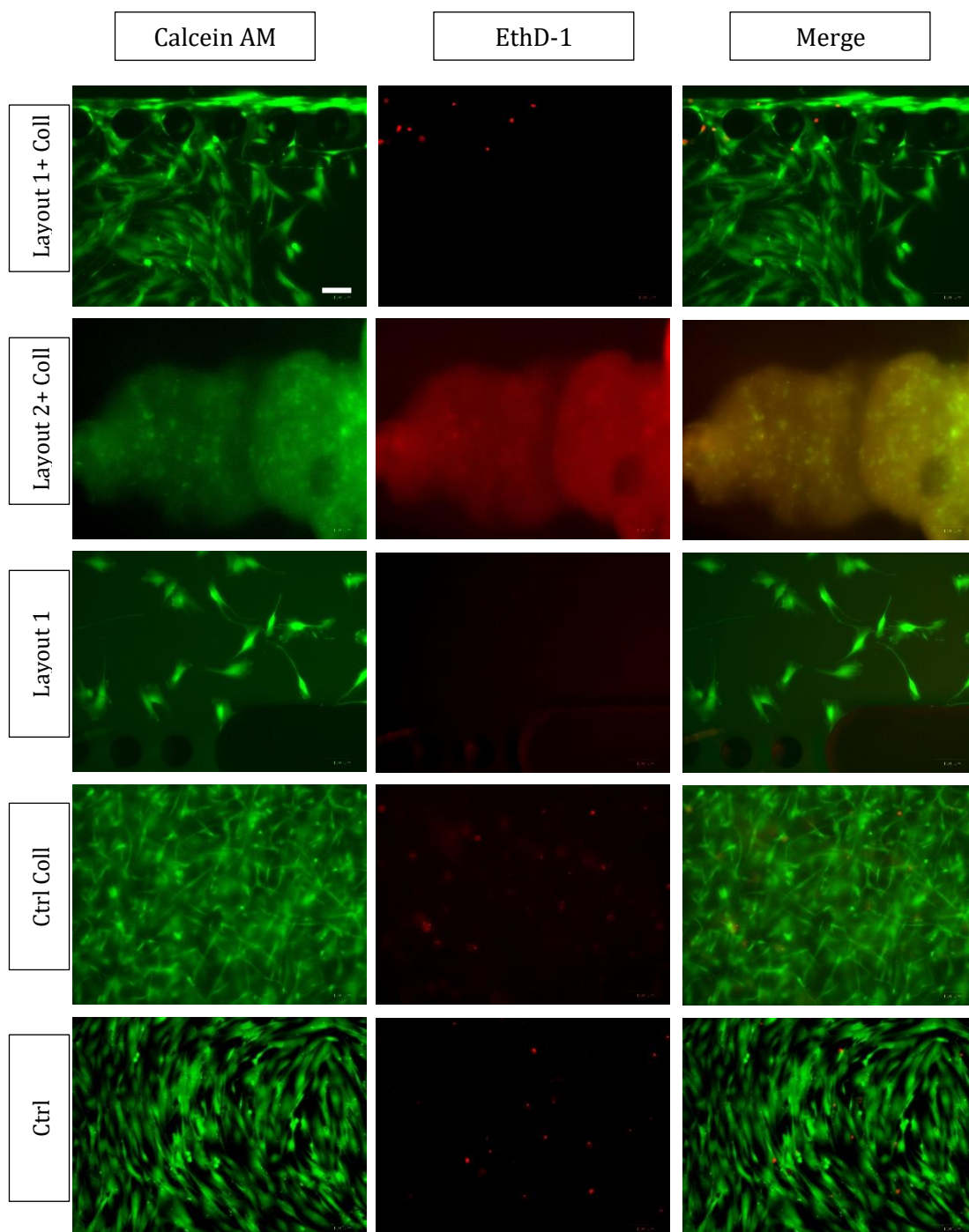


**Figure 4.4.2** Cells were stained with calcein AM and EthD-1 after 72h of culture. The scale bar is the same for all images and corresponds to 100  $\mu$ m.

The Figure 4.4.2 reports the images of LIVE/DEAD. In accordance with both experimental works of Lee et al<sup>116</sup>. and Kyung Eun Sung et al<sup>117</sup>, HFF-1 cells cultured into the bottom layer with reservoir in PDMS loaded with collagen hydrogel (Layout 1+ Coll) are vital and show the typical morphology of fibroblasts, with large areas of flattened cytoplasm surrounding a centralised nucleus. In addition, although some studies in

literature show a higher gap between the micropillars these results demonstrate that the cell vitality is not affected by a lower distance between each micropillar<sup>116</sup>. Cells are vital even in the chip with the layout 1 without collagen hydrogel despite the number of cells is lower in the hydrogel-free chip than the hydrogel containing chip.

Instead, the hydrogel in the sample with the second configuration is dry and the cells dead, furthermore, the control chip with layout 2 has not been reported because the cells were already dead after 48 hours. These results are attributable to the use of needles as reservoirs, since they did not allow the passaging of the medium.

Thus, collagen hydrogel in microfluidic channel allows the formation of chemical and biological gradients that have ensured the vitality of the cells and their 3D conformation as claimed by Fahima Akther et al <sup>118</sup>.

Moreover, in agreement with Bott et al <sup>114</sup>, fibroblasts encapsulated within collagen gels exhibit a higher degree of cell spreading and the formation of interconnected multicellular networks at earlier time points. In accordance with Vanesa Olivares et al., collagen properties such as biocompatibility, porosity, biodegradability, and collagen-to-cell ligand binding make collagen an excellent choice to reproduce the physiological cell behaviour<sup>119</sup>.

#### 4.4.2 PSCs culture

The PSCs were selected as they are the most important cellular component of the stroma of PDAC and play a key role in tumour progression. This experiment with PSCs has been executed to investigate the effect that the bottom layer of the device and the collagen hydrogel have on the pancreatic stromal cells. The experiment has been performed on the bottom layer with PDMS reservoir bonded on microscope slide. Controls without hydrogel were also implemented. In this experiment, PSCs were monitored, and their growth was observed with digital imaging system up to 4 days. The captured images of cells and hydrogel are shown in Figure 4.4.3.

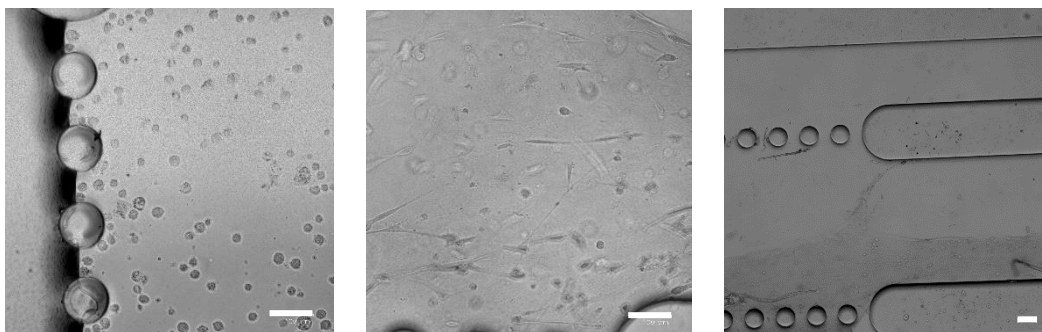


**Figure 4.4.3** PSCs growth in collagen hydrogel in the bottom layer. A) Just seeded B) 48h after seeded C) 72h after seeded. The scale bar corresponds to 100  $\mu$ m.

Cellular vitality was studied with LIVE/DEAD assay only at 48 hours after seeding and the images of the samples and controls are reported in Figure 4.4.4.

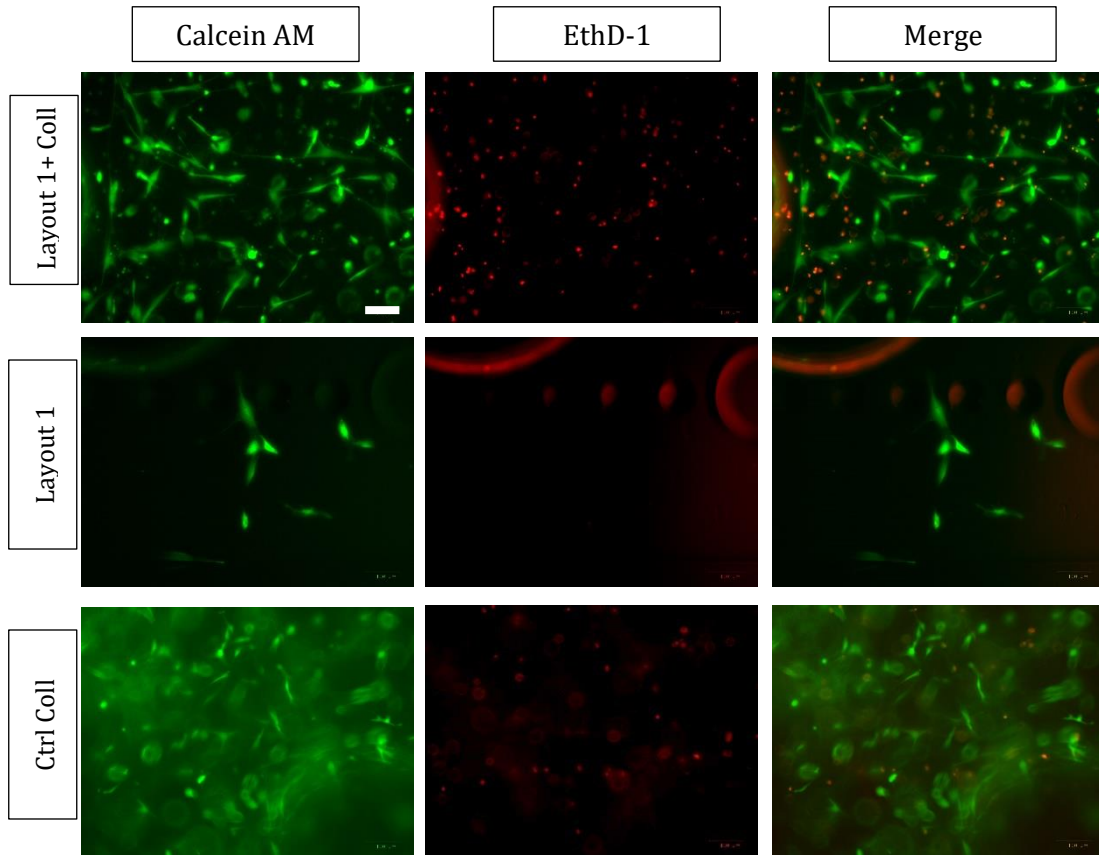


**Figure 4.4.4** Cells were stained with calcein AM and EthD-148h after seeded . The scale bar is the same for all images and corresponds to 100  $\mu\text{m}$ .

In accordance with Hyun Ju Hwang et al<sup>120</sup>, in the mono-culture of PSCs cells into bottom layer with reservoir in PDMS loaded with collagen hydrogel, PSCs are vital and present their typical elongated morphology.

Although the cell density was the same, a lower the number of cells in hydrogel-free chips can be observed. This is a result of a too short adhesion time of the cells before the addition of the medium, and the time was then modified in later seeding.

In addition, it is possible to observe that the formation of a gradient in collagen hydrogel in the device favours greater cellular growth of PSCs than cells embedded in the scaffold collagen hydrogel.

To study the morphology of PSCs under normal conditions, therefore in the absence of cancer cells, staining with DAPI and Phalloidin was carried out at 48h and 4 days after seeding.

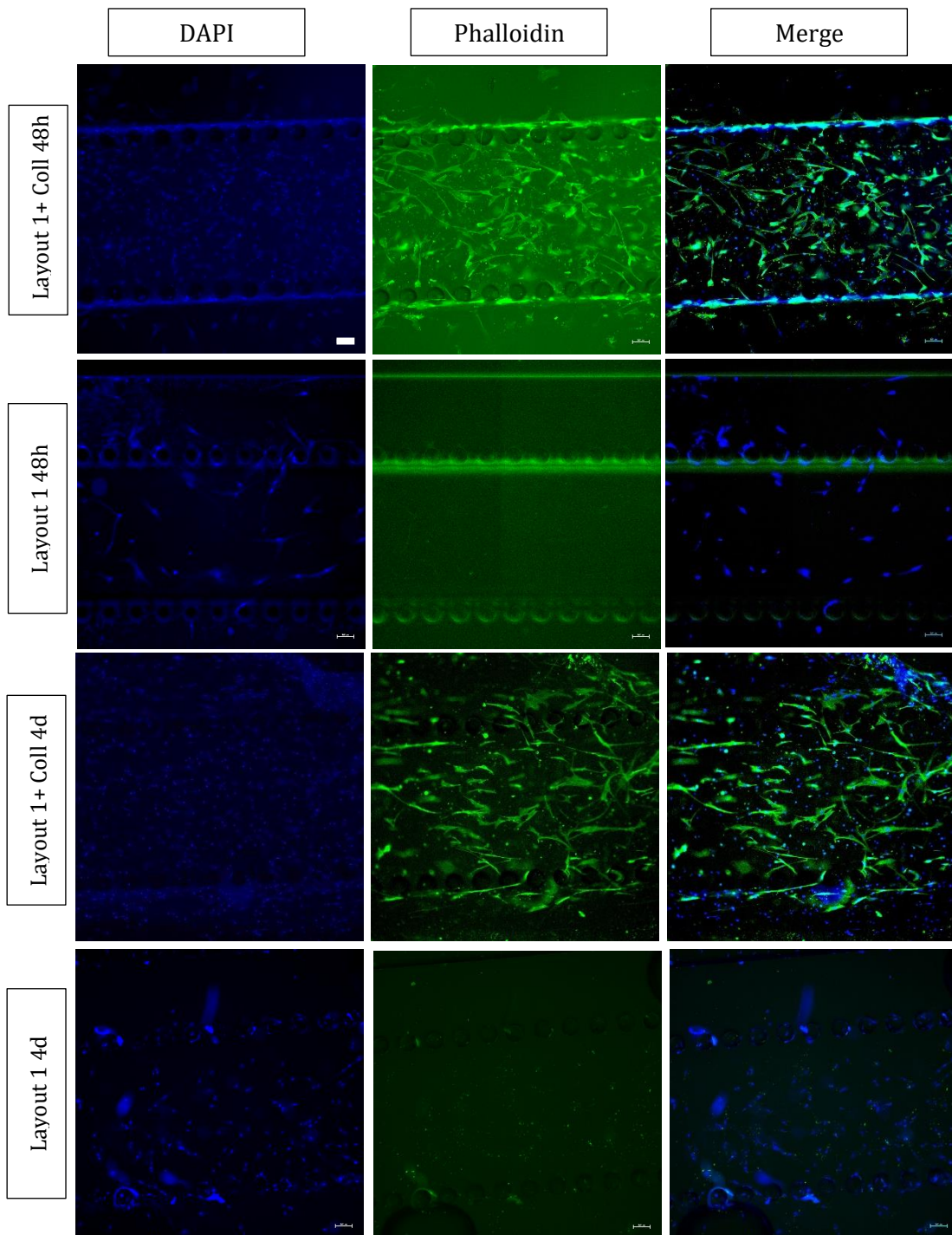


**Figure 4.4.5** Comparison of morphology and structure of PSCs in microfluidic culture with collagen hydrogel and without it, 48h after seeded and 4 days after seeded. Cells were stained with DAPI and phalloidin. The scale bar is the same for all images and corresponds to 100  $\mu\text{m}$ .

The images in the Figure 4.4.5 display that PSCs cells after 48 hours from seeding have the typical star morphology that is even more noticeable after four days of culture. So as demonstrated by for the culture of PSCs from Ji-Hyun Lee et al<sup>121</sup>, PSCs grown in 3D collagen hydrogel in the device show the relatively short, starry form of inactive PSCs. Focusing on gel-free controls at both 48 hours and 4 days, actin filaments are not present, this may be due to the short adhesion time left to the cells during the cellular seeding process.

#### **4.4.3 HPDE-KRAS culture**

The HPDE -KRAS were used as they are epithelial cell line derived from human pancreatic duct epithelial cells with mutation on gene KRAS and therefore allow to mimic the *PanINs-I* of PDAC.

This first experiment with HPDE-KRAS has been performed to investigate the effect that the top layer of the device and the PCL/Gel nanofibrous membrane have on the behaviour of cells. The experiment has been executed on the top layer with PDMS reservoir bonded on glass laboratory and on glass slides covered with PCL/Gel membrane. To compare the cellular response the controls on plastic well were implemented. In this experiment, HPDE-KRAS were monitored, and their growth was observed with digital imaging system for 3 days, and the captured images of cells in microfluidic device (coded as chip) and PCL/Gel membrane are shown below in Figure 4.4.6.

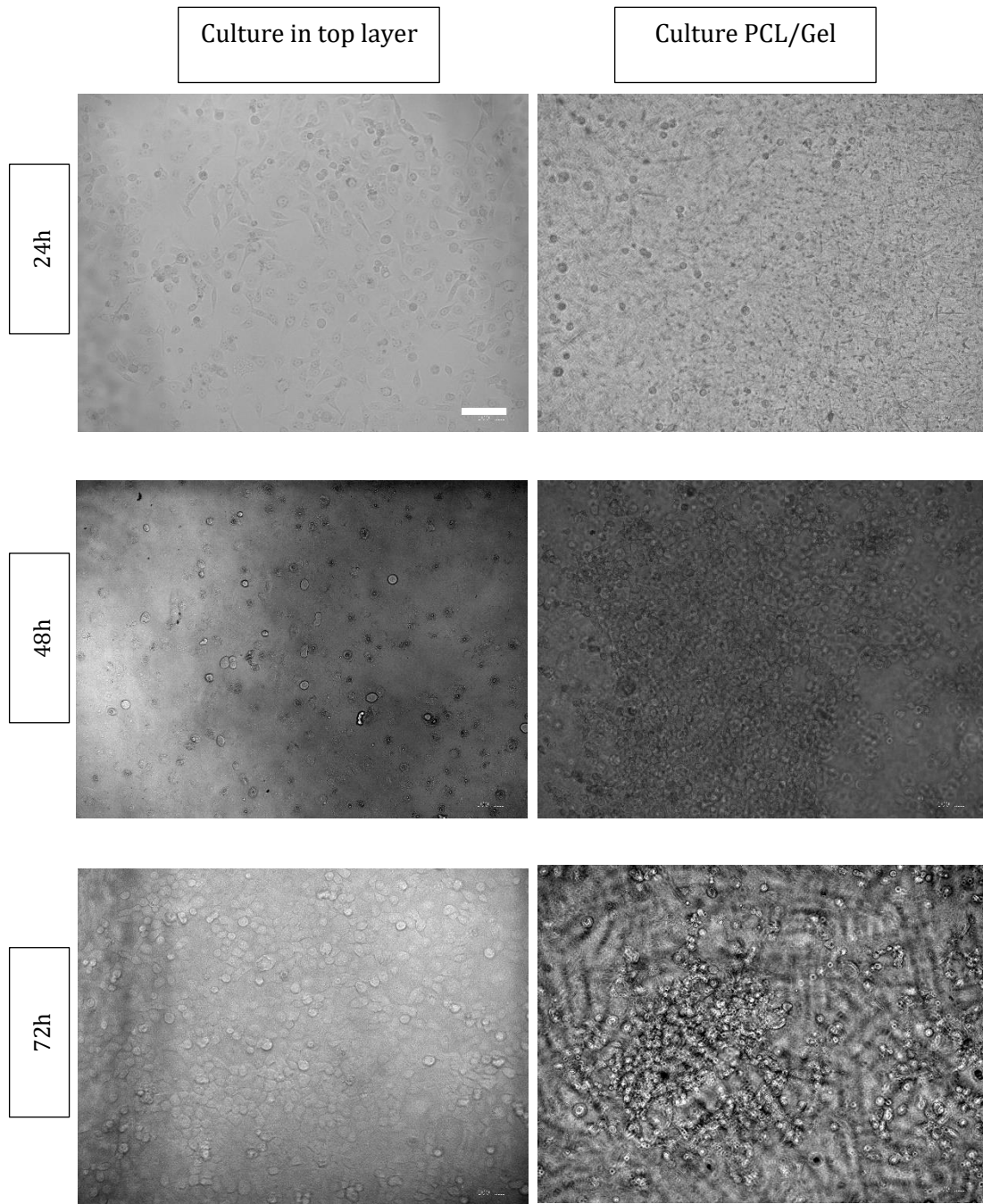


**Figure 4.4.6** Comparison of HPDE growth in microfluidic culture (i) and on PCL/Gel membrane (ii). A) 24h after seeded B) 48h after seeded C) 72h after seeded. The scale bar is the same for all images and corresponds to 100  $\mu\text{m}$ .

Cellular vitality was evaluated with LIVE/DEAD assay after 24 hours, 48 hours and 72 hours from seeding and the images of the samples and controls were reported in Figure 4.4.7.

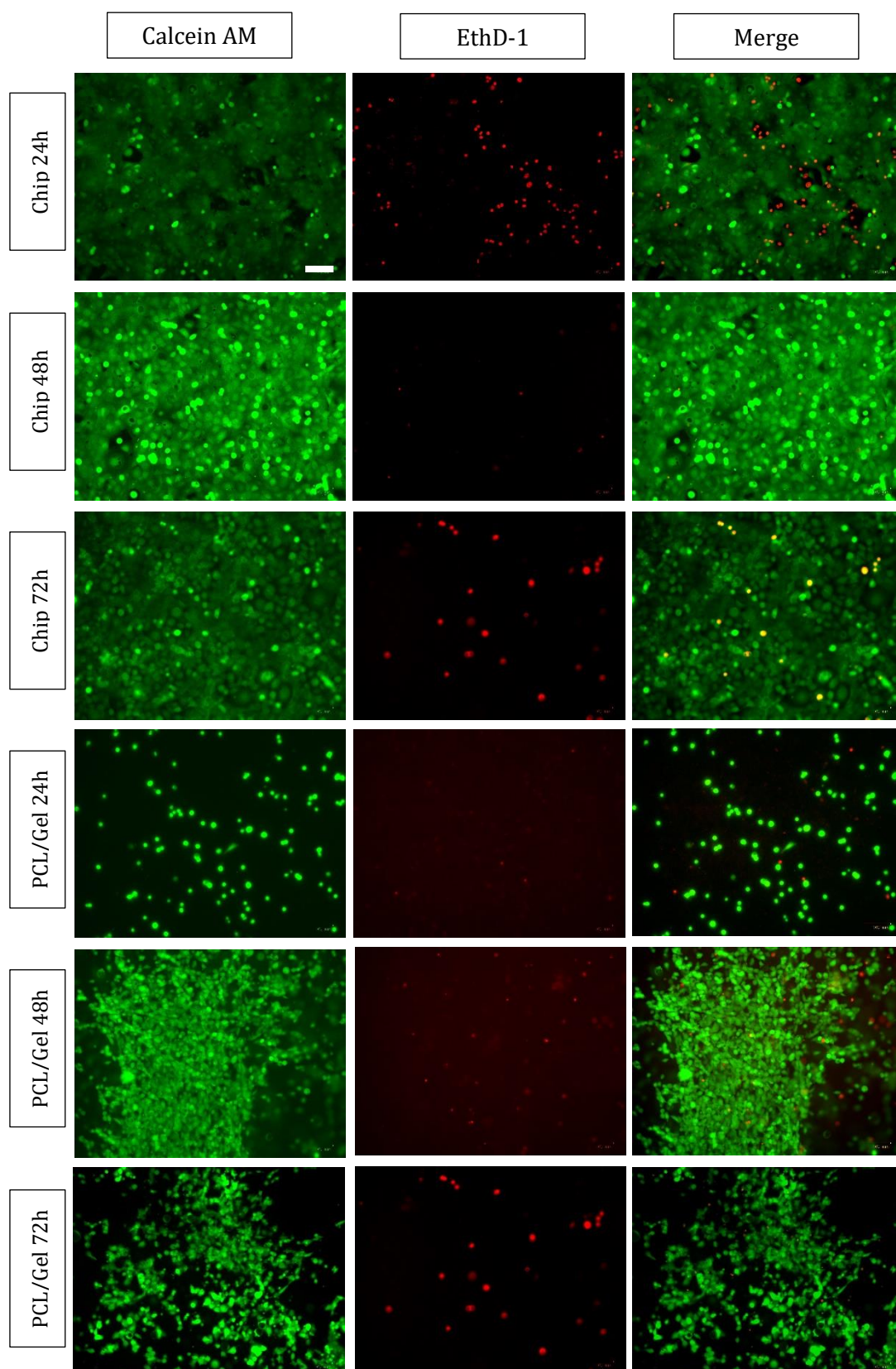


**Figure 4.4.7** Comparison between HPDE seeded in microfluidic and in PCL/Gel membrane. Cells were stained with calcein AM and EthD-1 24h, 48h and 72h after seeded. The scale bar is the same for all images and corresponds to 100  $\mu\text{m}$ .

HPDE-KRAS are vital and proliferative both within the chip and on the PCL/Gel membrane. In accordance with the work done by Kuppan et al. cell proliferation on PCL-gelatin nanofibrous membrane is high and PCL-gelatin nanofibers exhibit good cell adhesion<sup>122</sup>.

To study the morphology of HPDE-KRAS both in microfluidic device and on PCL/Gel membrane, staining with DAPI and Phalloidin was carried out at 24h 48h and 72h after seeding.

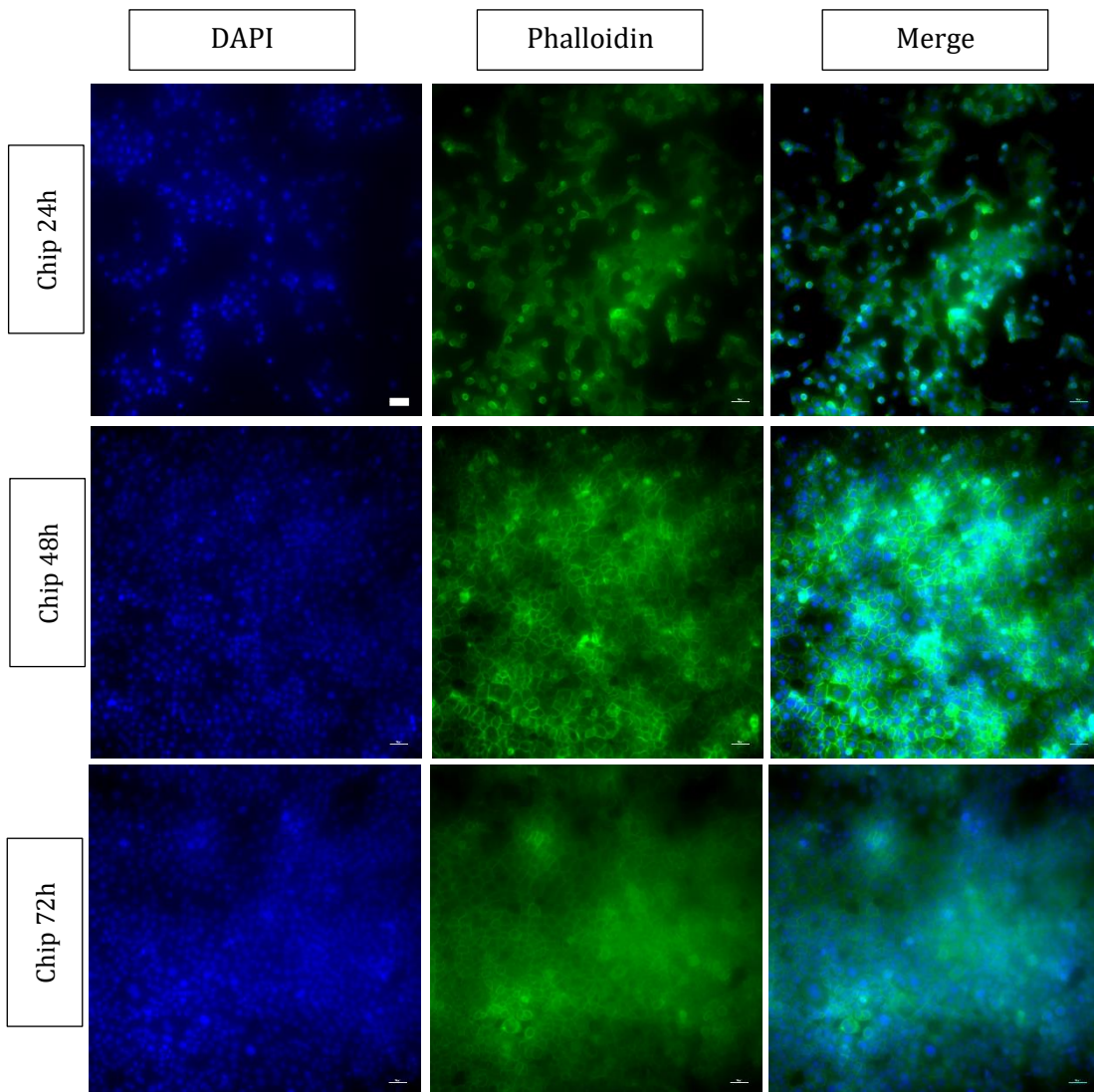


**Figure 4.4.8** Comparison of morphology and structure of HPDE in microfluidic device. Cells were stained with DAPI and phalloidin 24h,48h and 72h after seeded. The scale bar is the same for all images and corresponds to 100  $\mu\text{m}$ .

In Figure. 4.4.8 the cytoskeletal morphology of HPDE-KRAS can be observed within the top layer of the platform, and the formation of the characteristic cobblestone morphology confirms that cells are functionally active. Furthermore, focusing on staining images with DAPI an increase in cell nuclei within time can be noted confirming a good cell proliferation in the chip.

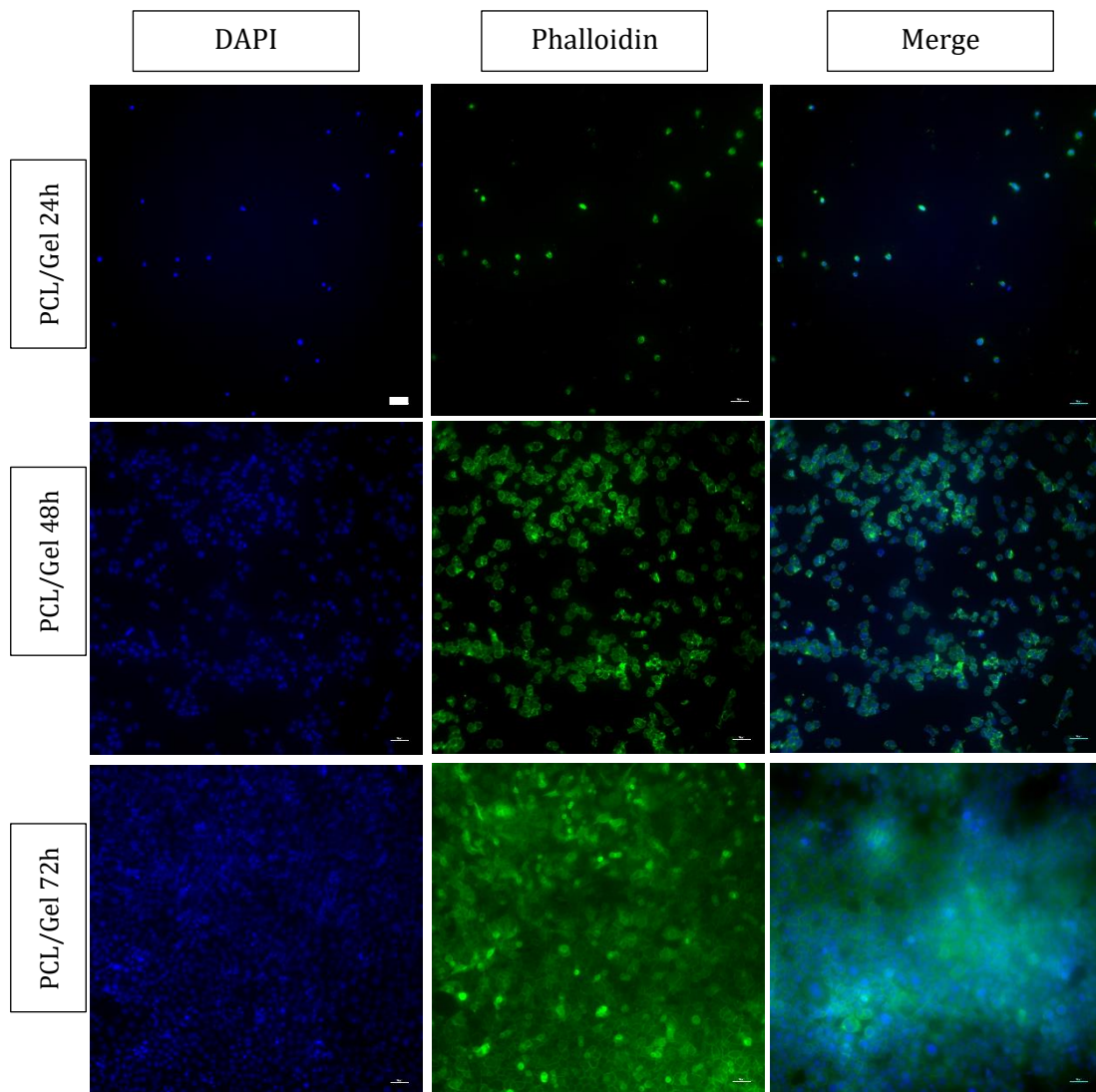


**Figure 4.4.9** Comparison of morphology and structure of HPDE on PCL/Gel membrane. Cells were stained with DAPI and phalloidin 24h, 48h and 72h after seeded. The scale bar is the same for all images and corresponds to 100  $\mu\text{m}$ .

Figure. 4.4.9 shows the cytoskeletal morphology of HPDE-KRAS on PCL/Gel membrane, and the formation of the characteristic cobblestone morphology which proves that cells are functionally active on PCL/Gel membrane.

In accordance with Kuppam et al<sup>122</sup>, the immunostaining for cytoskeletal protein actin shows that the phenotype of the HPDE-KRAS cells is retained on both scaffolds.

#### 4.4.4 Co-culture

Co-culture in the microfluidic device has been implemented to mimic the physiological stroma-PDAC crosstalk. This experiment has been executed on the complete device and two types of controls were also employed, PSCs embedded in the collagen hydrogel and HPDE-KRAS seeded on plastic wells.

The evolution of the co-culture was observed with digital imaging system for 3 days, and the captured images of cells in microfluidic device. Referring to Figure 4.4.10 it can be concluded that the double layer of PDMS and the membrane do not allow to observe growth of cells in the device with a microscope system.

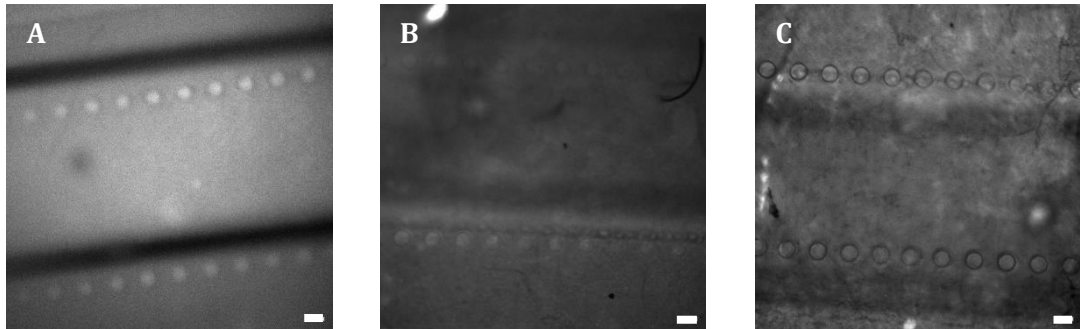


**Figure 4.4.10** Co-culture growth. A) 24h after seeded B) 48h after seeded C) 72h after seeded. The scale bar corresponds to 100  $\mu$ m.

To evaluate cellular vitality of co-culture and controls after 24 hours, 48 hours and 72 hours from seeding a LIVE/DEAD assay was used.

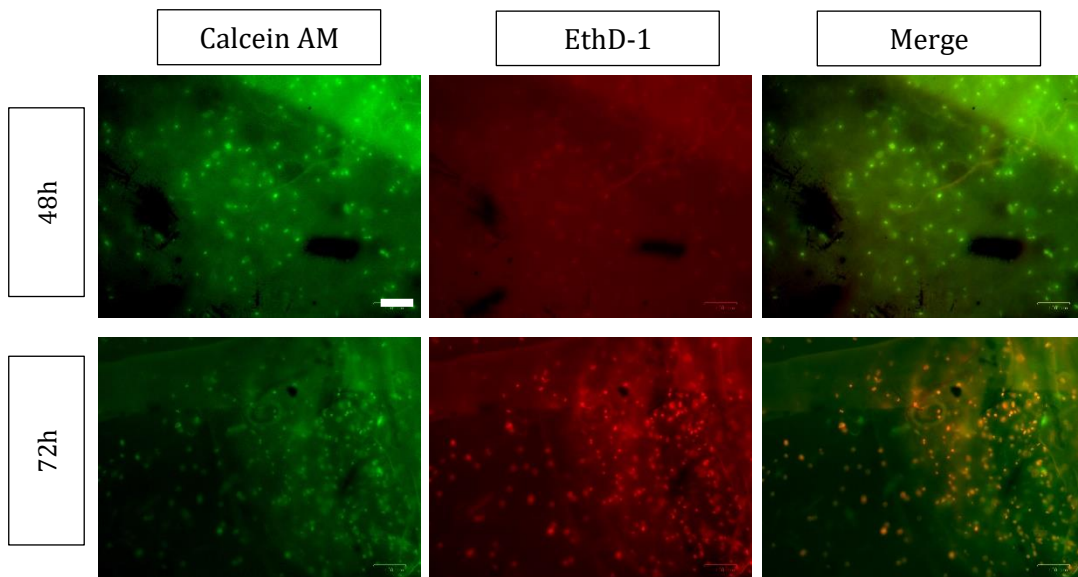


**Figure 4.4.11** Comparison of cell viability of co-culture in microfluidic device, at 24h, 48h and 72h. The scale bar is the same for all images and corresponds to 100  $\mu$ m.

As can be seen from Figure 4.4.11, LIVE/DEAD assay reveals that HPDE-KRAS are viable and proliferative in the co-culture environment. By focusing on PSCs in co-culture, LIVE/DEAD assay shows that these cells are viable, but the degree of proliferation is lower than mono-culture. This behaviour is also observed in gel controls where PSCs are vital, but the number of cells do not significantly increase in the 72h of observation. In addition, collagen hydrogel has been largely absorbed by the membrane when it was inserted, as can be seen from Figure.4.4.13. This is a possible cause of the low number of PSCs.

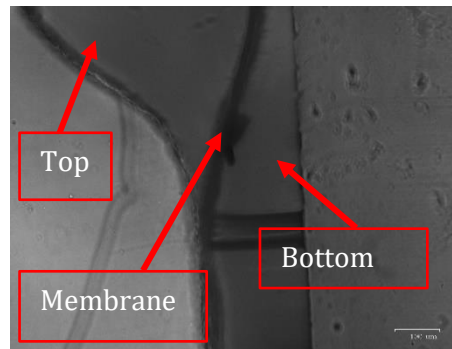


**Figure 4.4.13** Section of microfluidic device after 48h of culture (Graduated scale 100 µm).

In order to assess the vitality of the cells on the membrane, the devices have been disassembled and only the membrane mounted between two microscope slides was analysed by fluorescence microscopy.

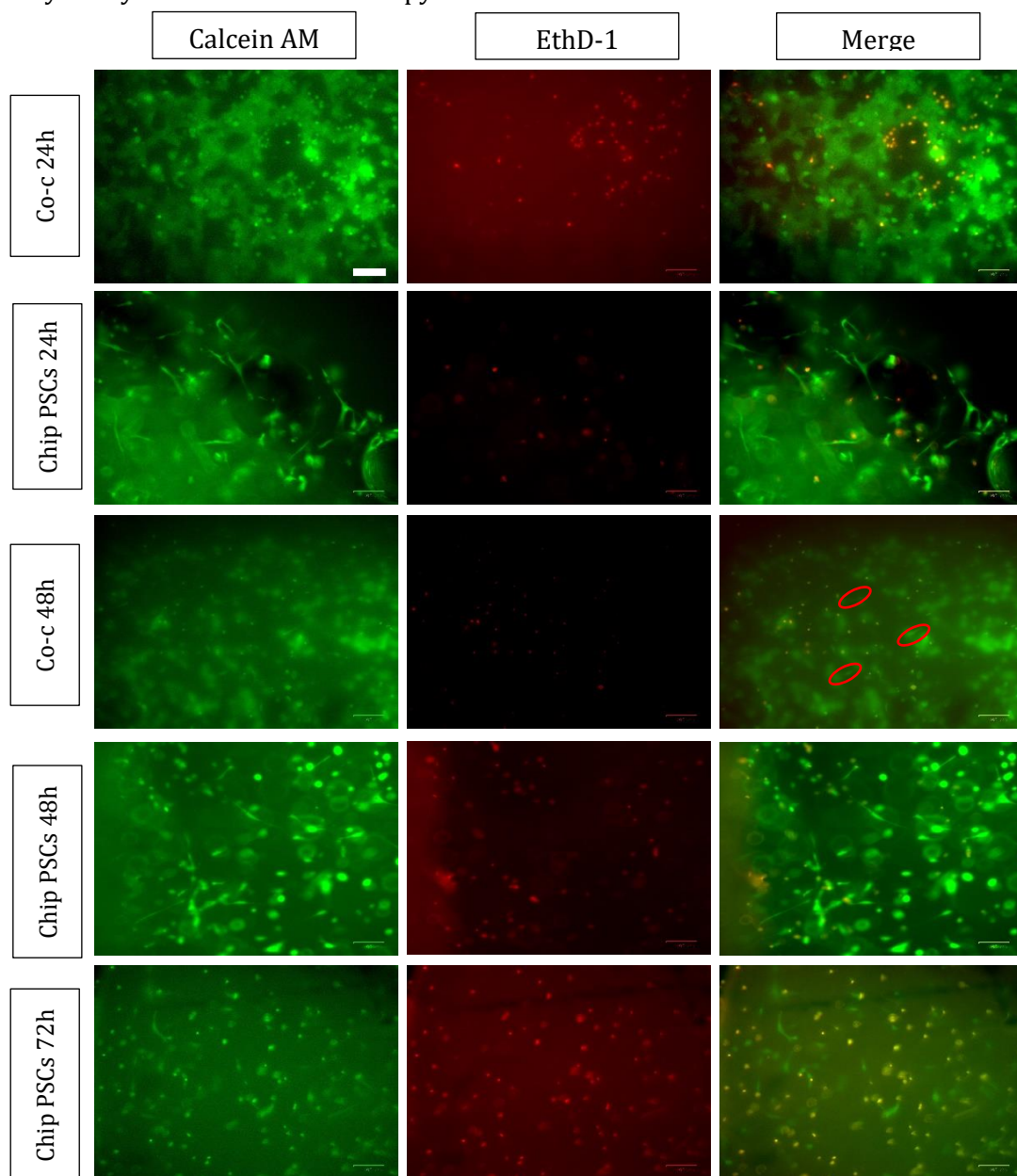


**Figure 4.4.12** Comparison of cell viability of co-culture in microfluidic device 24h, 48h and 72h after seeded. The scale bar is the same for all images and corresponds to 100 µm.

The images from LIVE/DEAD assay relative to the membrane are shown in Figure 4.4.12 and confirm the vitality of the HPDE-KRAS cells observed in the assembled device and the adhesion of these cells to the membrane.

Staining with DAPI and Phalloidin was carried out after 24h 48h and 72h to evaluate the morphology of both HPDE-KRAS and PSCs cells in the complete microfluidic device.

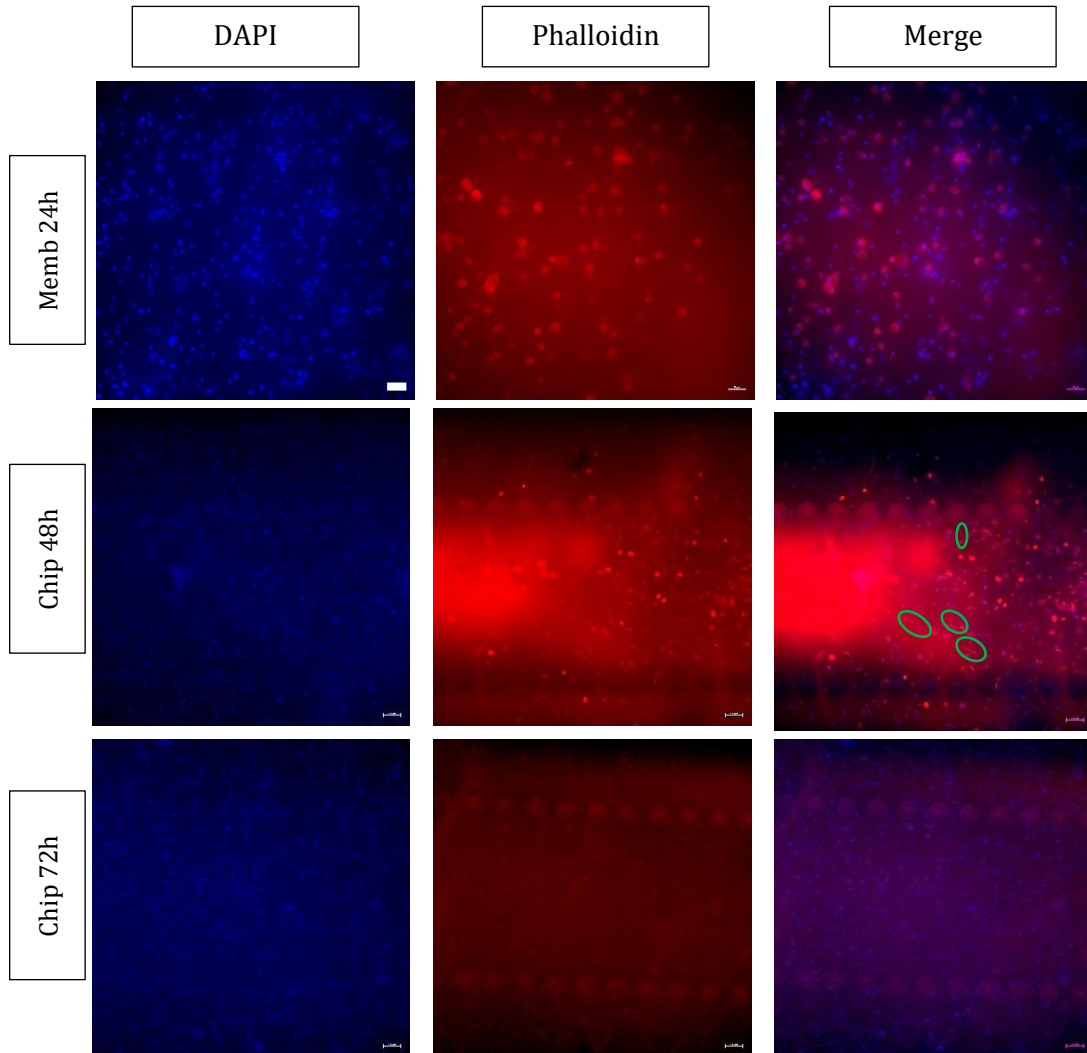


**Figure 4.4.14** Comparison of morphology and structure of HPDE and PSCs microfluidic device. Cells were stained with DAPI and phalloidin 24h,48h and 72h after seeded. The green circles highlight the PSCs cells. The scale bar is the same for all images and corresponds to 100  $\mu\text{m}$ .

In Figure 4.4.14 showing the images from DAPI/phalloidine assay, HPDE-KRAS cells show their classic cuboidal shape, while PSCs show an elongated shape. Furthermore, the large number of HPDE-KRAS cells in the bottom layer is a sign of cell migration in the bottom layer, indicating the stimulatory effect of PSCs on the migration of cancer, according to the work of Ji-Hyun Lee et al <sup>121</sup>.

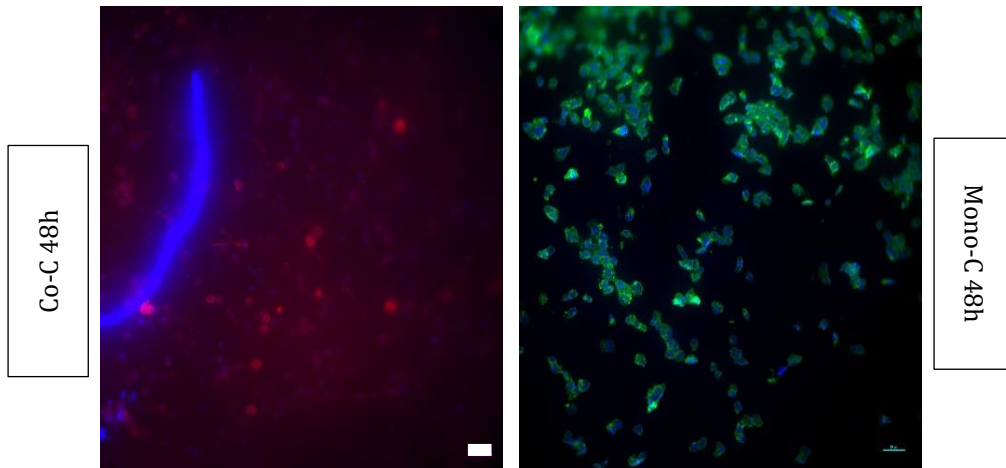


**Figure 4.4.15** Comparison between the morphology of HPDE-KRAS on PCL/gel membrane in the co-culture and monoculture 48h after seeded. The scale bar is the same for all images and corresponds to 100  $\mu\text{m}$ .

From the comparison between the morphology of HPDE-KRAS on PCL/gel membrane in the co-culture and monoculture shown in Figure 4.4.15 it can be seen that in both types the cells have a cuboidal form, a sign of proliferation and vitality.

The Figure 4.4.16 shows 60X focus co-culture at 48 h. In Figure 4.1.16-C it is possible to observe the beginning of the formation of an acino, while in Figure 4.1.16 -A and -B one can observe the PSCs.

PSCs cultured three dimensionally by embedding in a collagen matrix, underwent morphological changes from a relatively short and stellate shape to a long spindle shape with stress fiber formation. PSCs cells assume an elongated spindle shape resulting in a significant decrease in F-actin area, indicating their activation<sup>121</sup>.

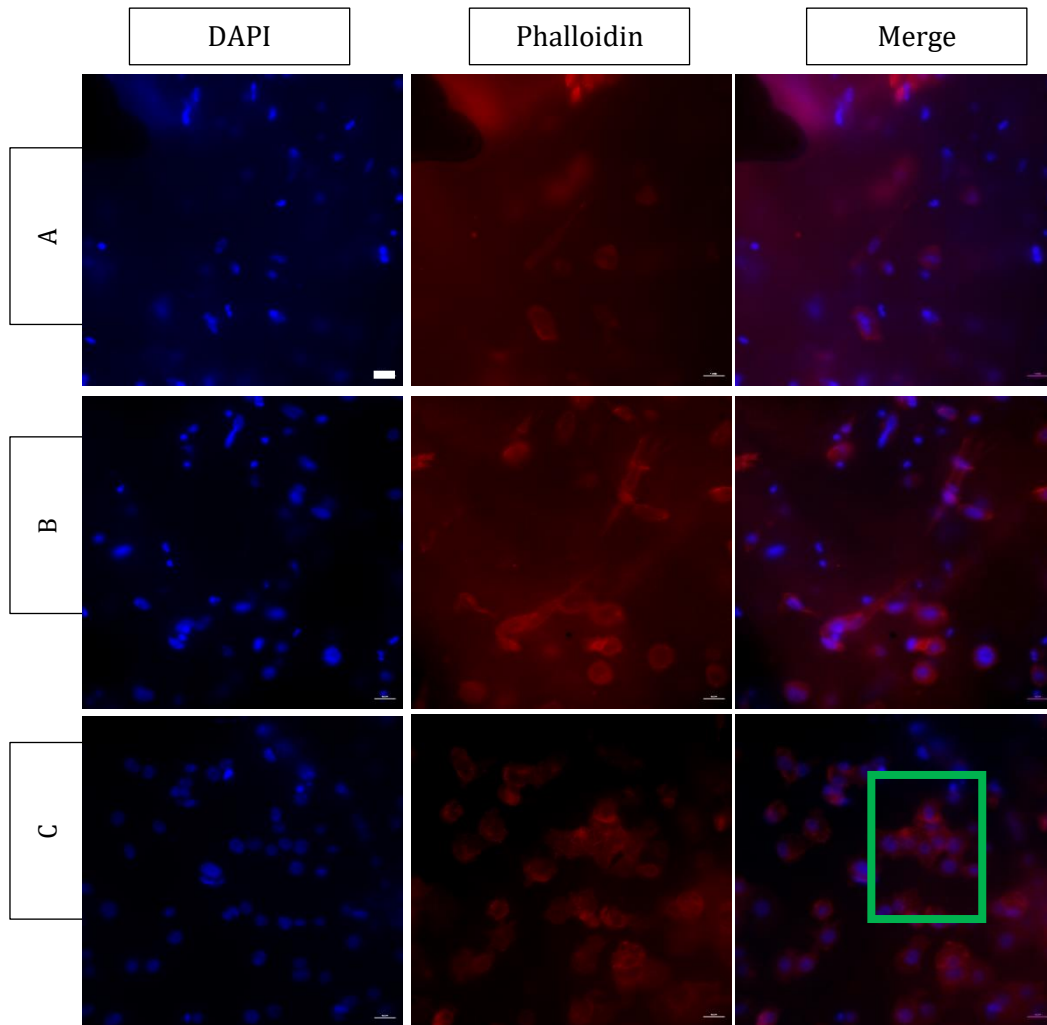


**Figure 4.4.16** Comparison of morphology and structure of HPDE and PSCs on PCL/Gel membrane in microfluidic device with focus of 60X. Cells were stained with DAPI and phalloidin 24h,48h and 72h after seeded. The scale bar is the same for all images and corresponds to 20  $\mu\text{m}$ .

## 5. Conclusion and future work

The pancreatic adenocarcinoma (PDAC) is the tumour that mostly affects the exocrine pancreas and it is characterized by a low survival rate associated with the incapacity to make an early diagnosis. PDAC has also a high resistance to treatments due to the presence of a dense desmoplastic tissue known as stroma. The stroma-PDAC crosstalk significantly affects the cancer evolution. In this context, the development of an *in vitro* model that mimics PDAC and its interactions with the tumour microenvironment (TME) is necessary to study the tissue and to facilitate the drugs discovery.

Microfluidic devices represent powerful approaches that recapitulate organ substructures in a controlled microenvironment. A microfluidic system is composed by various microchannels or microchambers that can be loaded with different biomaterials in order to mimic to the native microenvironment where cells grow.

The main goal of this thesis project is to develop an *in vitro* model of pancreatic acino-ductal unit using a microfluidic device in order to study PDAC and the crosstalk between the tumour and its stroma. To this aim, a multilayer PDMS platform combining with a thermosensitive collagen-based hydrogel and a PCL/Gel membrane was fabricated. Specifically, this system is constituted by two compartments: a bottom layer mimicking the stromal component which is composed of three channels delimited by micropillars and a top layer which resembles the tumour component. These two compartments are separated by an electrospun PCL/Gel membrane.

The microfluidic device was fabricated by replica molding technique. The molds of the bottom and top layers were produced respectively using SU-8 photolithography and laser ablation techniques, and both processes were optimized. The PCL/gel membrane was obtained using the electrospinning technique starting from an already optimized protocol. The obtained results demonstrate that the microfluidic device made of the top layer and the bottom layer composed by micropillar of 100  $\mu\text{m}$  of diameter and gap of 75  $\mu\text{m}$  (Model B) is the best performing. Replicas have the desired dimensions and a low number of defects, furthermore the model B confines well the collagen hydrogel into the central channel, and it represents the best compromise between collagen retention inside the channel and nutrient diffusion through the pillars gap. Furthermore, HFF-1s and PSCs were used to mimic the stromal component while the HPDE-KRAS cells have been used to mimic the PDAC tissue. Cell viability analyses demonstrate that this microfluidic device facilitates adhesion, growth and proliferation of HFF-1, PSCs and HPDE-KRAS cells. PSCs cells embedded into collagen hydrogel grown in mono-culture show their typical elongated morphology while they assume an elongated spindle shape

when seeded in co-culture with HPDE-KRAS cells, indicating their activation. The HPDE-KRAS cells show the characteristic cobblestone morphology both in mono- and co-culture, confirming the correct effect of microfluidic device on cells.

This experimental work allowed to obtain an *in vitro* pathological model of the pancreatic acino-ductal unit. The innovative aspect of this study is represented by the original layout of the microfluidic device.

Compared to the other models developed to study PDAC, this device consists of a membrane allowing a direct interaction between the channels of PDMS layers. In this way, the two different cell lines are in direct contact in order to better mimic the *in vivo* interaction and to investigate the crosstalk between the stroma and tumour cells in a scalable and biomimetic platform. The high number of micropillars with a shorter gap between them are demonstrated able to generate the chemical and biological gradients needed to guarantee a physiological microenvironment. Further implementations could include the optimization of the cellular density in order to reproduce the physiological PSCs/HPDE-KRAS ratio. The influence of shear stresses on the co-culture could be investigated and the *in situ* dynamic environment could be reproduced. For instance, constant and intermittent flows could be applied to evaluate the effects on PSCs activation and HPDE-KRAS migration. In addition, the cellular activity in response to drugs could be also evaluated.

To conclude, this *in vitro* pathological model of the pancreatic acino-ductal unit represents an interesting and promising start point to improve the knowledge on PDAC and to investigate new therapies.

## 6. Bibliography

1. Mcguigan A *et al.* Pancreatic cancer: A review of clinical diagnosis, epidemiology, treatment and outcomes MINIREVIEWS 4862 Cryotherapy in the management of premalignant and malignant conditions of the esophagus 4870 Acute acalculous cholecystitis in children *Ba.* **24**, 43 (2018).
2. Tomás-Bort, E., Kieler, M., Sharma, S., Candido, J. B. & Loessner, D. 3D approaches to model the tumor microenvironment of pancreatic cancer. *Theranostics* **10**, 5074–5089 (2020).
3. Totti, S., Allenby, M. C., Dos Santos, S. B., Mantalaris, A. & Velliou, E. G. A 3D bioinspired highly porous polymeric scaffolding system for: In vitro simulation of pancreatic ductal adenocarcinoma. *RSC Adv.* **8**, 20928–20940 (2018).
4. Gupta, P. *et al.* A Novel Scaffold-Based Hybrid Multicellular Model for Pancreatic Ductal Adenocarcinoma—Toward a Better Mimicry of the in vivo Tumor Microenvironment. *Front. Bioeng. Biotechnol.* **8**, (2020).
5. Silgbernagl. *Fisiologia.* (2002).
6. Longnecker, D. The Pancreapedia: Exocrine Pancreas Knowledge Base. <https://www.pancreapedia.org/reviews/anatomy-and-histology-of-pancreas> (2014).
7. Haschek, W. M., Rousseaux, C. G., & Wallig, M. A. Pancreas. in *Fundamentals of Toxicologic Pathology* 237–260 (2010). doi:10.1016/b978-0-12-370469-6.00010-6.
8. Molinaro, M., Rizzoli, C., Siracusa, G. & Stefanini, M. *Istologia di V.Monesi.* (1998).
9. Bardeesy, N. & DePinho, R. A. Pancreatic cancer biology and genetics. *Nat. Rev. Cancer* **2**, 897–909 (2002).
10. Saif, M. W. Pancreatic neoplasm in 2011: An update. *J. Pancreas* **12**, 316–321 (2011).
11. Ying, H. *et al.* Genetics and biology of pancreatic ductal adenocarcinoma. *Genes Dev.* **30**, 355–385 (2016).
12. Li, C. *et al.* Identification of pancreatic cancer stem cells. *Cancer Res.* **67**, 1030–1037 (2007).
13. *Pancreatic Cancer and Tumor Microenvironment.* (Transworld Research Network, 2012).
14. Iacobuzio-Donahue, C. A. Genetic evolution of pancreatic cancer: Lessons learnt from the pancreatic cancer genome sequencing project. *Gut* **61**, 1085–1094 (2012).

15. Tang et al., 2005. 基因的改变 NIH Public Access. *Bone* **23**, 1–7 (2008).
16. Koorstra, J. B. M., Feldmann, G., Habbe, N. & Maitra, A. Morphogenesis of pancreatic cancer: Role of pancreatic intraepithelial neoplasia (PanINs). *Langenbeck's Arch. Surg.* **393**, 561–570 (2008).
17. Distler, M., Aust, D., Weitz, J., Pilarsky, C. & Grützmann, R. Precursor lesions for sporadic pancreatic cancer: PanIN, IPMN, and MCN. *Biomed Res. Int.* **2014**, (2014).
18. Wanebo, H. J. & Vezeridis, M. P. Pancreatic cancer: An overview. *Semin. Surg. Oncol.* **11**, 168–180 (1995).
19. Kalluri, R. & Zeisberg, M. Fibroblasts in cancer. *Nat. Rev. Cancer* **6**, 392–401 (2006).
20. Bachem, M. G., Zhou, S., Buck, K., Schneiderhan, W. & Siech, M. Pancreatic stellate cells - Role in pancreas cancer. *Langenbeck's Arch. Surg.* **393**, 891–900 (2008).
21. Karamitopoulou, E. The tumor microenvironment of pancreatic cancer. *Cancers (Basel)*. **12**, 1–4 (2020).
22. Chu, G. C., Kimmelman, A. C., Hezel, A. F. & DePinho, R. A. Stromal biology of pancreatic cancer. *J. Cell. Biochem.* **101**, 887–907 (2007).
23. Koenig, A., Mueller, C., Hasel, C., Adler, G. & Menke, A. Collagen type I induces disruption of E-cadherin-mediated cell-cell contacts and promotes proliferation of pancreatic carcinoma cells. *Cancer Res.* **66**, 4662–4671 (2006).
24. Mueller, M. M. & Fusenig, N. E. Friends or foes - Bipolar effects of the tumour stroma in cancer. *Nat. Rev. Cancer* **4**, 839–849 (2004).
25. Hu, D. *et al.* Stromal fibronectin expression in patients with resected pancreatic ductal adenocarcinoma. *World J. Surg. Oncol.* **17**, 1–8 (2019).
26. Veenstra, V. L. *et al.* Stromal SPOCK1 supports invasive pancreatic cancer growth. *Mol. Oncol.* **11**, 1050–1064 (2017).
27. Vonlaufen, A. *et al.* Pancreatic stellate cells: Partners in crime with pancreatic cancer cells. *Cancer Res.* **68**, 2085–2093 (2008).
28. Xu, Z. *et al.* Role of pancreatic stellate cells in pancreatic cancer metastasis. *Am. J. Pathol.* **177**, 2585–2596 (2010).
29. Castells-sala, C., Ribes, M. A., Children, B. & Recha, L. Current Applications of Tissue Engineering in Biomedicine. *J. Biochips Tissue Chips* **s2**, (2015).
30. Lee, J., Cuddihy, M. J. & Kotov, N. A. Three-dimensional cell culture matrices: State of the art. *Tissue Eng. - Part B Rev.* **14**, 61–86 (2008).
31. Andersen, M. L. & Winter, L. M. F. ): e20170238 (Annals of the Brazilian Academy of Sciences) *An Acad Bras Cienc. An Acad Bras Cienc* **91**, 1–14 (2019).
32. Hingorani, S. R. *et al.* Erratum: Preinvasive and invasive ductal pancreatic cancer

- and its early detection in the mouse (Cancer Cell (4) (437-450)). *Cancer Cell* **5**, 103 (2004).
33. Ijichi, H. *et al.* Aggressive pancreatic ductal adenocarcinoma in mice caused by pancreas-specific blockade of transforming growth factor- $\beta$  signaling in cooperation with active Kras expression. *Genes Dev.* **20**, 3147–3160 (2006).
  34. Qiu, W. & Su, G. H. *Challenges and advances in mouse modeling for human pancreatic tumorigenesis and metastasis. Cancer and Metastasis Reviews* vol. 32 (2013).
  35. Radhakrishnan, J., Varadaraj, S., Dash, S. K., Sharma, A. & Verma, R. S. Organotypic cancer tissue models for drug screening: 3D constructs, bioprinting and microfluidic chips. *Drug Discov. Today* **25**, 879–890 (2020).
  36. Baker, L. A., Tiriach, H., Clevers, H. & Tuveson, D. A. Modeling pancreatic cancer with organoids The Need for Accurate Model Systems of Pancreatic Cancer. *Trends in Cancer* **2**, 176–190 (2016).
  37. Kolenda, T. *et al.* State of the art paper 2D and 3D cell cultures-a comparison of different types of cancer cell cultures. (2016) doi:10.5114/aoms.2016.63743.
  38. Longati, P. *et al.* 3D pancreatic carcinoma spheroids induce a matrix-rich, chemoresistant phenotype offering a better model for drug testing. *BMC Cancer* **13**, 1–13 (2013).
  39. Cave, D. D. *et al.* The revolutionary roads to study cell–cell interactions in 3d in vitro pancreatic cancer models. *Cancers (Basel)*. **13**, 1–19 (2021).
  40. Sgarminato, V., Tonda-Turo, C. & Ciardelli, G. Reviewing recently developed technologies to direct cell activity through the control of pore size: From the macro- to the nanoscale. *J. Biomed. Mater. Res. Part B Appl. Biomater.* **108**, 1176–1185 (2020).
  41. Puls, T. J., Tan, X., Whittington, C. F. & Voytik-Harbin, S. L. 3D collagen fibrillar microstructure guides pancreatic cancer cell phenotype and serves as a critical design parameter for phenotypic models of EMT. *PLoS One* **12**, 1–25 (2017).
  42. Langer, E. M. *et al.* Modeling Tumor Phenotypes In Vitro with Three-Dimensional Bioprinting. *Cell Rep.* **26**, 608-623.e6 (2019).
  43. Hoshiba, T., Lu, H., Kawazoe, N. & Chen, G. Decellularized matrices for tissue engineering. *Expert Opin. Biol. Ther.* **10**, 1717–1728 (2010).
  44. Vennin, C. *et al.* Reshaping the Tumor Stroma for Treatment of Pancreatic Cancer. *Gastroenterology* **154**, 820–838 (2018).
  45. Wan, J. *et al.* Culture of iPSCs Derived Pancreatic  $\alpha$ 1/2-Like Cells In Vitro Using Decellularized Pancreatic Scaffolds: A Preliminary Trial. (2017) doi:10.1155/2017/4276928.

46. Ware, M. J. *et al.* Generation of an in vitro 3D PDAC stroma rich spheroid model HHS Public Access. doi:10.1016/j.biomaterials.2016.08.041.
47. Doctor, A., Seifert, V., Ullrich, M., Hauser, S. & Pietzsch, J. Three-dimensional cell culture systems in radiopharmaceutical cancer research. *Cancers (Basel)*. **12**, 1–28 (2020).
48. Moreira, L. *et al.* Pancreas 3D Organoids: Current and Future Aspects as a Research Platform for Personalized Medicine in Pancreatic Cancer. *Cmgh* **5**, 289–298 (2018).
49. Chio, I. I. C. *et al.* NRF2 Promotes Tumor Maintenance by Modulating mRNA Translation in Pancreatic Cancer. *Cell* **166**, 963–976 (2016).
50. Huang, L. *et al.* Ductal pancreatic cancer modeling and drug screening using human pluripotent stem cell- and patient-derived tumor organoids. *Nat. Med.* **21**, 1364–1371 (2015).
51. Swayden, M., Soubeyran, P. & Iovanna, J. Upcoming Revolutionary Paths in Preclinical Modeling of Pancreatic Adenocarcinoma. *Front. Oncol.* **9**, 1–12 (2020).
52. Kurth, F. *et al.* *Organs-on-a-chip engineering. Organ-on-a-chip: Engineered Microenvironments for Safety and Efficacy Testing* (2019). doi:10.1016/B978-0-12-817202-5.00003-6.
53. Wang, Z., Volinsky, A. A. & Gallant, N. D. Crosslinking effect on polydimethylsiloxane elastic modulus measured by custom-built compression instrument. *J. Appl. Polym. Sci.* **131**, 1–4 (2014).
54. Antoine, E. E., Vlachos, P. P. & Rylander, M. N. Tunable collagen I hydrogels for engineered physiological tissue micro-environments. *PLoS One* **10**, 1–18 (2015).
55. Nnebe, I. M. & Schneider, J. W. Dynamic Atomic Force Microscopy Studies to Characterize Heterogeneous Surfaces. *Dekker Encycl. Nanosci. Nanotechnol.* **10**, 987–1000 (2007).
56. Wang, C., Tran, V., Ma, Z. & Wen, X. *Rapid prototyping technologies for tissue regeneration. Rapid Prototyping of Biomaterials: Techniques in Additive Manufacturing* (2019). doi:10.1016/B978-0-08-102663-2.00006-X.
57. Nur, O. & Willander, M. *Conventional nanofabrication methods. Low Temperature Chemical Nanofabrication* (2020). doi:10.1016/b978-0-12-813345-3.00003-4.
58. Sinha, S. K. & Bit, A. *23. Microfluidics in tissue engineering. Biomaterials for Organ and Tissue Regeneration* (LTD, 2020). doi:10.1016/B978-0-08-102906-0.00010-6.
59. Martinez-duarte, R. & Madou, M. J. Lattice Boltzmann Method and Its Applications in Microfluidics. *Microfluid. Nanofluidics Handb.* 229–244 (2012) doi:10.1201/b11188-11.

60. Chung, C. K., Long, H. P. & Lai, C. C. Microfluidic chip using foil-assisted CO<sub>2</sub> laser ablation for suspended particle separation. *Micro Nano Lett.* **10**, 500–503 (2015).
61. Hsieh, Y. K. *et al.* Direct micromachining of microfluidic channels on biodegradable materials using laser ablation. *Polymers (Basel)*. **9**, (2017).
62. Ravi-Kumar, S., Lies, B., Lyu, H. & Qin, H. Laser ablation of polymers: A review. *Procedia Manuf.* **34**, 316–327 (2019).
63. Trujillo-De Santiago, G. *et al.* materials The Tumor-on-Chip: Recent Advances in the Development of Microfluidic Systems to Recapitulate the Physiology of Solid Tumors. (2019) doi:10.3390/ma12182945.
64. Beer, M. *et al.* A novel microfluidic 3D platform for culturing pancreatic ductal adenocarcinoma cells: Comparison with in vitro cultures and in vivo xenografts. *Sci. Rep.* **7**, 1–12 (2017).
65. Lee, J. H. *et al.* Microfluidic co-culture of pancreatic tumor spheroids with stellate cells as a novel 3D model for investigation of stroma-mediated cell motility and drug resistance. *J. Exp. Clin. Cancer Res.* **37**, 1–12 (2018).
66. Nguyen, D. H. T. *et al.* A biomimetic pancreatic cancer on-chip reveals endothelial ablation via ALK7 signaling. *Sci. Adv.* **5**, 1–10 (2019).
67. PDMS SYLGARD.  
[https://www.sigmaaldrich.com/catalog/product/aldrich/761036?lang=it&region=IT&gclid=EAIaIQobChMIoLWYhq7V8AIVh5eyCh00xA-9EAAAYASAAEgIhUfD\\_BwE](https://www.sigmaaldrich.com/catalog/product/aldrich/761036?lang=it&region=IT&gclid=EAIaIQobChMIoLWYhq7V8AIVh5eyCh00xA-9EAAAYASAAEgIhUfD_BwE).
68. Ruben, B. *et al.* Oxygen plasma treatments of polydimethylsiloxane surfaces: Effect of the atomic oxygen on capillary flow in the microchannels. *Micro Nano Lett.* **12**, 754–757 (2017).
69. Del Campo, A. & Greiner, C. SU-8: A photoresist for high-aspect-ratio and 3D submicron lithography. *J. Micromechanics Microengineering* **17**, (2007).
70. Epoxy, P. & Photoresist, N. SU-8 2000 Permanent Epoxy Negative Photoresist PROCESSING GUIDELINES FOR : *Exposure* (2000).
71. Nitride, G. *et al.* MICROTECH LASER WRITER Specification.
72. Lawson, R. A. & Robinson, A. P. G. *Overview of materials and processes for lithography. Frontiers of Nanoscience* vol. 11 (Elsevier, 2016).
73. Kapton Tape. <https://www.professionalplastics.com/KaptonTape-siliconeadhesive>.
74. Micro-Laser Ablation. <https://www.micro-la.com/open/design-detail/7/marcatura-laser-standalone-laser-slider>.
75. Yang, S., Leong, K. F., Du, Z. & Chua, C. K. The design of scaffolds for use in tissue engineering. Part I. Traditional factors. *Tissue Eng.* **7**, 679–689 (2001).

76. Gunatillake, P. A., Adhikari, R. & Gadegaard, N. Biodegradable synthetic polymers for tissue engineering. *Eur. Cells Mater.* **5**, 1–16 (2003).
77. Azimi, B., Nourpanah, P., Rabiee, M. & Arbab, S. Poly ( $\epsilon$ -caprolactone) fiber: An overview. *J. Eng. Fiber. Fabr.* **9**, 74–90 (2014).
78. Mahmood Lubowa Muhammad, K., Ariffin, F., Kamilah, H. & Sulaiman, S. Review of Fish Gelatin Extraction, Properties and Packaging Applications. *Food Sci. Qual. Manag.* **56**, (2016).
79. Nikkiah, M., Akbari, M., Memic, A., Dolatshahi-pirouz, A. & Khademhosseini, A. for Tissue Engineering and. *Biomater. from Nat. Adv. Devices Ther.* 37–62 (2016).
80. GPTMS. <https://www.sigmaaldrich.com/IT/it/product/aldrich/440167>.
81. Melt. <http://novaspider.com/equipment-and-services/>.
82. Pasirayi, G. *et al.* Microfluidic Bioreactors for Cell Culturing: A Review. *Micro Nanosyst.* **3**, 137–160 (2012).
83. J. M. Berg, and S. G. S. B. A. D. Studies on Surface Wettability of Poly ( Dimethyl ) Siloxane ( PDMS ) and Glass Under Oxygen-Plasma. *J. MicroElecMechSys* **14**, 590–597 (2005).
84. Systeme, N. P. Atto ( Low Cost / Low Budget ) Niederdruck Plasma Systeme Low pressure plasma systems Atto.
85. Sanjeeva Murthy, N. Techniques for analyzing biomaterial surface structure, morphology and topography. *Surf. Modif. Biomater. Methods Anal. Appl.* 232–255 (2011) doi:10.1533/9780857090768.2.232.
86. KLA. Profilometer TENCOR P-10 SURFACE PROFILER. <https://www.kla-tencor.com/products/instruments/stylus-profilers/innovation-history>.
87. Leica. <https://www.leica-microsystems.com/it/prodotti/>.
88. Janssen, G.-J. 1.1. What does the word FESEM mean? *Scanning* 1–5 (2005).
89. FE-SEM. <https://www.zeiss.com/microscopy/int/products/scanning-electron-microscopes/geminisem.html>.
90. Shoulders, M. D. & Raines, R. T. Collagen structure and stability. *Annu. Rev. Biochem.* **78**, 929–958 (2009).
91. Image of Collagen. <https://basicmedicalkey.com/5-protein-structure-and-function/>.
92. Walters, B. D. & Stegemann, J. P. Strategies for directing the structure and function of three-dimensional collagen biomaterials across length scales. *Acta Biomater.* **10**, 1488–1501 (2014).
93. Dinescu, S. *et al.* Collagen-Based Hydrogels and Their Applications for Tissue Engineering and Regenerative Medicine. 1643–1664 (2019) doi:10.1007/978-3-319-77830-3\_54.

94. Collagen. <https://advancedbiomatrix.com/fibricol.html>.
95. Graf, B. W. & Boppart, S. A. Imaging and analysis of three-dimensional cell culture models. *Methods Mol. Biol.* **591**, 211–227 (2010).
96. Nikon-Inverted Reserch Microscope. Ti2\_e\_2CE-MPLH-8.pdf.
97. DMEM. <https://www.thermofisher.com/it/en/home/life-science/cell-culture/mammalian-cell-culture/classical-media/dmem.html#:~:text=Gibco Dulbecco's Modified Eagle Medium,7%2C and PC-12>.
98. FBS. <https://www.thermofisher.com/it/en/home/life-science/cell-culture/mammalian-cell-culture/fbs.html>.
99. L-Glu.  
<https://www.thermofisher.com/order/catalog/product/25030149#/25030149>  
.
100. P/S.  
<https://www.thermofisher.com/order/catalog/product/15140122#/15140122>  
.
101. Chua, F. & Laurent, G. J. Fibroblasts. *Encycl. Respir. Med. Four-Volume Set* 213–219 (2006) doi:10.1016/B0-12-370879-6/00156-3.
102. Stellate Cell Growth Medium-iXCells Biotech.  
<https://www.ixcellsbiotech.com/product/cell-media-reagents/stellate-cell-growth-medium>.
103. Antimycotic 100X.  
<https://www.thermofisher.com/order/catalog/product/15240062#/15240062>  
.
104. RPMI. [https://www.thermofisher.com/it/en/home/life-science/cell-culture/mammalian-cell-culture/classical-media/rpmi.html?gclid=EAIaIQobChMIjKmD5c6c8QIVQ\\_hRCh05CQ4iEAAYASA AEgJ48fD\\_BwE&s\\_kwid=AL!3652!3!345664549641!p!!g!!gibco rpmi&ef\\_id=EAIaIQobChMIjKmD5c6c8QIV](https://www.thermofisher.com/it/en/home/life-science/cell-culture/mammalian-cell-culture/classical-media/rpmi.html?gclid=EAIaIQobChMIjKmD5c6c8QIVQ_hRCh05CQ4iEAAYASA AEgJ48fD_BwE&s_kwid=AL!3652!3!345664549641!p!!g!!gibco rpmi&ef_id=EAIaIQobChMIjKmD5c6c8QIV).
105. Radulovich, N., Qian, J. ying & Tsao, M. S. Human Pancreatic Duct Epithelial Cell Model for KRAS Transformation. *Methods Enzymol.* **439**, 1–13 (2008).
106. Gunetti, M. *et al.* Validation of analytical methods in GMP: The disposable Fast Read 102® device, an alternative practical approach for cell counting. *J. Transl. Med.* **10**, (2012).
107. Invitrogen Molecular Probes. LIVE/DEAD Viability/Cytotoxicity Kit for mammalian cells. *Prod. Information, Cat. number MP 03224* 1–7 (2005).
108. Promega. CellTiter-Glo ® Luminescent Cell Viability Assay Cell Viability Assay. 8–10 (2002).

109. chemical structure of resazurin. <https://en.wikipedia.org/wiki/Resazurin>.
110. Invitrogen. alamarBlue™ Cell Viability Reagent PIS. 1–2 (2019).
111. CalceinAM. <https://en.wikipedia.org/wiki/Calcein>.
112. Kapuscinski, J. DAPI: A DMA-Specific fluorescent probe. *Biotech. Histochem.* **70**, 220–233 (1995).
113. No, P. & Rev, M. A. N. Phalloidins说明书. (2000).
114. Repository, Z. O. & Library, M. The effect of matrix characteristics on fibroblast proliferation in 3D gels 1 . Tissue Repair and Regeneration Program , Institute of Health and Biomedical Innovation ( IHBI ), Queensland University of Technology , Brisbane , Australia 2 . Department of C. **31**, 8454–8464 (2010).
115. Tabatabaei, F., Moharamzadeh, K. & Tayebi, L. Fibroblast encapsulation in gelatin methacryloyl (GelMA) versus collagen hydrogel as substrates for oral mucosa tissue engineering. *J. Oral Biol. Craniofacial Res.* **10**, 573–577 (2020).
116. Jeong, S. Y., Lee, J. H., Shin, Y., Chung, S. & Kuh, H. J. Co-culture of tumor spheroids and fibroblasts in a collagen matrix-incorporated microfluidic chip mimics reciprocal activation in solid tumor microenvironment. *PLoS One* **11**, 1–17 (2016).
117. Sung, K. E. *et al.* Control of 3-dimensional collagen matrix polymerization for reproducible human mammary fibroblast cell culture in microfluidic devices. *Biomaterials* **30**, 4833–4841 (2009).
118. Akther, F., Little, P., Li, Z., Nguyen, N. T. & Ta, H. T. Hydrogels as artificial matrices for cell seeding in microfluidic devices. *RSC Adv.* **10**, 43682–43703 (2020).
119. Olivares, V. *et al.* Image-based characterization of 3d collagen networks and the effect of embedded cells. *Microsc. Microanal.* **25**, 971–981 (2019).
120. Hwang, H. J., Oh, M. S., Lee, D. W. & Kuh, H. J. Multiplex quantitative analysis of stroma-mediated cancer cell invasion, matrix remodeling, and drug response in a 3D co-culture model of pancreatic tumor spheroids and stellate cells. *J. Exp. Clin. Cancer Res.* **38**, 1–14 (2019).
121. Lee, J. H. *et al.* Microfluidic co-culture of pancreatic tumor spheroids with stellate cells as a novel 3D model for investigation of stroma-mediated cell motility and drug resistance. *J. Exp. Clin. Cancer Res.* **37**, (2018).
122. Kuppam, P., Sethuraman, S. & Krishnan, U. M. PCL and PCL-gelatin nanofibers as esophageal tissue scaffolds: Optimization, characterization and cell-matrix interactions. *J. Biomed. Nanotechnol.* **9**, 1540–1555 (2013).
123. Orth, M. *et al.* Pancreatic ductal adenocarcinoma: Biological hallmarks, current status, and future perspectives of combined modality treatment approaches. *Radiat. Oncol.* **14**, 1–20 (2019).

124. Carter, E. P. *et al.* cells Dissecting FGF Signalling to Target Cellular Crosstalk in Pancreatic Cancer. *Pancreat. Cancer. Cells* 10 (2021) doi:10.3390/cells10040847.
125. Ruano, P. *et al.* We are IntechOpen , the world ' s leading publisher of Open Access books Built by scientists , for scientists TOP 1 %. *Intech* 13 (2016).
126. Singh, J. P. *et al.* *Fabrication of magnetic tunnel junctions. Advanced Applications in Manufacturing Engineering* (Elsevier Inc., 2018). doi:10.1016/B978-0-08-102414-0.00002-1.